NASA TN D-919

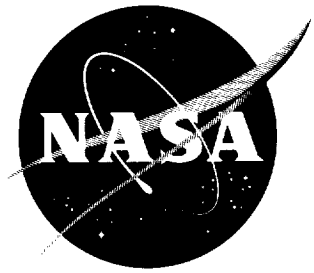

TECHNICAL NOTE

D-919

WIND-TUNNEL INVESTIGATION OF A BALLOON AS A TOWED DECELERATOR AT MACH NUMBERS FROM 1.47 TO 2.50

By John T. McShera and J. Wayne Keyes

Langley Research Center
Langley Field, Va.

NATIONAL AERONAUTICS AND SPACE ADMINISTRATION
WASHINGTON August 1961

NATIONAL AERONAUTICS AND SPACE ADMINISTRATION

TECHNICAL NOTE D-919

WIND-TUNNEL INVESTIGATION OF A BALLOON AS A TOWED DECELERATOR AT MACH NUMBERS FROM 1.47 TO 2.50

By John T. McShera and J. Wayne Keyes

SUMMARY

A wind-tunnel investigation has been conducted to study the characteristics of a towed spherical balloon as a drag device at Mach numbers from 1.47 to 2.50, Reynolds numbers from 0.36×10^6 to 1.0×10^6, and angles of attack from -15° to 15°. Towed spherical balloons were found to be stable at supersonic speeds. The drag coefficient of the balloon is reduced by the presence of a tow cable and a further reduction occurs with the addition of a payload. The balloon inflation pressure required to maintain an almost spherical shape is about equal to the free-stream dynamic pressure. Measured pressure and temperature distribution around the balloon alone were in fair agreement with predicted values. There was a pronounced decrease in the pressure coefficients on the balloon when attached to a tow cable behind a payload.

INTRODUCTION

Along with the current development of high-strength-fabric materials capable of withstanding high temperatures, there has been an increased interest in the use of drogue parachutes and balloon-type devices which may be deployed in recovery systems as decelerators and stabilizers under high-speed conditions. Flexible porous parachutes have a limited range of stable operation at supersonic speeds, as illustrated in reference 1. Stability can also be obtained at high porosities; however, the drag decreases rapidly with increasing porosity. Spherical balloons, however, are stable at supersonic speeds and have a relatively high drag coefficient depending upon the flow field surrounding the balloon. (See ref. 1.)

Small spheres (without payloads) have been investigated from subsonic to high supersonic velocities (refs. 2 and 3); however, the flow field surrounding a sphere towed behind a payload at supersonic speeds will undoubtedly be different from that about an independent sphere at the same velocity. An investigation has therefore been conducted in the Langley Unitary Plan wind tunnel to study the drag characteristics of a

spherical balloon (under simulated towed conditions) at Mach numbers from 1.47 to 2.50. In addition to drag measurements of the balloon and payload combination, pressure and temperature distributions around the balloon were measured and compared with predicted values. The results include some effects of Reynolds number, angle of attack, balloon inflation-pressure, tow-cable length, payload shape, and Mach number. A few tests were conducted to study the stability of a balloon under towed conditions.

SYMBOLS

C_D drag coefficient, $\frac{F_D}{qS}$

C_{D_p} pressure drag coefficient (defined in eq. 2)

C_p pressure coefficient, $\frac{p_l - p_\infty}{q_\infty}$

$C_{p,max} = \frac{p_{t,2} - p_\infty}{q_\infty}$

d diameter of model, ft

F_D force along X-stability axis, lb

l tow-cable length, in.

M Mach number

N_{Pr} Prandtl number

p pressure, lb/sq ft

q dynamic pressure, $0.7p_\infty M^2$, lb/sq ft

R Reynolds number, $\frac{\rho_\infty U_\infty d}{\mu_\infty}$

S frontal area, sq ft

s included angle between the separation point and the stagnation point

T	temperature, ^{o}R
U	velocity, ft/sec
α	angle of attack, deg
η	recovery factor (defined in eq. 3)
θ	angular position of thermocouples and pressure orifices (See fig. 2)
μ	viscosity, lb-sec/ft^2
ρ	mass density, lb-sec^2/ft^4

Subscripts:

e	equilibrium conditions
l	local conditions outside of boundary layer
2	conditions behind normal shock
t	total
∞	free-stream conditions
o	stagnation point
nom	nominal

APPARATUS

Wind Tunnel

The tests were conducted in the low Mach number test section of the Langley Unitary Plan wind tunnel. The tunnel is a variable-pressure return-flow type. The test section is 4 feet square and approximately 7 feet long. The nozzle leading to the test section is of the asymmetric sliding block type, and Mach numbers may be varied through a range from approximately 1.47 to 2.80 without tunnel shutdown. Further description of the tunnel may be found in reference 4.

Models and Instrumentation

Three balloon models 8 inches in diameter were constructed for the investigation. The first was a rigid model constructed of a spherical-shaped metal shell covered with a rubber-impregnated fabric having an average roughness of 125 microinches. This model was mounted on a six-component strain-gage balance supported on a sting from the downstream side of the balloon as shown in figure 1. The installation of a simulated tow cable is also shown in figure 1. This tow cable was simulated either by a rough steel rod with a nominal diameter of 0.25 inch or by telescoping tubes with a maximum diameter of 0.75 inch which could be remotely actuated to simulate three different lengths of tow cable. Various types of payloads could be attached to the upstream end of the telescoping tube (called an actuator). Since unpublished data have shown that a burble fence is necessary to stabilize a spherical balloon at subsonic speeds, the model was provided with a metal ring having a cross-sectional diameter of 0.25 inch and located 105° from the stagnation point as shown in figure 1. The rigid model balloon was equipped with pressure orifices and thermocouples in both the vertical and horizontal planes as shown in figure 2. Details of the 30 gage iron-constantan thermocouples and pressure-orifice installations are shown also in figure 2. Figure 3 shows details of the various payloads which were attached to the upstream end of the simulated tow cable, and figure 4 shows photographs of the various model configurations.

The second balloon model, also sting mounted, was flexible and its internal pressure could be controlled. Excessive deformation of the fabric surface, when subjected to supersonic flow, was prevented by eight cables imbedded in the fabric surface. Pressure orifices were located at the same locations as on the first model. Photographs of this model at a Mach number of 1.5 with different internal pressures are shown in figures 4(g) and 4(h).

The third balloon model was an inflatable type attached to a flexible steel tow cable of 1/16-inch diameter. A photograph of this third model is shown in figure 4(i). The upstream end of the flexible tow cable was attached to the base of the asymmetric body as illustrated in figures 4(j) and 4(k).

A fourth model illustrated in figure 4(k) and in figure 5 was constructed of clear plastic with a diameter of 6.75 inches. The balloon was attached to a flexible tow cable. In order to prevent the balloon from striking the tunnel walls when the starting shock wave passed through the test section, a trailing cable was attached to the downstream side of the balloon. After supersonic flow was established in the test section, the trailing cable remained slack. Only high-speed schlieren motion pictures were made during tests of this model.

Pressure orifices on the first and second models were connected to valves that sequentially sample 48 pressures on a single electrical transducer. The transducer output is recorded on digitized self-balancing potentiometers. The stagnation temperature was determined from probes located in the vicinity of the base of the balloon and outboard from the balloon wake. The temperatures were recorded on self-balancing potentiometers.

TESTS

The various configurations of the four models investigated are listed in table I and the test conditions are listed in table II. The two sting-supported models were tested through an angle-of-attack range of $\pm 15^{\circ}$. The Reynolds numbers listed in table II are based on a balloon diameter of 8 inches. The dewpoint temperature for all tests was maintained below -30° F to prevent adverse condensation effects. The stagnation temperature was maintained at 125° F for all Mach numbers except 2.50, where it was 150° F. In the tests of the sting-supported inflatable balloon model the internal pressure of the balloon was varied to determine the differential pressure necessary to maintain an almost spherical shape.

MEASUREMENTS AND ACCURACY

The maximum deviation of the local Mach number in the portion of the tunnel occupied by the model was ± 0.015 from the average values listed in table II. The angles of attack are corrected for deflection of the sting and balance under load. The angles of attack are also corrected for flow angularity and are estimated to be within $\pm 0.1^{\circ}$ of the indicated values.

The accuracy of the drag coefficients, based on balance calibration and repeatability of data is estimated to be within ± 0.02. The accuracy of the values of temperatures based on the calibrated accuracy of the self-balancing potentiometer recorders used is $\pm 0.5^{\circ}$. The accuracy of the pressure coefficients based on the calibrated accuracy of the measuring device used is a maximum of ± 0.033. Separation-point measurement is estimated to be accurate within $\pm 1^{\circ}$.

The data at $M = 1.50$, $\alpha = 0^{\circ}$ for the rigid balloon with a 24-inch tow cable and various payloads are influenced by shock reflections on and close to the balloon; the difference noted in drag coefficient values, however, is within the experimental accuracy.

RESULTS AND DISCUSSION

The results of an investigation of a balloon as a towed decelerator at Mach numbers from 1.47 to 2.50 are shown in figures 6 to 19. A motion-picture film supplement showing the towed balloons has also been prepared and is available on loan. A request card form and a description of the film will be found at the back of this paper on the page immediately preceding the abstract page.

STABILITY

The motion picture of the inflated balloon indicated that the random oscillation had an amplitude less than 1/8 the diameter of the balloon (24-inch tow cable) although the balloon was not fully inflated. The tow cable failed and no data were obtained for the fully inflated condition.

Schlieren motion pictures of the rigid towed balloon with a 24-inch tow cable showed oscillations of a very low frequency and a maximum total amplitude of two-thirds of the diameter of the balloon. In comparison with parachutes tested under the same conditions, both the inflated and the rigid plastic balloons were very stable at the supersonic speeds investigated, although flow separation and the resultant shock pattern varied with time at a given Mach number. There was a rapid movement of the separation point back and forth along the tow cable and this movement indicated the influence of the interaction between the balloon bow shock and the boundary layer on the tow cable. These fluctuations in the shock pattern may be seen in the motion-picture film supplement. Typical schlieren photographs of the sting-supported model balloons are shown in figure 6.

Drag Characteristics

Figure 7 shows the effect of Reynolds number on the drag characteristics of a clean rigid balloon. As can be seen, Reynolds number had little effect on the drag except at Mach numbers of 1.47 and 1.5. The Reynolds number range covered was small and the changes in drag coefficient due to Reynolds number effects were within the accuracy of the results. Based on data obtained in references 2 and 3, it appears that the tests were conducted above the critical Reynolds number range. At a critical Reynolds number there is generally a reduction in drag resulting from a rapid rearward movement of the separation point. However, in the Reynolds number range of the tests (0.36×10^6 to 1.0×10^6) this reduction in drag did not occur. There is a correlation between the changes in the location of the separation point and changes in drag.

Figure 8 shows the effect of the addition of a fence on the separation point on a balloon. Once a fence is added to the balloon, the separation point remains fixed on the model with increases in Mach number.

Figure 9 shows the effect of the fence on the drag characteristics of the balloon. The drag increased rapidly on the clean rigid balloon at the low Mach numbers as the separation-point location moved aft to 90°. After the separation point passed 90°, the drag decreased with increasing Mach numbers. The addition of the fence at 105° held the separation point constant, the drag was thereby held constant with increasing Mach number.

The effect of a simulated tow cable is shown in figure 10. In general, there is a considerable reduction in drag once a tow cable is attached to the rigid balloon. The increase in the ratio of the length of tow cable to the diameter of the balloon l/d from 1 to 3 resulted in little difference in drag, as the difference shown in figure 10 is within the experimental accuracy. Schlieren photographs indicated that for an increase in l/d from 1 to 3, the separation point on the tow cable stays fixed at about one balloon diameter upstream. The separated flow over the 8-inch tow cable shows little or no evidence of unsteadiness. However, the 24-inch tow cable has some evidence of unsteady flow at $M = 2.5$, although the extent of the separated region remains unchanged. From a drag consideration in the Reynolds number range tested either a one- or three-balloon-diameter tow cable is satisfactory.

Unpublished data indicate that the fence is needed for stability at subsonic speeds. Figure 11 shows the fence has little effect upon holding the drag constant once a tow cable is attached to the rigid balloon. The drag increment gained by the use of a fence is nullified and the resultant drag is decreased; that is, at $M = 2.0$ the drag is approximately one-third of that of the clean balloon. A typical curve for drag coefficient plotted against angle of attack for various Mach numbers is shown in figure 12 for the rigid balloon with an 8-inch tow cable and a fence. The change in drag with angle of attack is indicative of the effect of the asymmetry of the flow due to the tow cable and fence; a similar condition would be expected to occur during the oscillations of a towed balloon.

Figure 13 compares C_D for the balloon with various payloads at different l/d ratios. Except for the asymmetric body, all payloads at a given l/d have approximately the same drag values. There is a definite increase in drag for the symmetrical body configurations when l/d is increased from 1.25 to 3.00. Except for the asymmetric body, it appears that an optimum tow-cable length has not been reached even at an l/d of 3. The drag coefficient is still increasing and the stability was unaffected. The asymmetric body, however, acts differently. At zero tow-cable length (payload attached to the balloon) there was a much lower

drag than for an l/d of 1.25. With an increase in l/d from 1.25 to 3, the drag decreased slightly. The asymmetric body at an l/d of 1.25 had a C_D approximately $1\frac{1}{2}$ to $1\frac{3}{4}$ times the value for symmetrical bodies at the same l/d.

The inflation pressure required to maintain an almost spherical shape of the balloon at supersonic speeds will vary with the balloon's construction and with the free-stream dynamic pressure. Visual observation of the balloon indicated that the inflation pressure required to maintain an almost spherical shape was about equal to the free-stream dynamic pressure.

Pressure Distribution

In figures 14 and 15, the pressure distribution predicted by modified Newtonian theory is shown for comparison with the measured pressure distribution on the balloon. The predicted pressure distribution is determined from the equation

$$C_p = C_{p,max} \cos^2\theta \qquad (1)$$

The predicted curves are in fair agreement with the experimental curves for the balloon. The deviation between predicted and measured values increases with increasing Mach numbers. This difference between the agreement of these curves with those in references 5 to 7 cannot be explained by the low Mach numbers or Reynolds numbers. Pressure distributions on other configurations are included in both figures 14 and 15 to show the reduction in pressure coefficient on the front part of the balloon when a tow cable and payload are attached. There was an increase in the pressure coefficients on the front part of the rigid balloon with increasing tow-cable length as the separation point moved from the tip of the tow cable to some point downstream of the tip. This same trend was observed in reference 8. The addition of the actuator and a given payload resulted in the same trend for increasing actuator lengths except for the asymmetric body.

There was a definite change in pressure between $\theta = 90^\circ$ and $\theta = 110^\circ$ when the fence was added to the balloon. In figure 15(a), the change in the pressure distribution on the inflated balloon with a symmetrical body and an internal pressure of 27C pounds per square foot can be explained by the change in shape of the model, which was pear-shaped instead of spherical. In most cases the local pressures are constant with increasing distance around the balloon in the separated region. No attempt has been made to compare the pressures measured in the vertical and horizontal planes at an angle of attack. However, the pressures

measured in the horizontal planes are in good agreement for a given positive and negative angle and for a given configuration as shown in figure 16.

Pressure drag coefficients were obtained by integrating the pressure distribution around the clean rigid balloon at an angle of attack of 0°:

$$C_{D_p} = \int_0^{\pi} C_p \sin 2\theta \, d\theta \qquad (2)$$

Estimates of the skin drag indicated this drag to be small. Therefore, it would be expected that the integrated pressure drag coefficients for the clean rigid balloon should be a good approximation of the total drag. A comparison of integrated and measured coefficients shows this to be true as indicated in the following table:

M	C_D	C_{D_p}
1.50	0.83	0.84
2.00	.95	.95
2.50	.79	.76

Temperature Distribution

The curves as determined from laminar and turbulent flow theory shown in figure 17 are computed from the expression,

$$\frac{T_e}{T_o} = \eta\left(1 - \frac{T_l}{T_o}\right) + \frac{T_l}{T_o} \qquad (3)$$

where the recovery factor $\eta = \sqrt{N_{Pr}}$ for the laminar-flow theory and $\eta = \sqrt[3]{N_{Pr}}$ for the turbulent flow theory. Due to the roughness of the model, the flow would be expected to be completely turbulent over the model. The Prandtl number is assumed constant at $N_{Pr} = 0.73$ for small temperature and pressure differences. The ratio of equilibrium to stagnation temperature at $\theta = 0°$ on the clean rigid balloon at zero angle of attack should be unity. The lower values of temperature ratio near $\theta = 0°$ shown in figure 17 could be caused by an instrumentation error. Platinum strips were added to the thermocouple junction to minimize the heat loss from the junction to the thermocouple wires. However a recent

unpublished theoretical method for predicting the loss in heating rate due to the ratio of wire size to skin thickness indicates the platinum strips were not adequate to compensate for the heat sink of the wires. Therefore, if the curves T_e/T_o were shifted to comply with a $\frac{T_e}{T_o} = 1$ at the stagnation point, then the slope of the measured curve would agree with the slope of the theoretical curve for turbulent flow.

There was a definite decrease in the equilibrium temperatures on the front of the rigid balloon when a tow cable and payload were attached as shown in figures 18 and 19. There is no appreciable change in the temperatures with a change in tow-cable length. In general, the temperature distributions in the horizontal plane at a positive and negative angle of attack are in good agreement for a given configuration. This agreement does not hold true for case of the rigid balloon and asymmetric body shown in figure 19(e) because of the unsymmetrical shock formation ahead of the model. The temperatures, like the pressures, remain nearly constant in the separated region.

CONCLUSIONS

The results of a wind-tunnel investigation of a balloon as a towed decelerator at Mach numbers from 1.47 to 2.50 lead to the following conclusions:

1. In comparison with other drogue devices, both the inflated and the rigid plastic balloons were very stable at the supersonic speeds investigated.

2. The addition of a fence on a clean rigid balloon fixes the separation point over the Mach number range of 1.50 to 2.50 and the drag remained constant with increases in Mach number. The effect of the fence was nullified when a tow cable and payload were added to the clean rigid balloon.

3. The drag coefficient of the balloon is reduced by the presence of a tow cable and further reduced by the addition of a payload.

4. The drag coefficient increases with increasing tow-cable length for the symmetrical payloads.

5. The balloon inflation pressure required to maintain an almost spherical shape is about equal to the free-stream dynamic pressure.

6. Measured pressure and temperature distributions around the balloon alone were in fair agreement with predicted values. There was a pronounced decrease in pressure coefficients and temperature ratios on the balloon when attached to a tow cable behind a payload.

7. The integrated pressure drag coefficients for the clean rigid balloon were good approximations of the total drag.

8. In the separated flow region, the equilibrium temperatures and the local pressures were essentially constant with increasing distance around the balloon.

Langley Research Center,
National Aeronautics and Space Administration,
Langley Field, Va., May 2, 1961.

REFERENCES

1. Maynard, Julian D.: Aerodynamics of Decelerators at Supersonic Speeds. Proc. of Recovery of Space Vehicles Symposium, Los Angeles, Calif., Aug. 31 - Sept. 1, 1960. (Sponsored by Inst. Aero. Sci. and Air Res. Dev. Command.)

2. Charters, A. C., and Thomas, Richard N.: The Aerodynamic Performance of Small Spheres From Subsonic to High Supersonic Velocities. Jour. Aero. Sci., vol. 12, no. 4, Oct. 1945, pp. 468-476.

3. May, Albert, and Witt, W. R., Jr.: Free-Flight Determination of the Drag Coefficients of Spheres. Jour. Aero. Sci., vol. 20, no. 9, Sept. 1953, pp. 635-638.

4. Anon.: Manual for Users of the Unitary Plan Wind Tunnel Facilities of the National Adivsory Committee for Aeronautics. NACA, 1956.

5. Beckwith, Ivan E., and Gallagher, James J.: Heat Transfer and Recovery Temperatures on a Sphere With Laminar, Transitional, and Turbulent Boundary Layers at Mach Numbers of 2.00 and 4.15. NACA TN 4125, 1957.

6. Lawson, Warren A., McDearmon, R. W., and Rainey, R. W.: Investigation of the Pressure Distributions on Reentry Nose Shapes at a Mach Number of 3.55. NASA TM X-244, 1960.

7. Stine, Howard A., and Wanlass, Kent: Theoretical and Experimental Investigation of Aerodynamic-Heating and Isothermal Heat-Transfer Parameters on a Hemispherical Nose With Laminar Boundary Layer at Supersonic Mach Numbers. NACA TN 3344, 1954.

8. Moeckel, W. E.: Flow Separation Ahead of a Blunt Axially Symmetric Body at Mach Numbers 1.76 to 2.10. NACA RM E51I25, 1951.

TABLE I.- CONFIGURATIONS OF SPHERICAL BALLOON MODELS

Balloon model	Balloon diameter, in.	Fence installed	Simulated tow-cable	Tow-cable length, in.	Payload	Data obtained
Sting-supported (rigid)	8	No	None	0	None	Drag, pressure and temperature distribution
Sting-supported (rigid)	8	No	Rigid 0.25-inch-diameter steel rod	24	None	Drag, pressure and temperature distribution
Sting-supported (rigid)	8	No	Rigid 0.25-inch-diameter steel rod	8	None	Drag, pressure and temperature distribution
Sting-supported (rigid)	8	Yes	Rigid 0.25-inch-diameter steel rod	24	None	Drag, pressure and temperature distribution
Sting-supported (rigid)	8	Yes	Rigid 0.25-inch-diameter steel rod	8	None	Drag, pressure and temperature distribution
Sting-supported (rigid)	8	Yes	None	0	Asymmetric body*	Drag, pressure and temperature distribution
Sting-supported (rigid)	8	Yes	Telescoping tubes (actuator)	10	Disk	Drag, pressure and temperature distribution
Sting-supported (rigid)	8	Yes	Telescoping tubes (actuator)	24	Disk	Drag, pressure and temperature distribution
Sting-supported (rigid)	8	Yes	Telescoping tubes (actuator)	10	Asymmetric body	Drag, pressure and temperature distribution
Sting-supported (rigid)	8	Yes	Telescoping tubes (actuator)	24	Asymmetric body	Drag, pressure and temperature distribution
Sting-supported (rigid)	8	Yes	Telescoping tubes (actuator)	10	Ball	Drag, pressure and temperature distribution
Sting-supported (rigid)	8	Yes	Telescoping tubes (actuator)	24	Ball	Drag, pressure and temperature distribution
Sting-supported (rigid)	8	Yes	Telescoping tubes (actuator)	10	Symmertic body	Drag, pressure and temperature distribution
Sting-supported (rigid)	8	Yes	Telescoping tubes (actuator	24	Symmetric body	Drag, pressure and temperature distribution
Sting-supported (inflated)	8 (approx.)	Yes	Telescoping tubes (actuator	10	Symmetric body	Drag, internal pressure, and pressure distributions
Towed (inflated)	8 (approx.)	Yes	1/16-inch-diameter flexible cable	24	Asymmetric body	Motion pictures
Towed (rigid plastic)	6.75	Yes	1/8-inch-diameter flexible cable	24	Asymmetric body	High-speed schlieren motion pictures
Towed (rigid plastic)	6.75	Yes	1/8-inch-diameter flexible cable	24	None	High-speed schlieren motion pictures

*Balloon model was attached directly to base of payload.

TABLE II.- TEST CONDITIONS OF SPHERICAL BALLOON MODELS

M	$p_{t,\infty}$, lb/sq ft	q_∞, lb/sq ft	R
1.47	429.6	184.8	0.55×10^6
1.47	625.6	269.3	.80
1.47	783.0	336.9	1.00
1.50	430.6	184.8	.55
1.50	521.0	223.7	.66
1.50	629.3	270.0	.80
1.50	785.9	337.2	1.00
1.54	435.7	185.9	.55
1.54	634.5	270.8	.80
1.54	792.8	338.2	1.00
1.57	446.1	189.3	.55
1.57	639.1	271.2	.80
1.57	802.7	340.6	1.00
1.70	461.0	189.0	.55
1.70	669.0	274.0	.80
1.70	810.0	331.8	1.00
1.90	498.0	188.0	.55
1.90	720.0	271.4	.80
1.90	899.0	338.9	1.00
2.00	506.0	180.9	.55
2.16	799.0	259.6	.80
2.16	1,002.0	325.9	1.00
2.50	435.0	111.1	.36

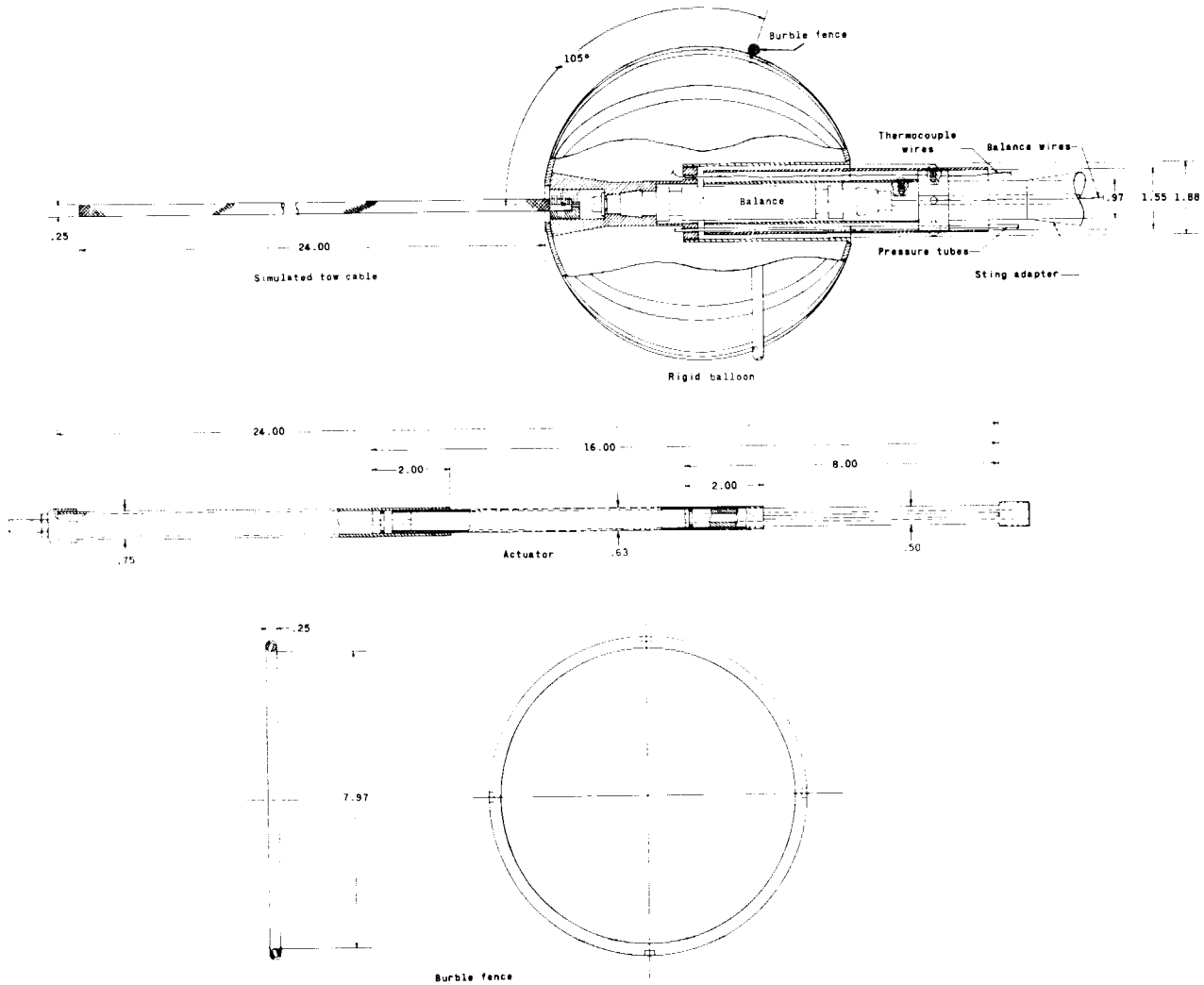

Figure 1.- Detail of balloon, sting adapter, actuator, simulated tow cable, and burble fence. All dimensions are in inches unless otherwise indicated.

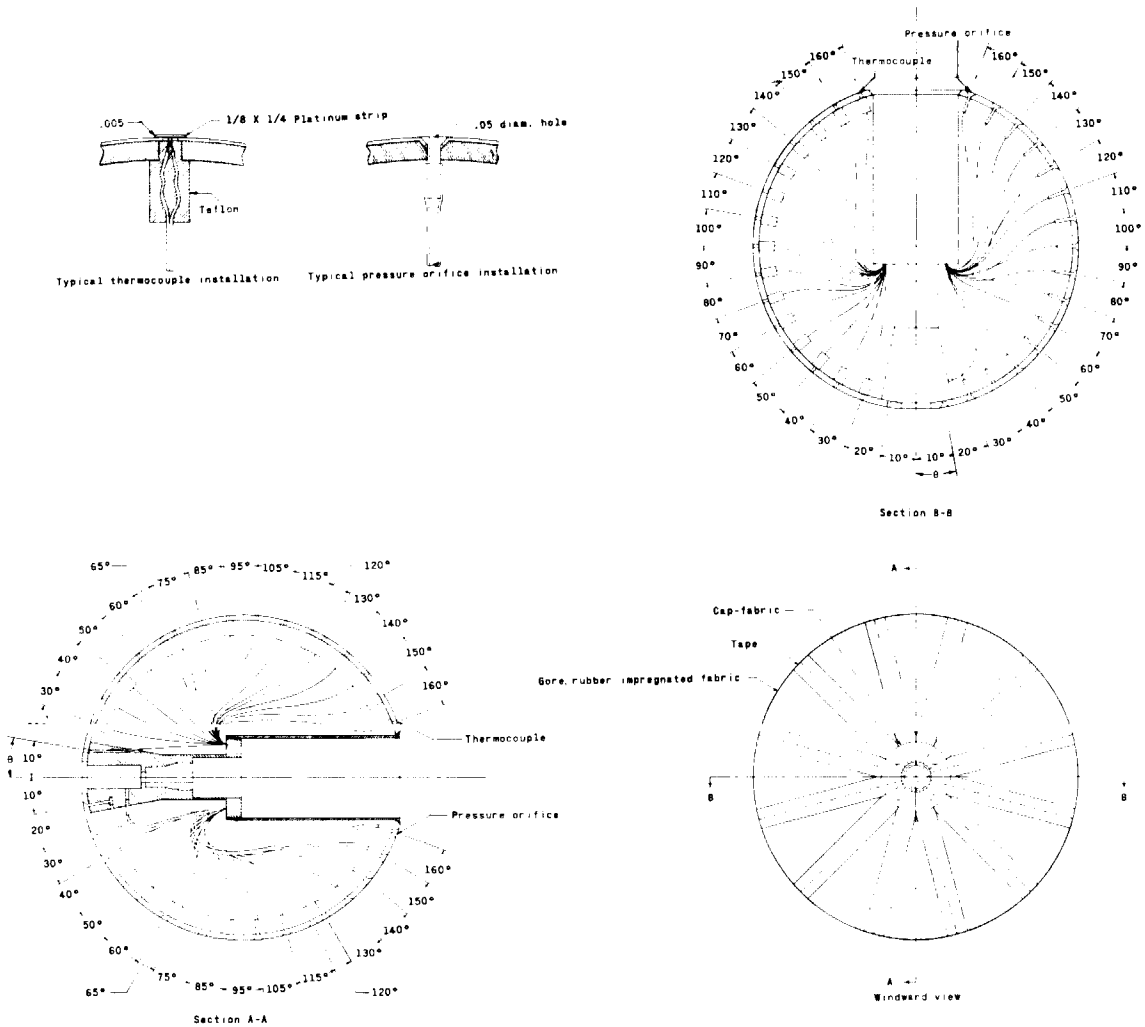

Figure 2.- Detail of model showing pressure orifices and thermocouple locations. All dimensions are in inches unless otherwise indicated.

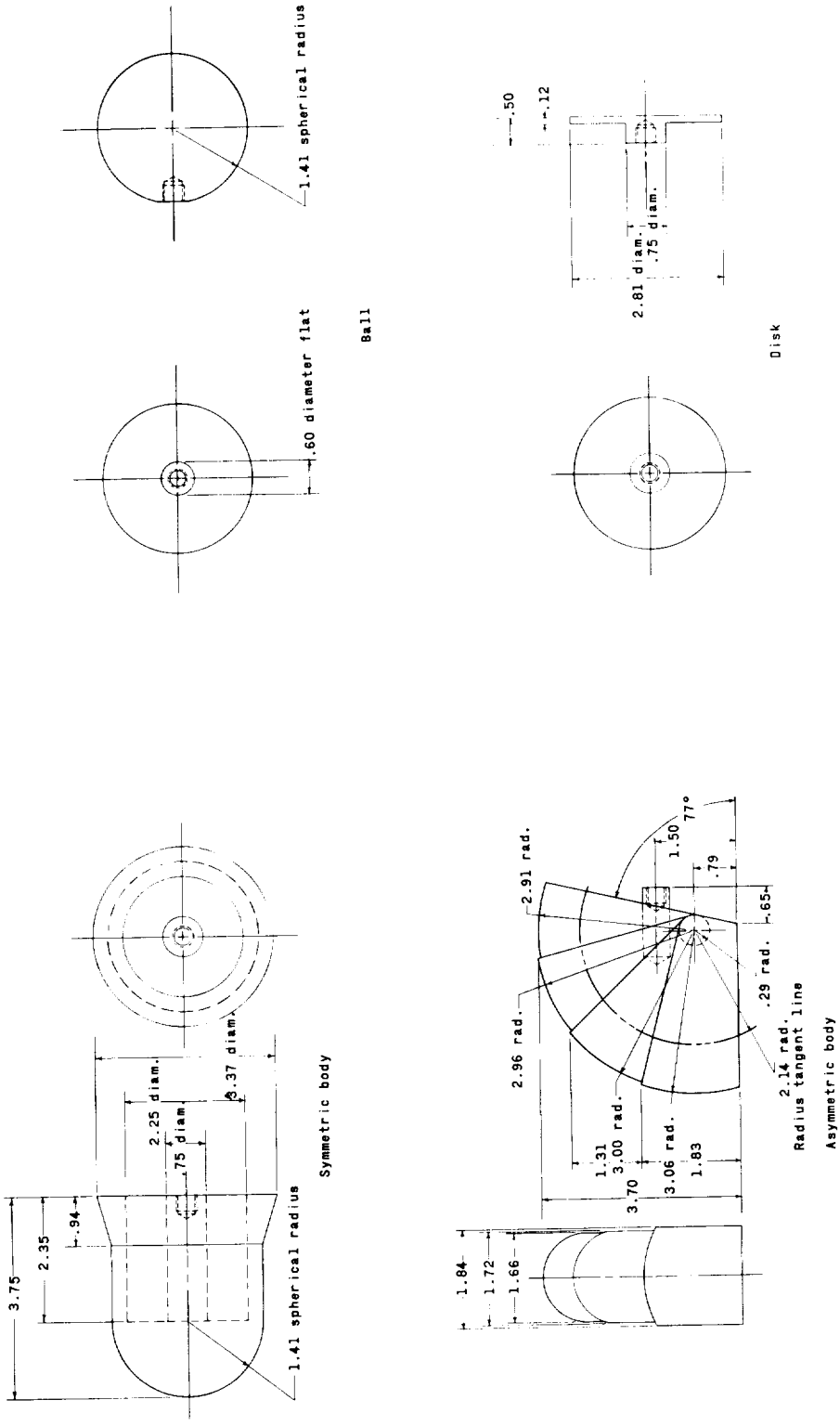

Figure 3.- Details of various payloads. All dimensions are in inches unless otherwise indicated.

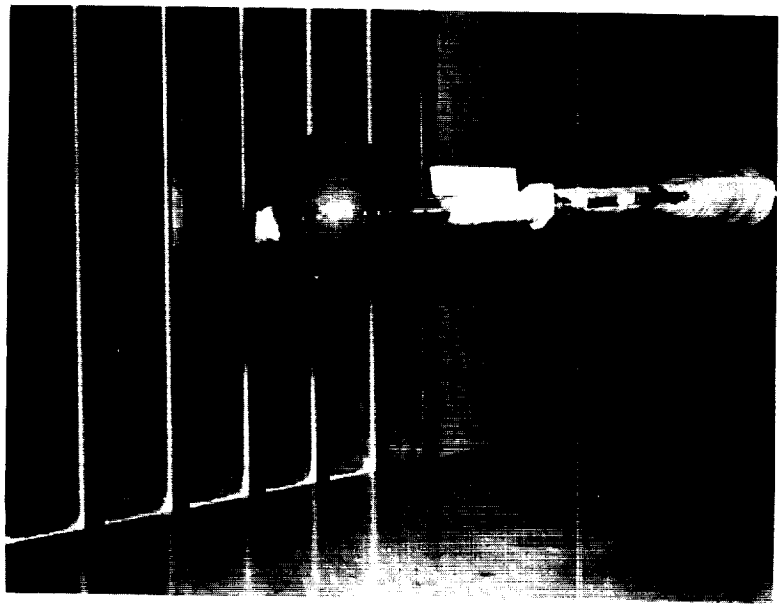

(a) Clean rigid balloon. L-59-4838

(b) Rigid balloon with fence, actuator, and disk. L-59-4845

Figure 4.- Typical model photographs.

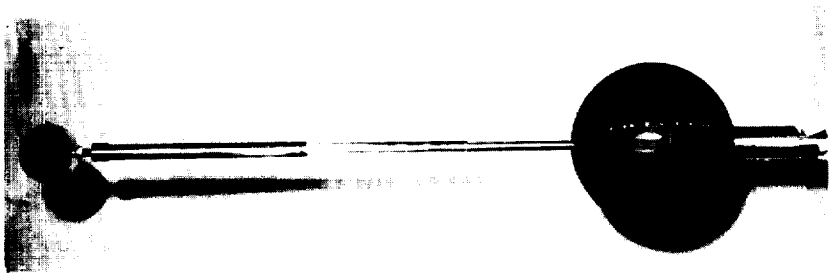

(c) Rigid balloon with 24-inch actuator and ball.

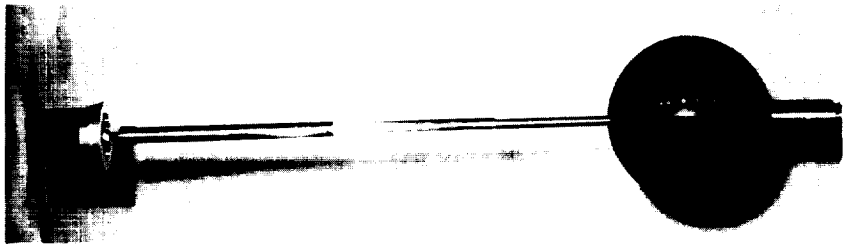

(d) Rigid balloon with 24-inch actuator and symmetric body.

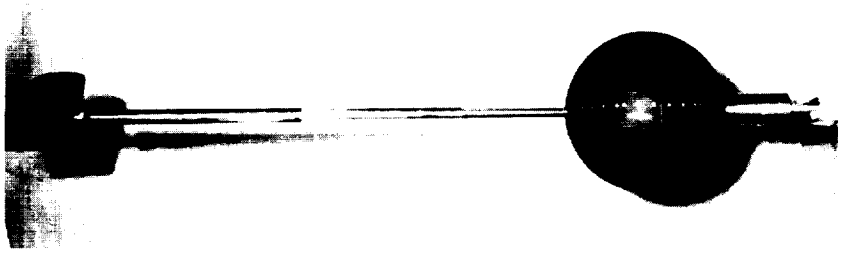

(e) Rigid balloon with 24-inch actuator and asymmetric body.

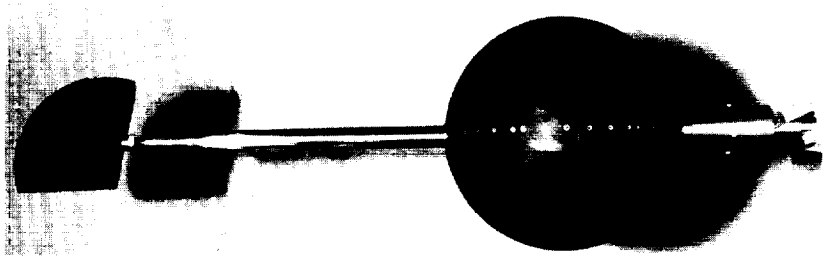

(f) Rigid balloon with 10-inch actuator and asymmetric body.

Figure 4.- Continued. L-61-2160

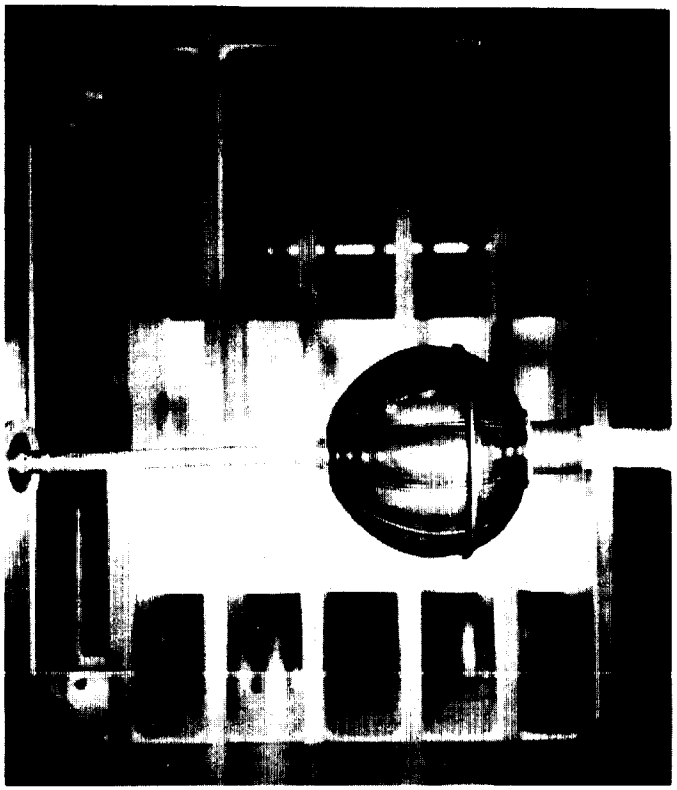

(g) Inflated balloon with fence, 10-inch actuator, and symmetric body at an internal pressure of 581.2 pounds per square foot. M = 1.50; $\alpha_{nom} = 0^{o}$.

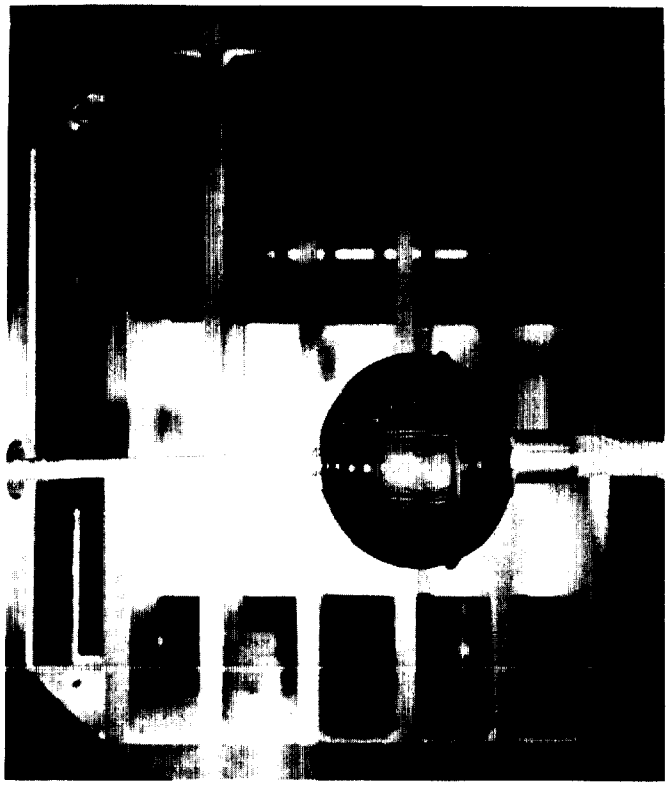

(h) Inflated balloon with fence, 10-inch actuator, and symmetric body at an internal pressure of 270.5 pounds per square foot. M = 1.50; $\alpha_{nom} = 0^{o}$.

Figure 4.- Continued. L-61-2161

(i) Towed inflatable balloon model.

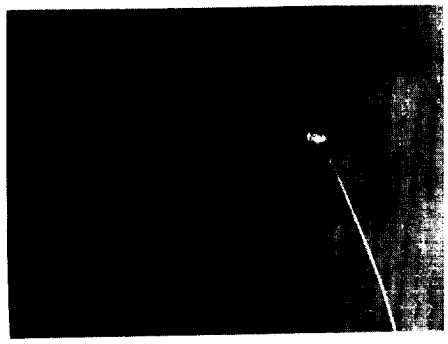

(j) Payload used with towed inflatable balloon model and towed rigid plastic model.

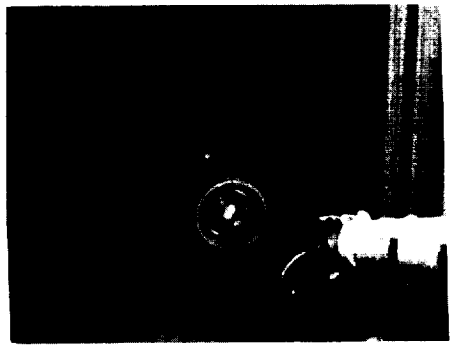

(k) Towed rigid plastic balloon model.

Figure 4.- Concluded. L-61-2162

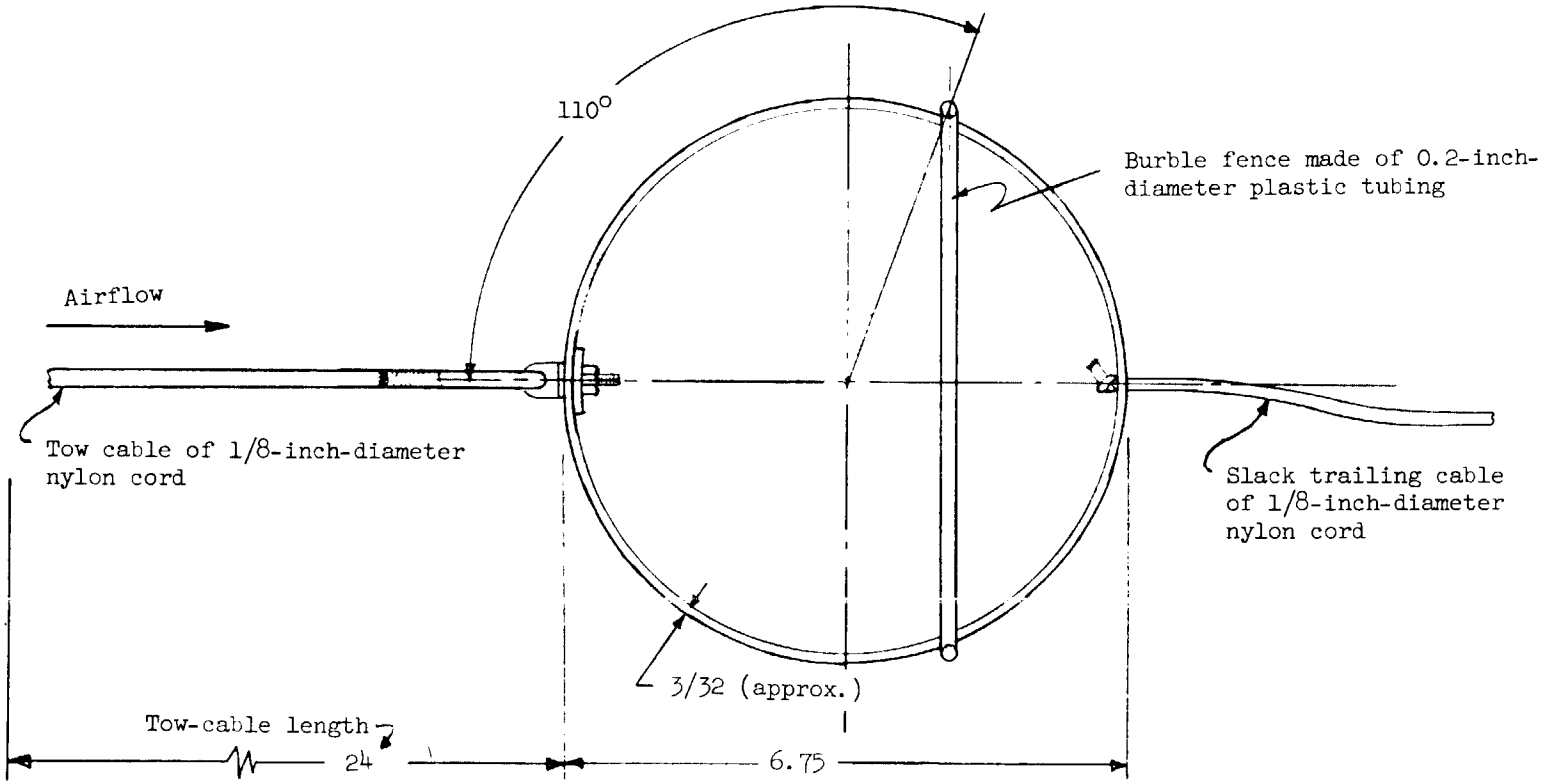

Figure 5.- Details of the plastic spherical-balloon model. All dimensions are in inches.

M = 1.50

M = 2.00

M = 2.50

(a) Clean rigid balloon. $\alpha_{nom} = 0^{o}$. L-61-2163

Figure 6.- Typical schlieren photographs.

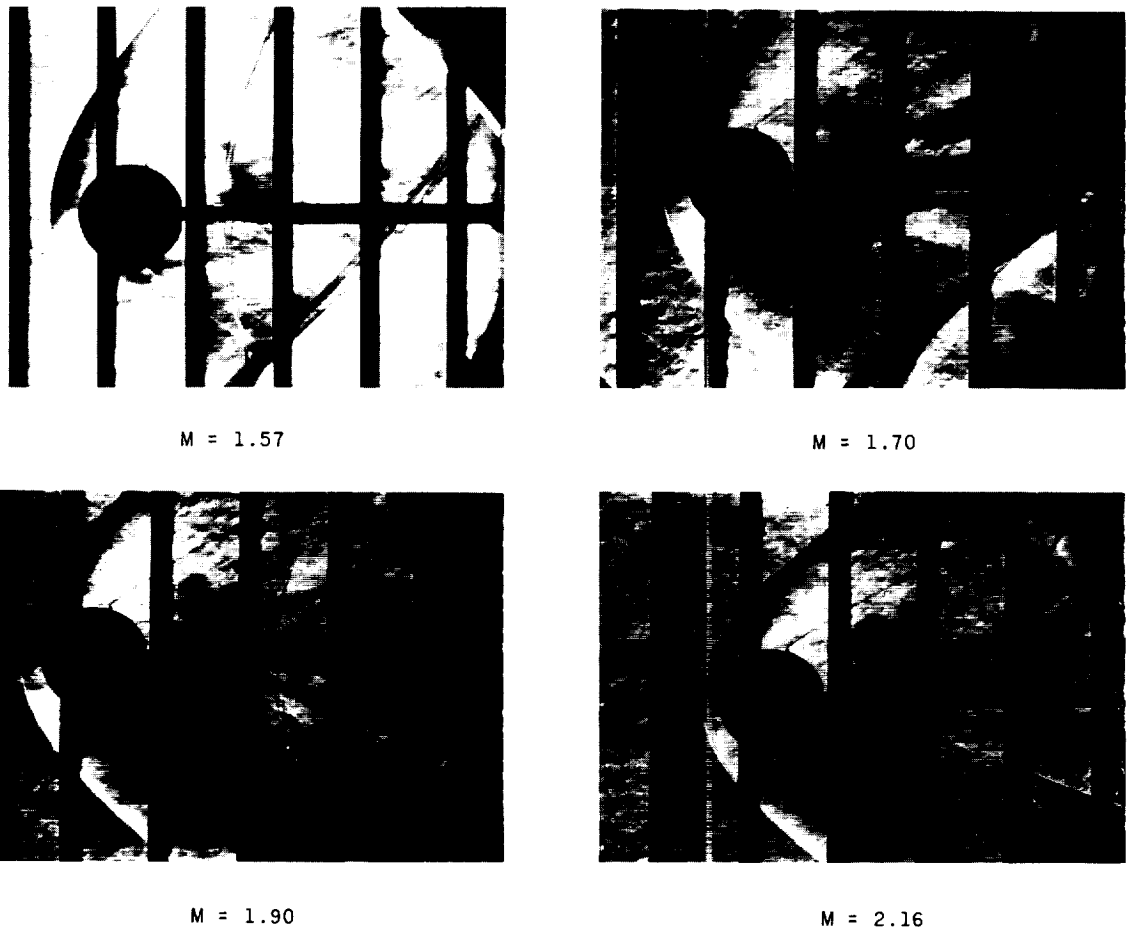

(b) Rigid balloon with fence. $c_{nom} = 0^{o}$.

Figure 6.- Continued. L-61-2164

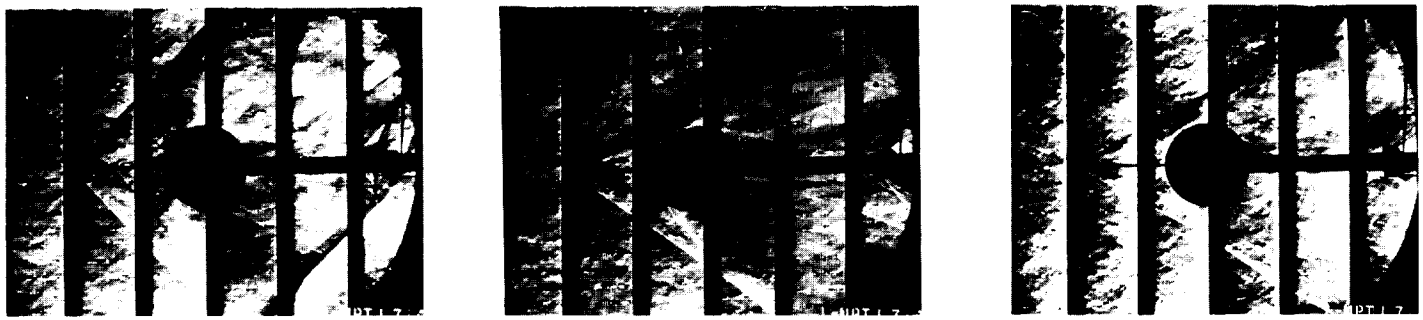

M = 1.50 M = 2.00 M = 2.50

(c) Rigid balloon with 8-inch tow cable. $\alpha_{nom} = 0^{\circ}$.

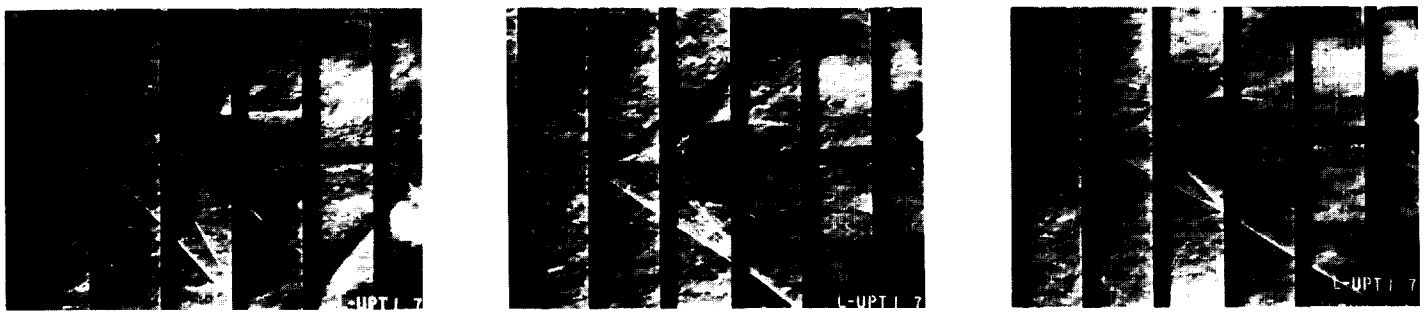

M = 1.50 M = 2.00 M = 2.50

(d) Rigid balloon with fence and 8-inch tow cable. $\alpha_{nom} = 0^{\circ}$.

Figure 6.- Continued. L-61-2165

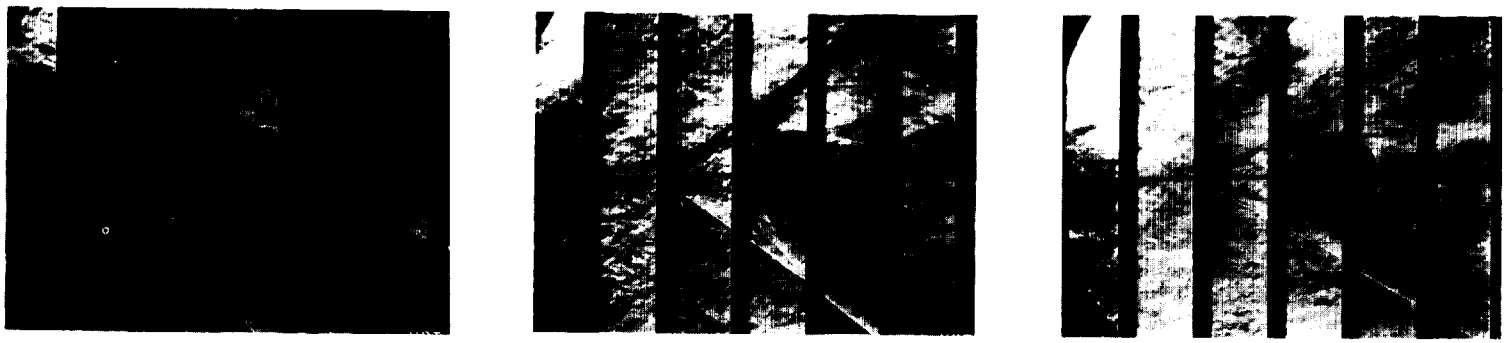

M = 1.50 M = 2.00 M = 2.50

(e) Rigid balloon with 24-inch tow cable.

M = 1.50 M = 2.00 M = 2.50

(f) Rigid balloon with 24-inch tow cable and fence.

Figure 6.- Continued. L-61-2166

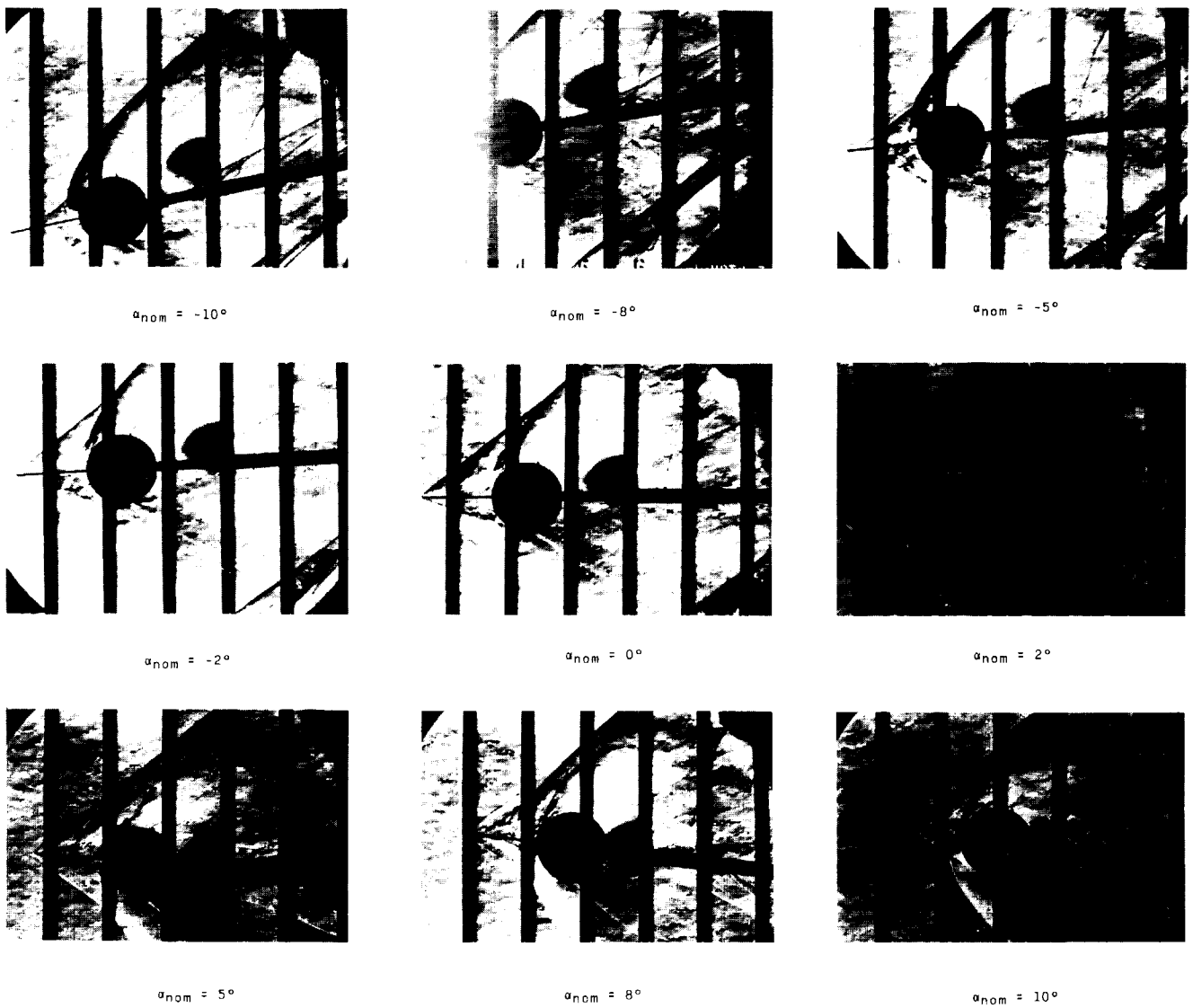

(g) Rigid balloon with fence and 8-inch tow cable at various angles of attack. M = 1.90.

Figure 6.- Continued. L-61-2167

Ball

Disk

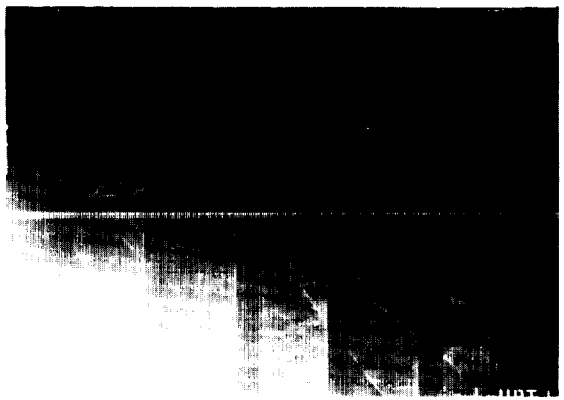

Symmetric body

Asymmetric body

M = 1.50

(h) Rigid balloon with fence, 10-inch actuator, and various payloads. $\alpha_{nom} = 0^{\circ}$.

Figure 6.- Continued. L-61-2168

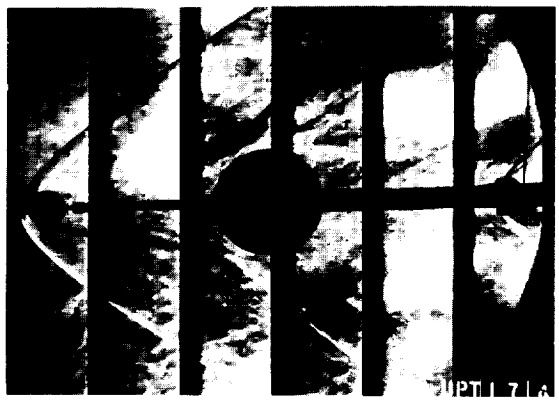

Ball

Disk

Symmetric body

Asymmetric body

M = 2.00

(h) Continued.

Figure 6.- Continued. L-61-2169

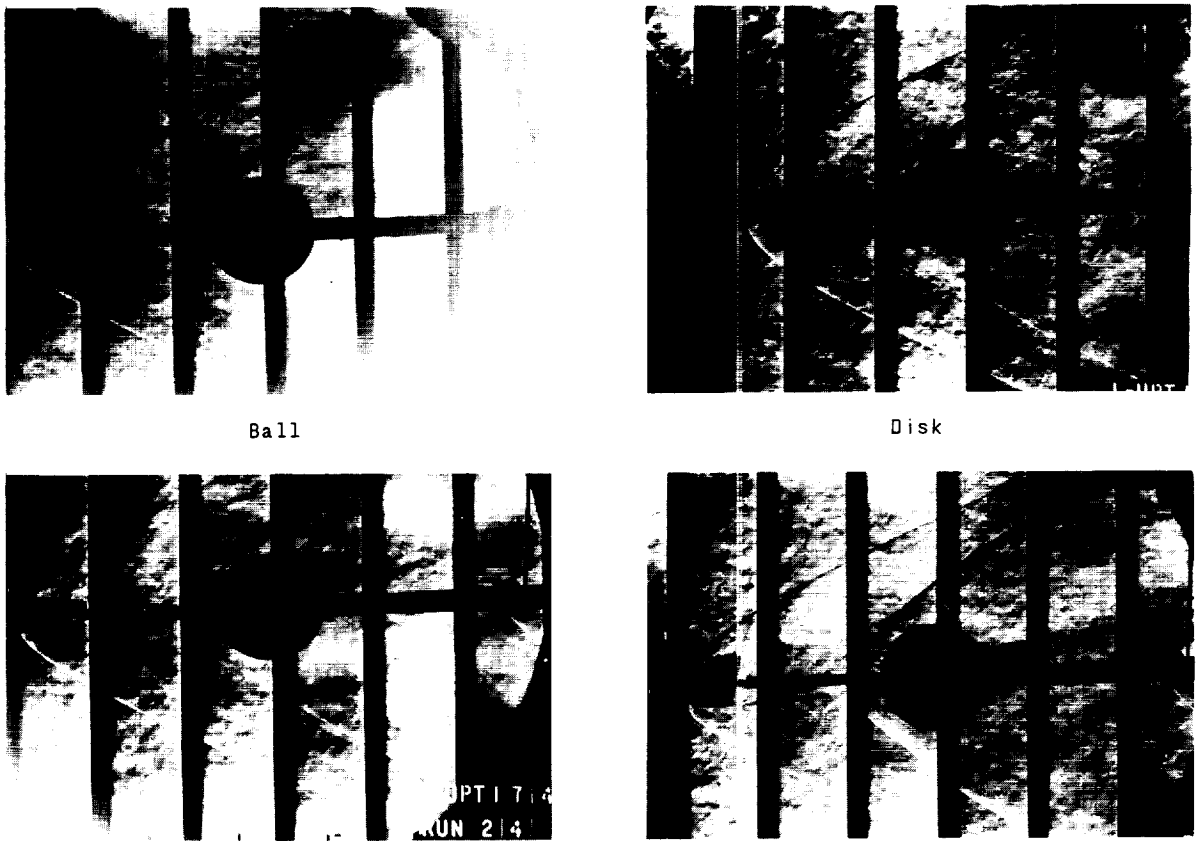

L-884

(h) Concluded. L-61-2170

Figure 6.- Continued.

M = 1.50

M = 2.00

M = 2.50

(i) Inflated balloon with fence. $\alpha_{nom} = 0^{\circ}$. L-61-2171

Figure 6.- Concluded.

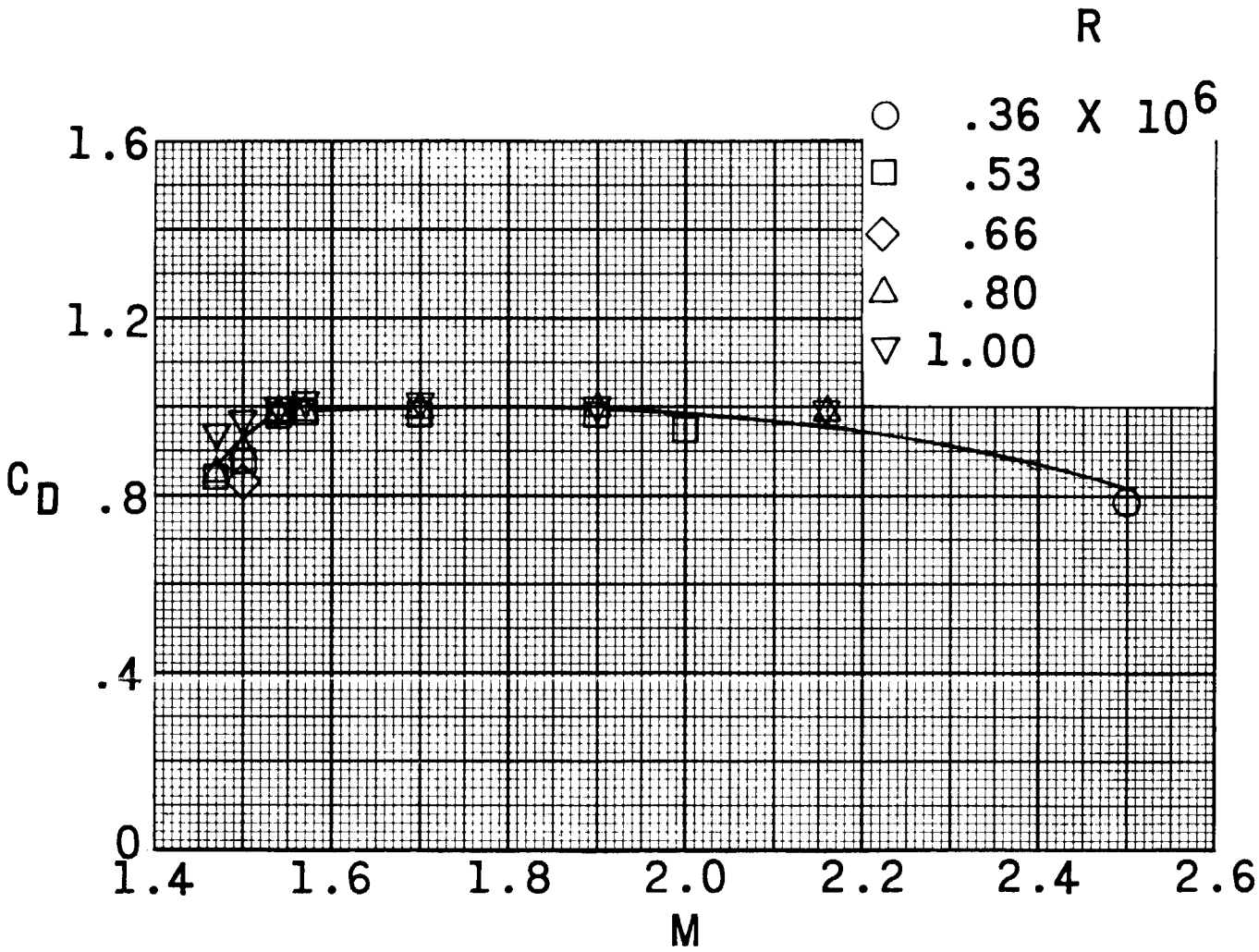

Figure 7.- Effect of Reynolds number on the drag characteristics of a clean rigid balloon. $\alpha_{nom} = 0^{o}$.

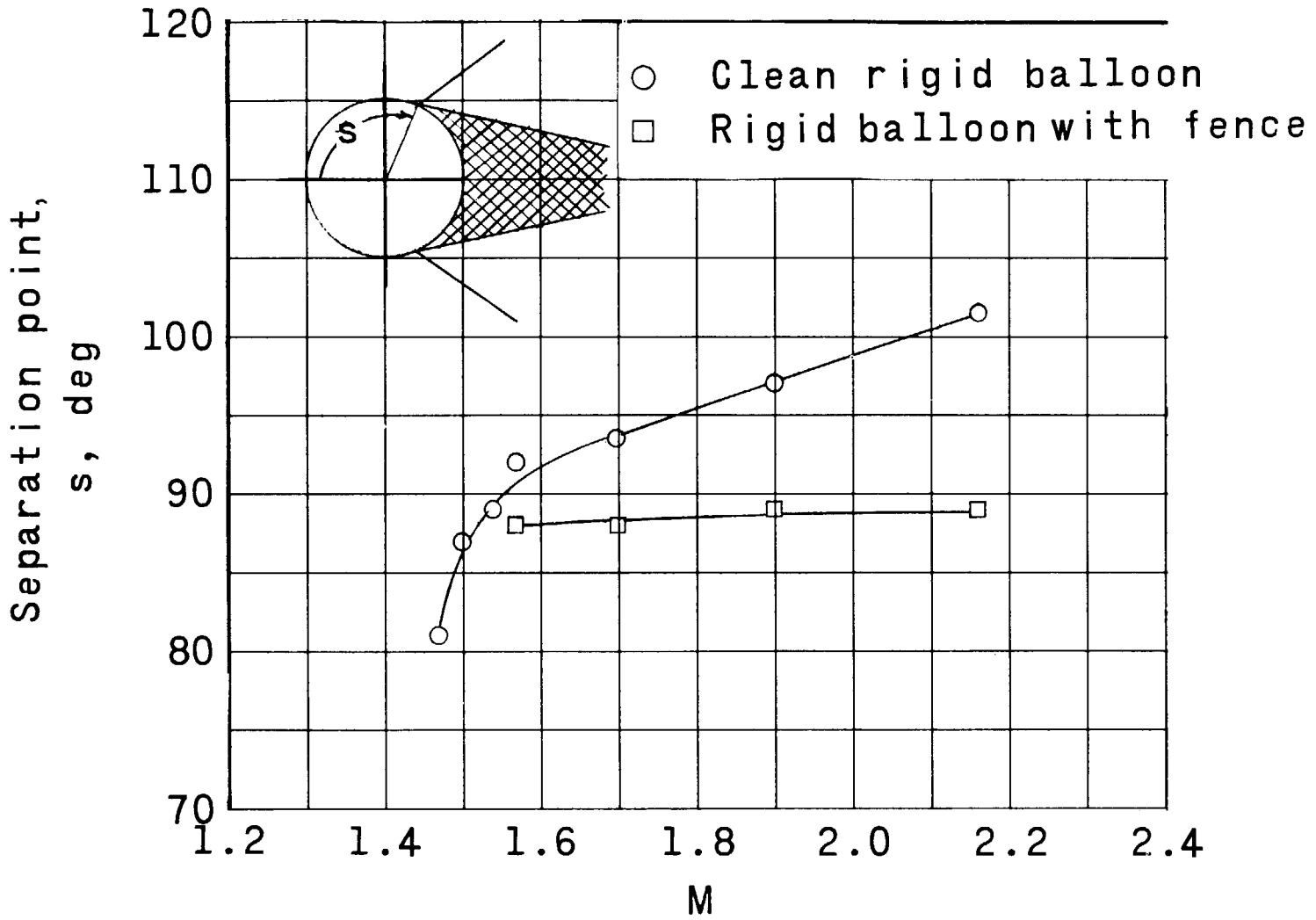

Figure 8.- Effect of the addition of a fence on the separation point of a rigid balloon. $\alpha_{nom} = 0^{o}$.

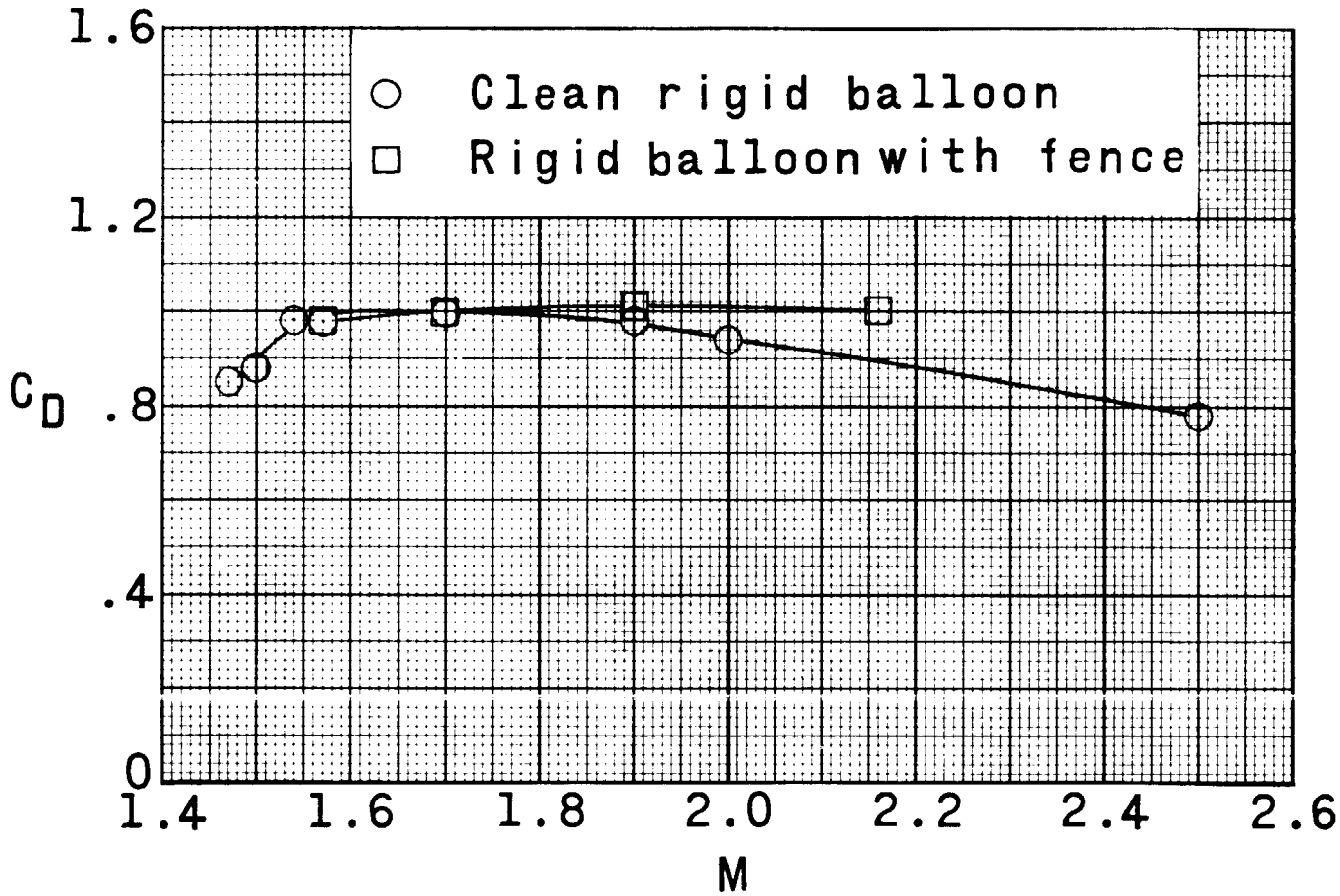

Figure 9.- Effect of the addition of a fence on the drag characteristics of a rigid balloon. $\alpha_{nom} = 0^{o}$.

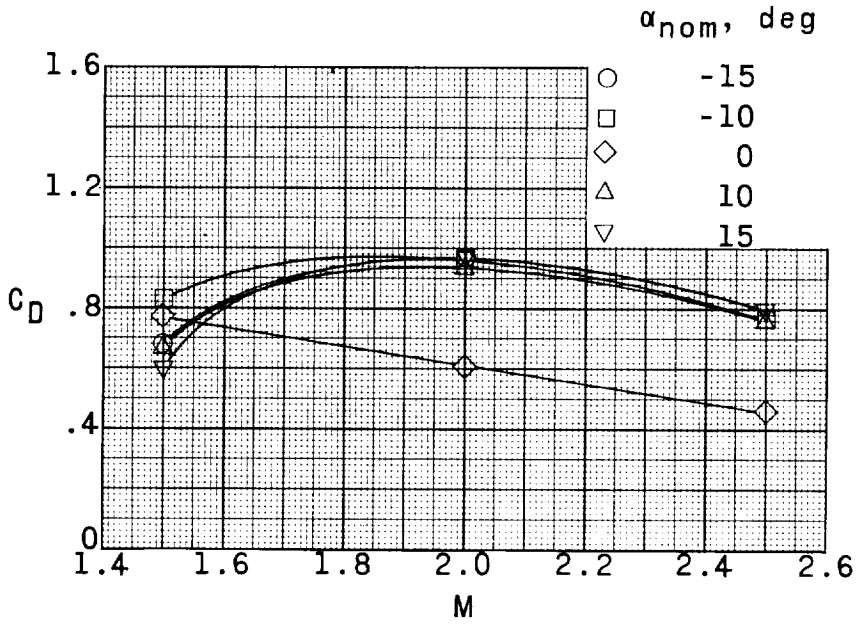

(a) 8-inch tow cable.

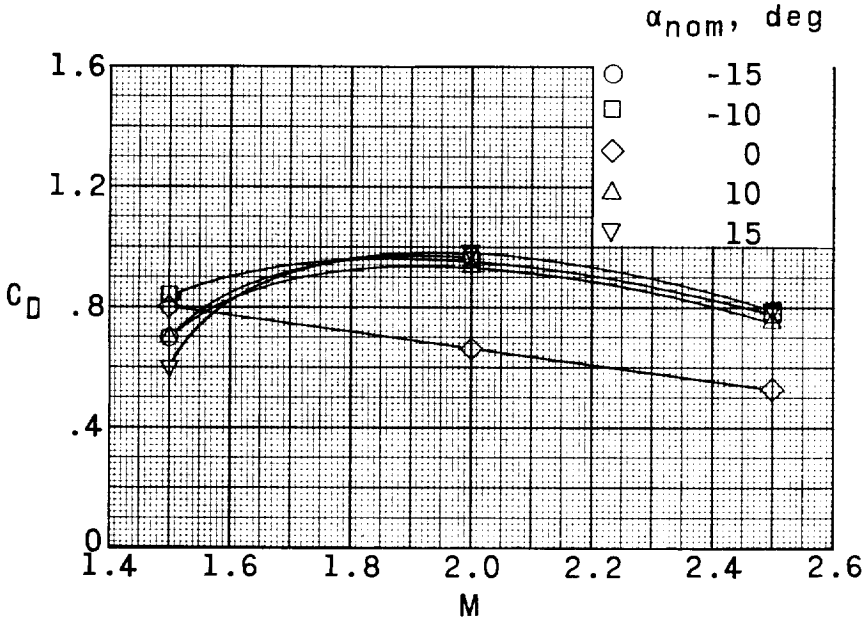

(b) 24-inch tow cable.

Figure 10.- Effect of simulated tow-cable length on the drag characteristics of a rigid balloon without fence.

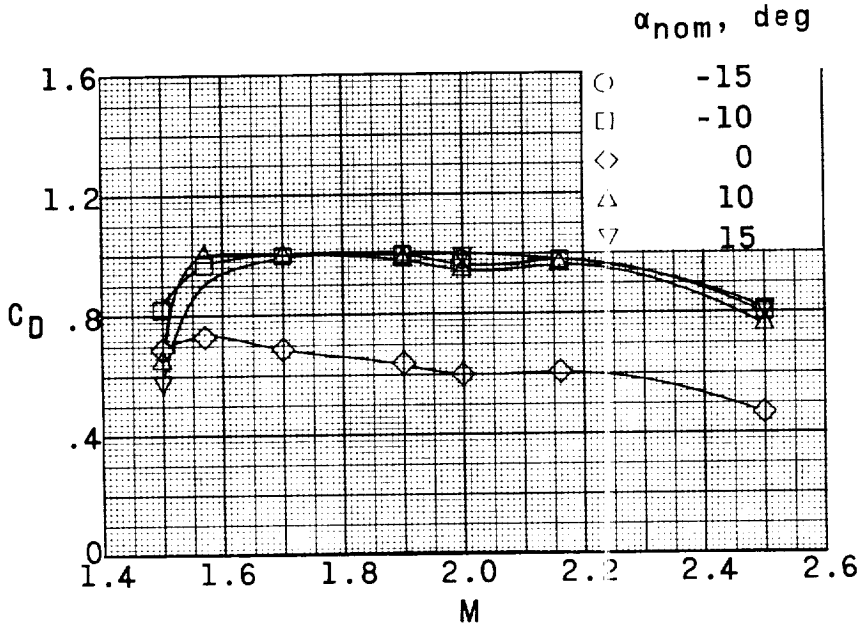

(a) 8-inch tow cable.

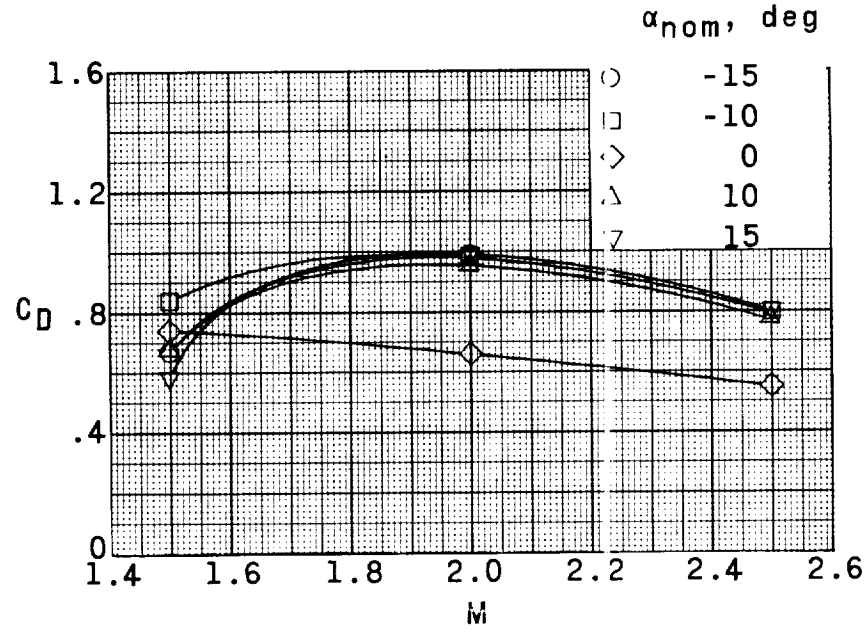

(b) 24-inch tow cable.

Figure 11.- Effect of simulated tow-cable length on the drag characteristics of a rigid balloon with fence.

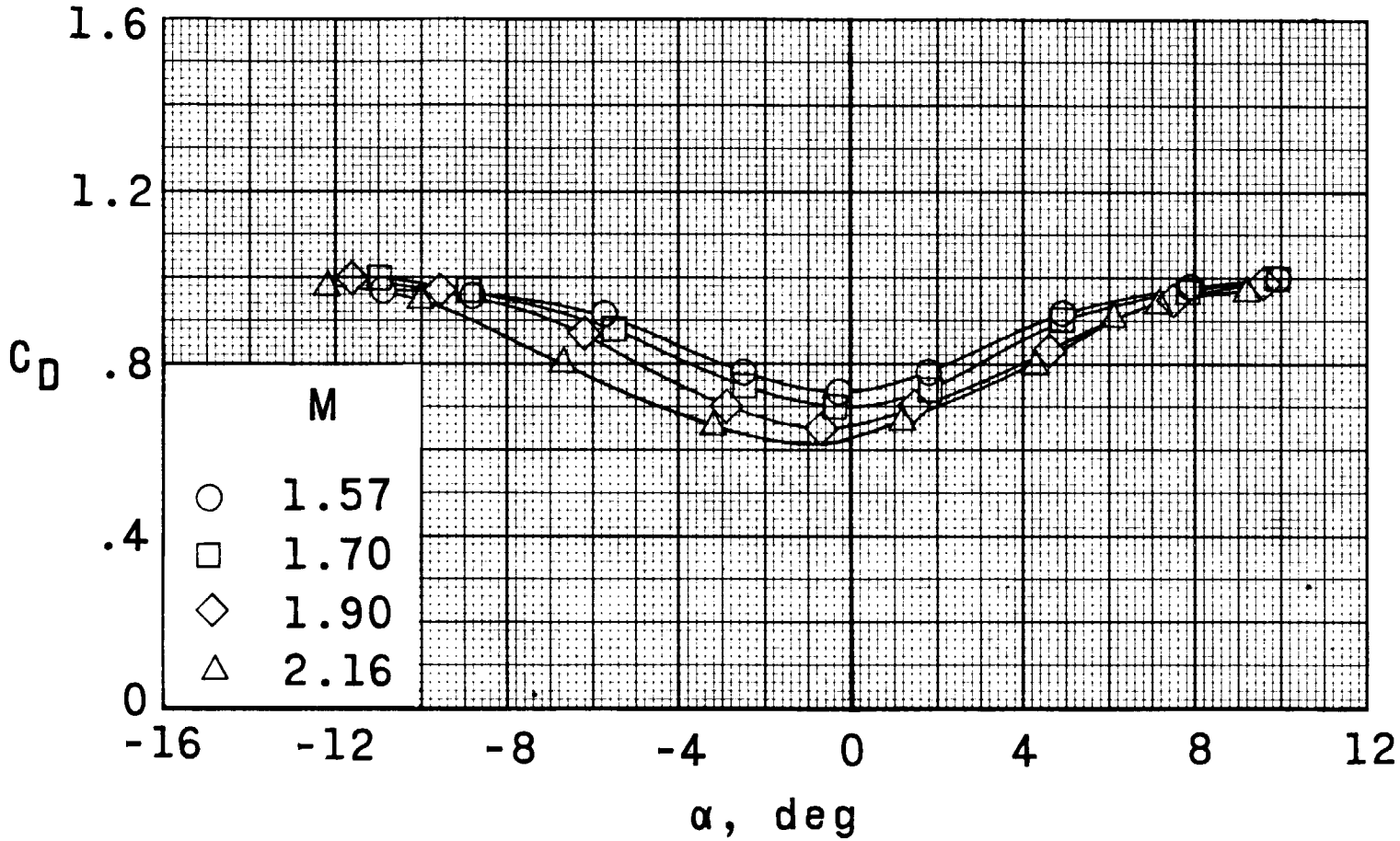

Figure 12.- Variation of the drag characteristics with angle of attack for the rigid balloon with fence and 8-inch tow cable.

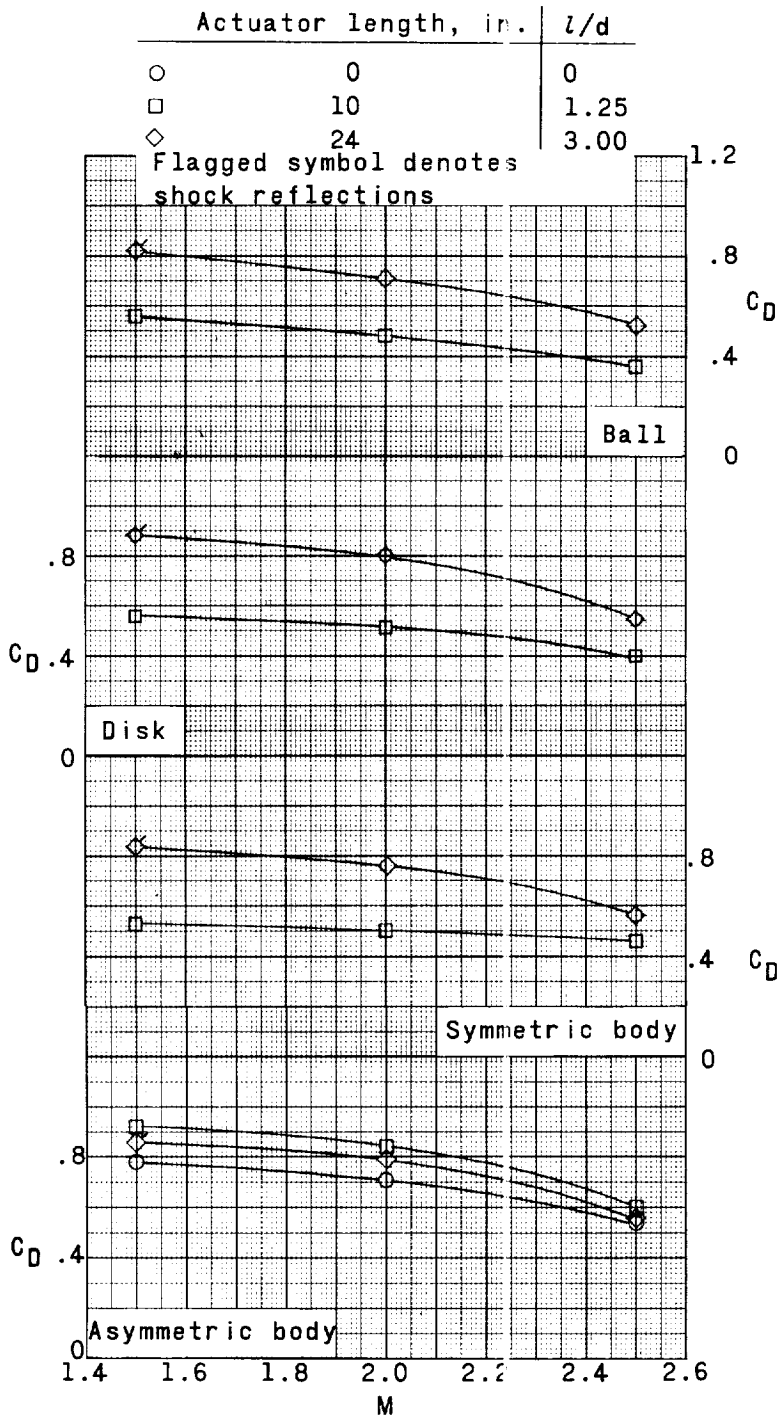

Figure 13.- Effect of payloads with varying actuator lengths on the drag characteristics of the rigid balloon with fence. $\alpha_{nom} = 0^{\circ}$.

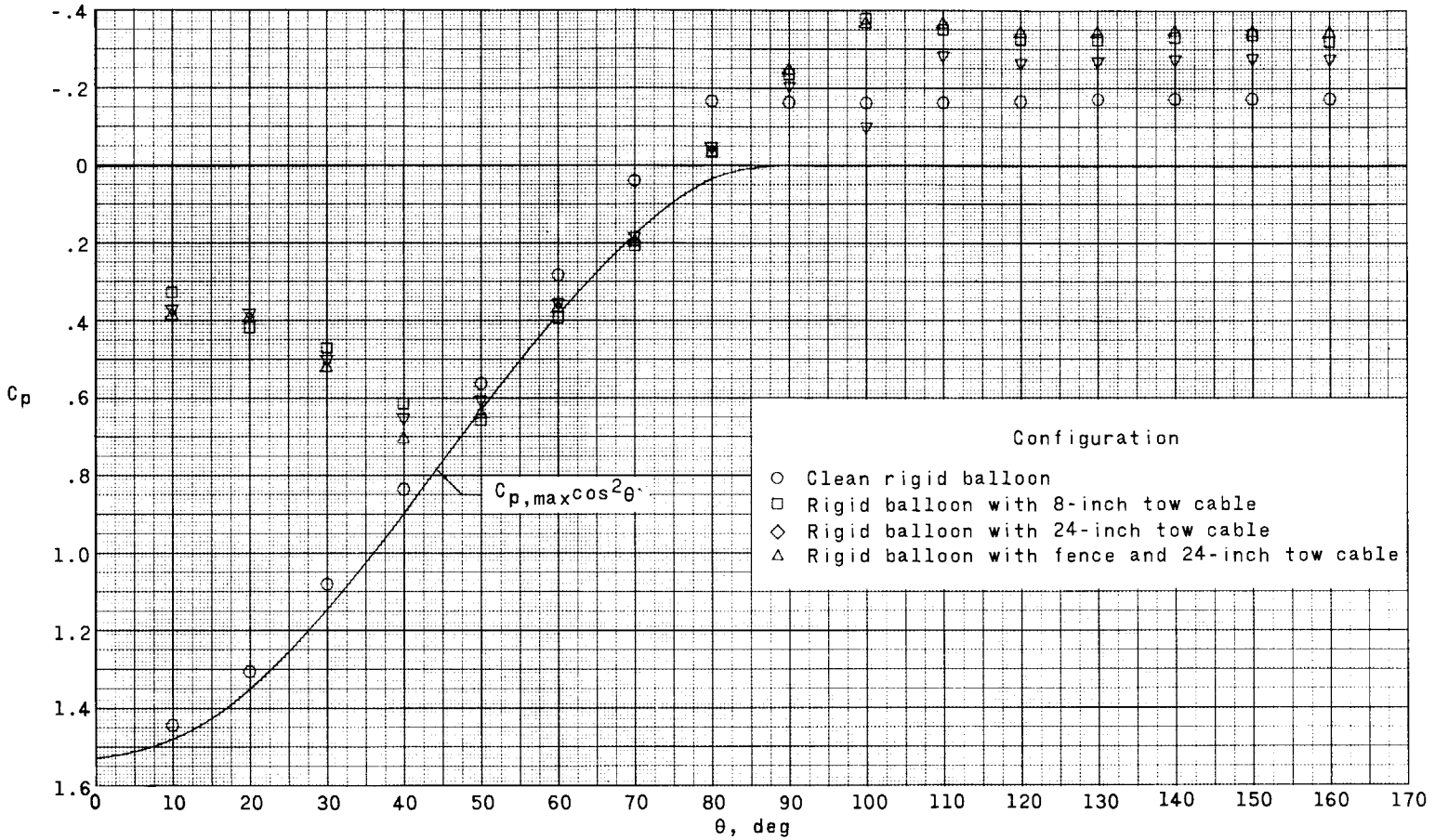

(a) Rigid balloon with and without fence and at various tow-cable lengths. M = 1.50.

Figure 14.- Comparison of experimental pressure coefficients with Newtonian distribution on the rigid balloon. $\alpha_{nom} = 0^o$.

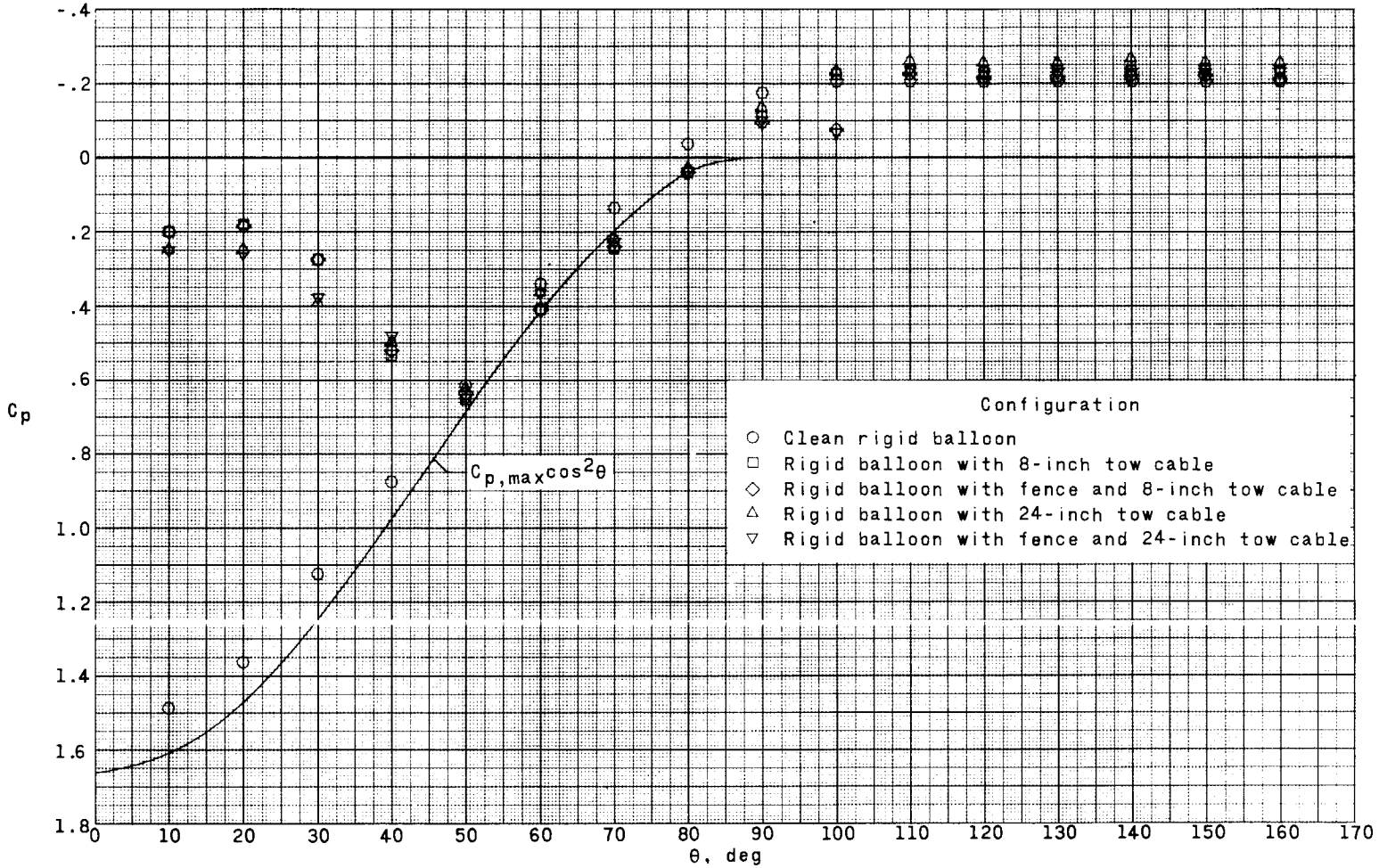

(b) Rigid balloon with and without fence and at various tow-cable lengths. M = 2.00.

Figure 14.- Continued.

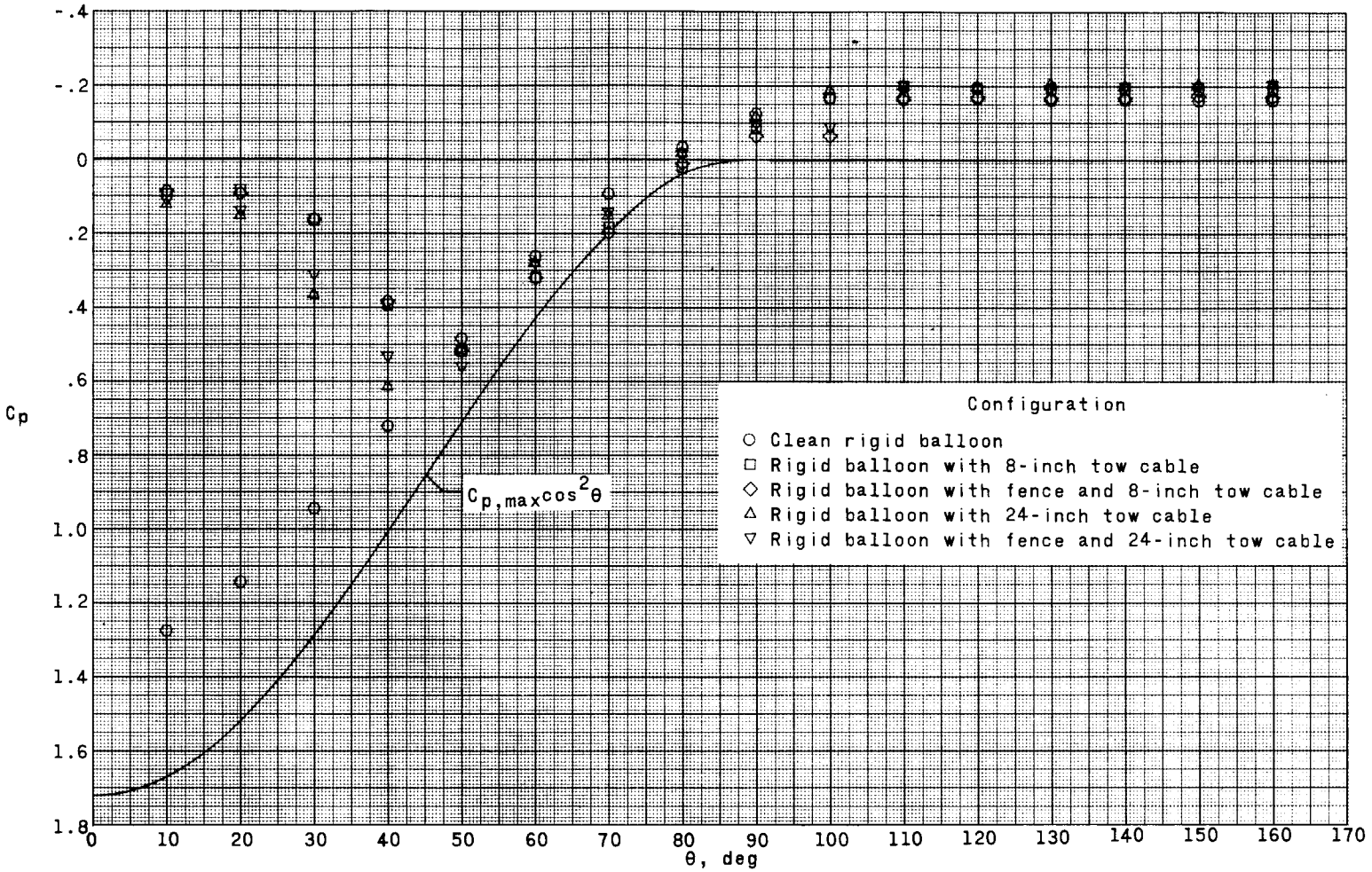

(c) Rigid balloon with and without fence and at various tow-cable lengths. M = 2.50.

Figure 14.- Continued.

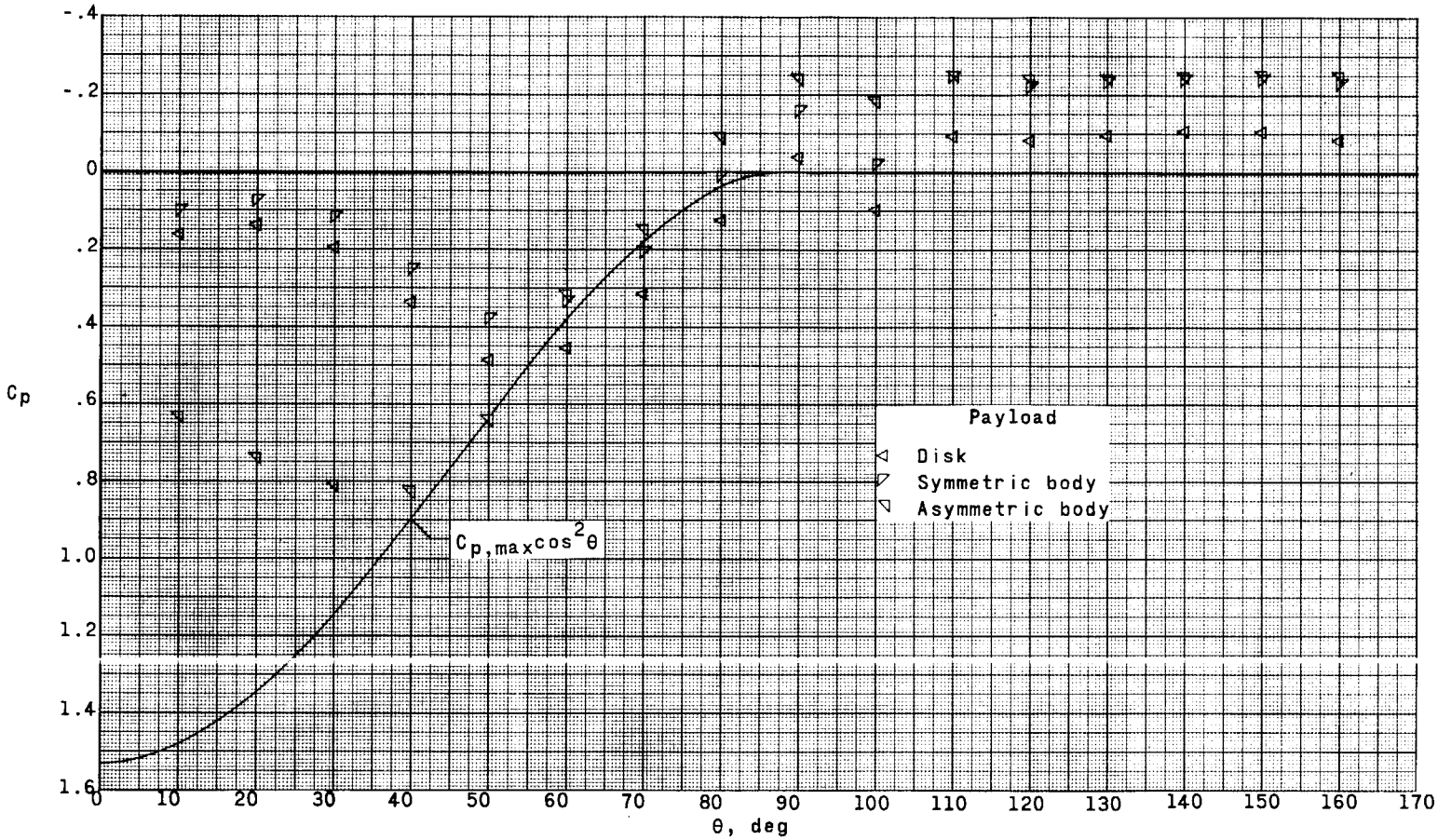

(d) Rigid balloon with fence, 10-inch actuator, and various payloads. M = 1.50.

Figure 14.- Continued.

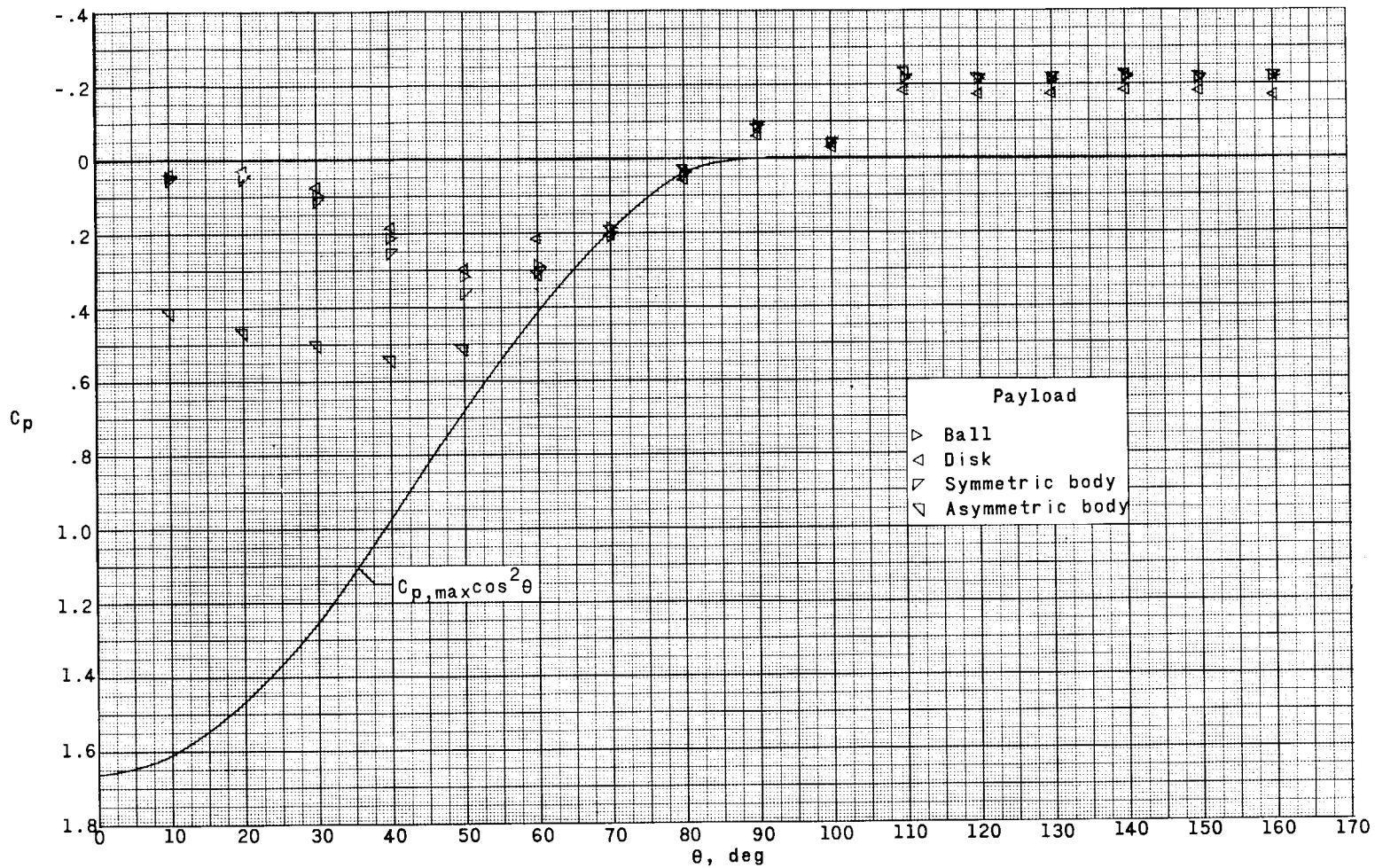

(e) Rigid balloon with fence, 10-inch actuator, and various payloads. M = 2.00.

Figure 14.- Continued.

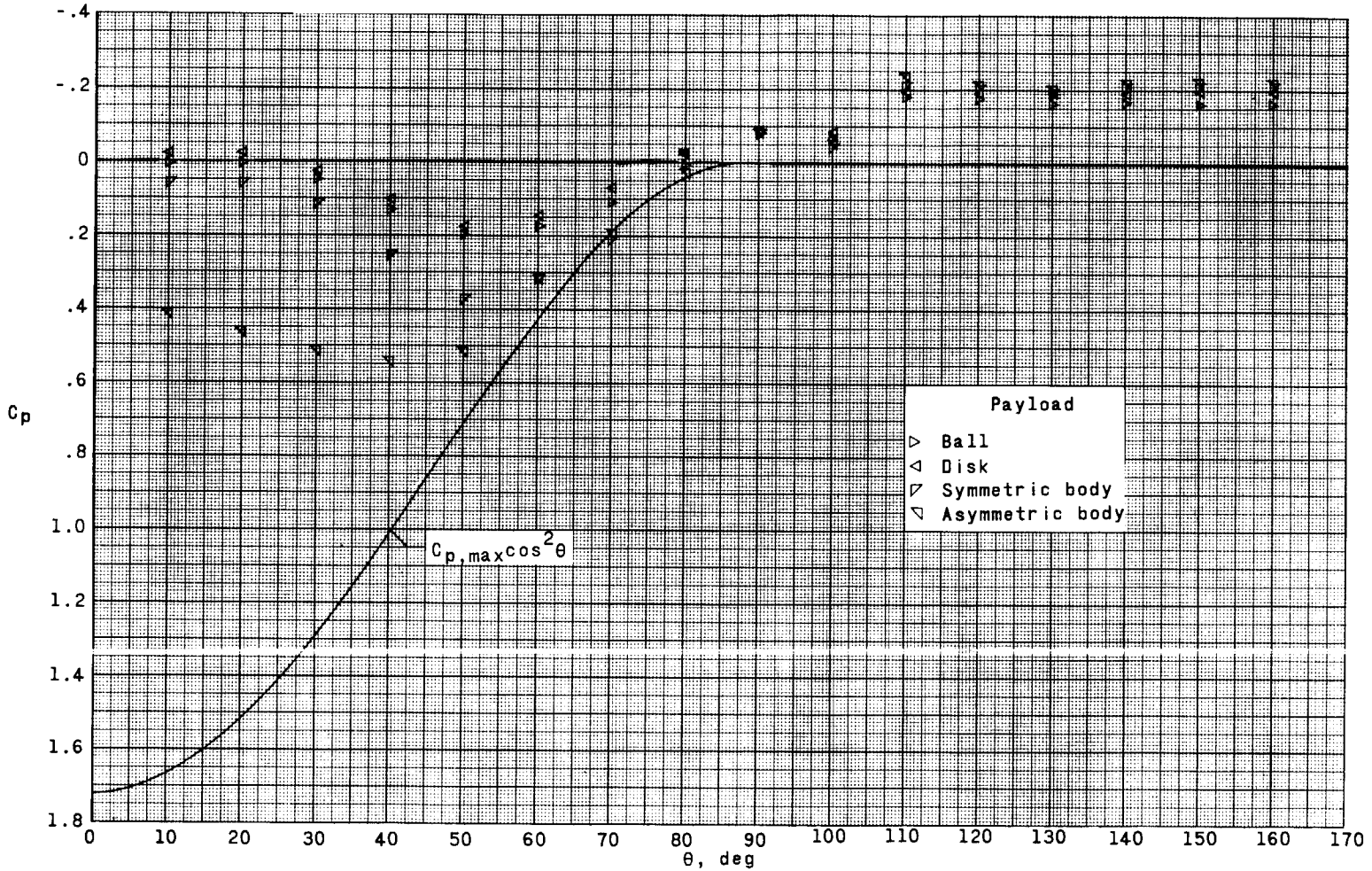

(f) Rigid balloon with fence, 10-inch actuator, and various payloads. M = 2.50.

Figure 14.- Continued.

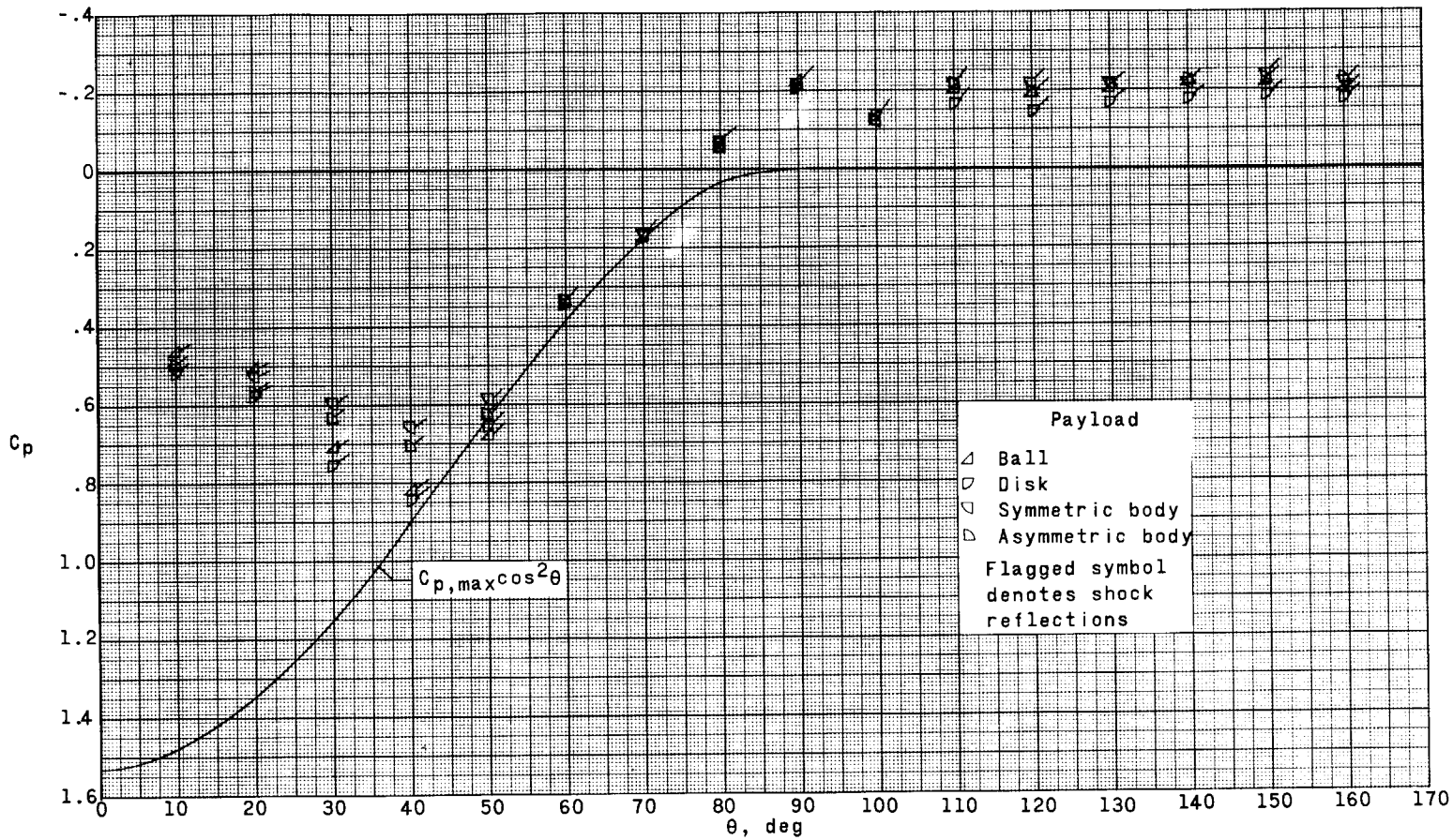

(g) Rigid balloon with fence, 24-inch actuator, and various payloads. M = 1.50.

Figure 14.- Continued.

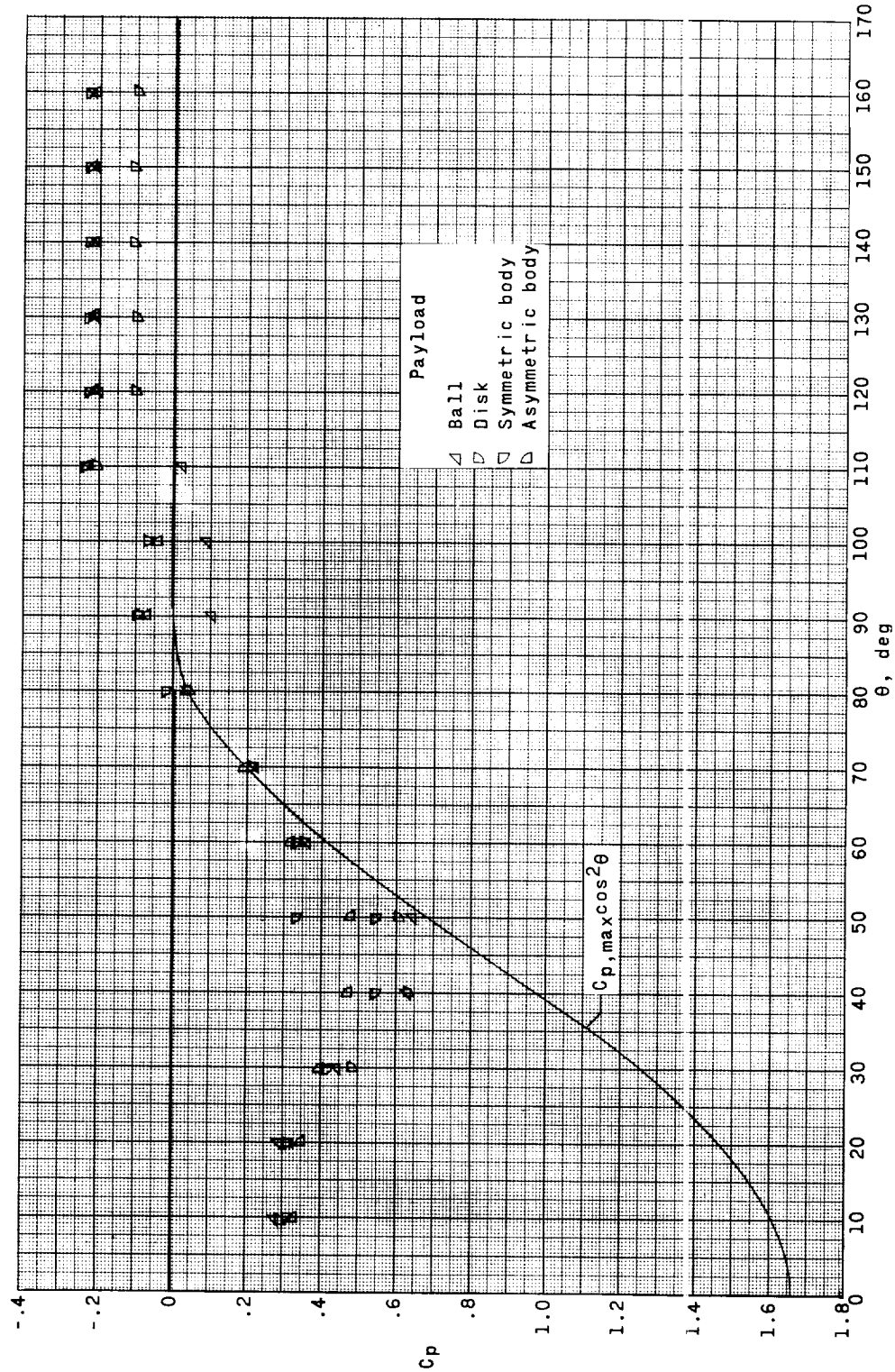

(h) Rigid balloon with fence, 24-inch actuator, and various payloads. M = 2.00.

Figure 14.- Continued.

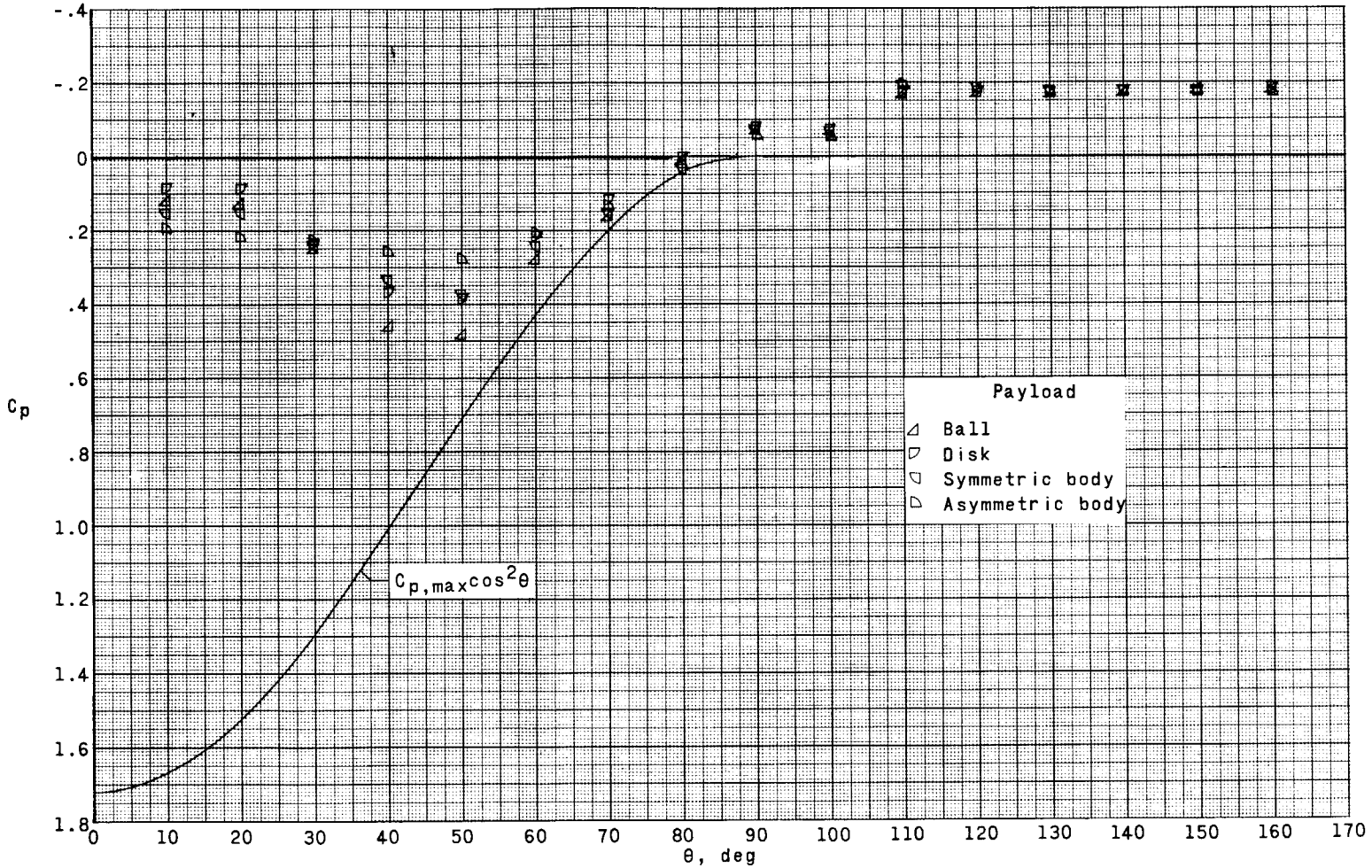

(i) Rigid balloon with fence, 24-inch actuator, and various payloads. M = 2.50.

Figure 14.- Continued.

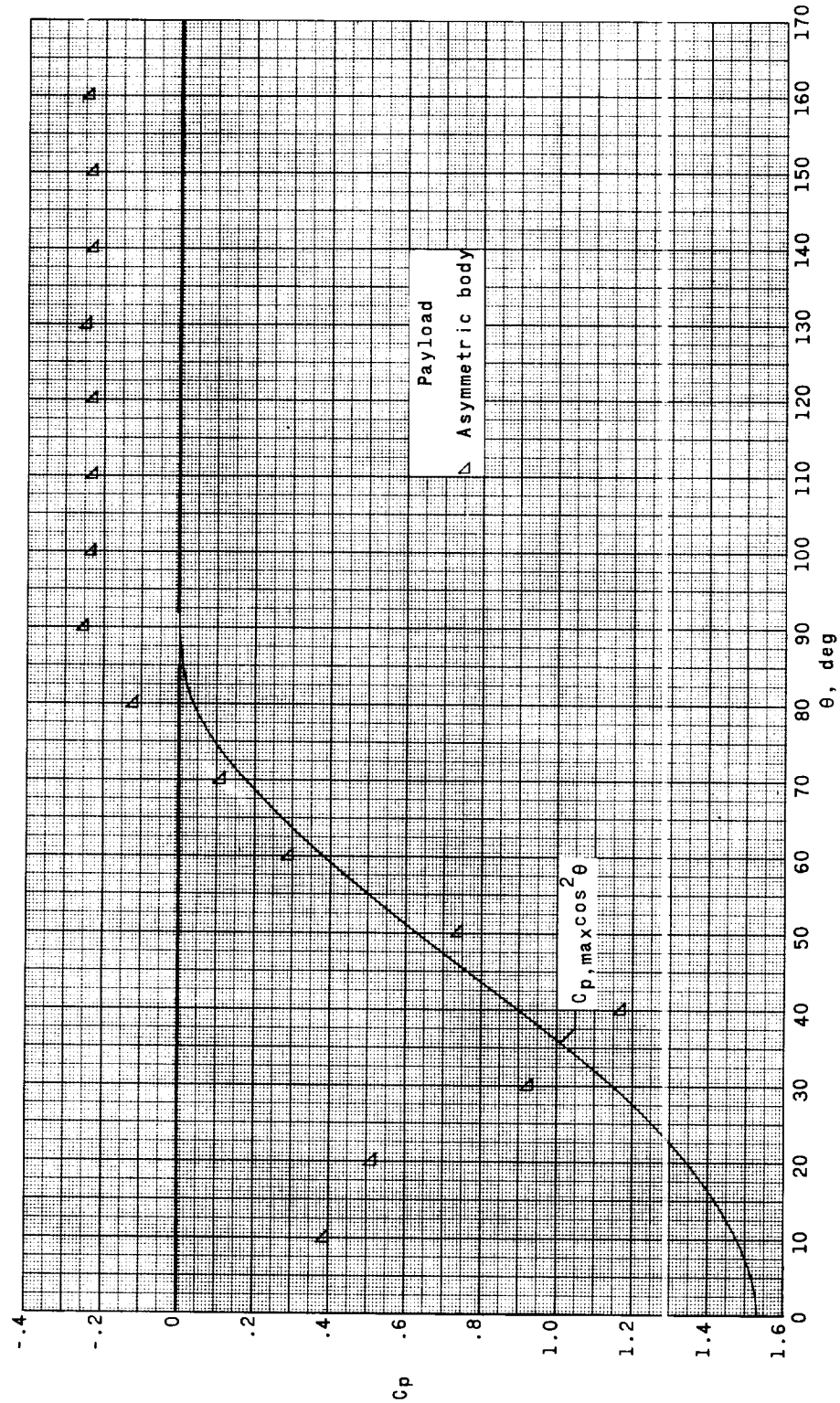

(j) Rigid balloon with fence and asymmetric body. M = 1.50.

Figure 14.- Continued.

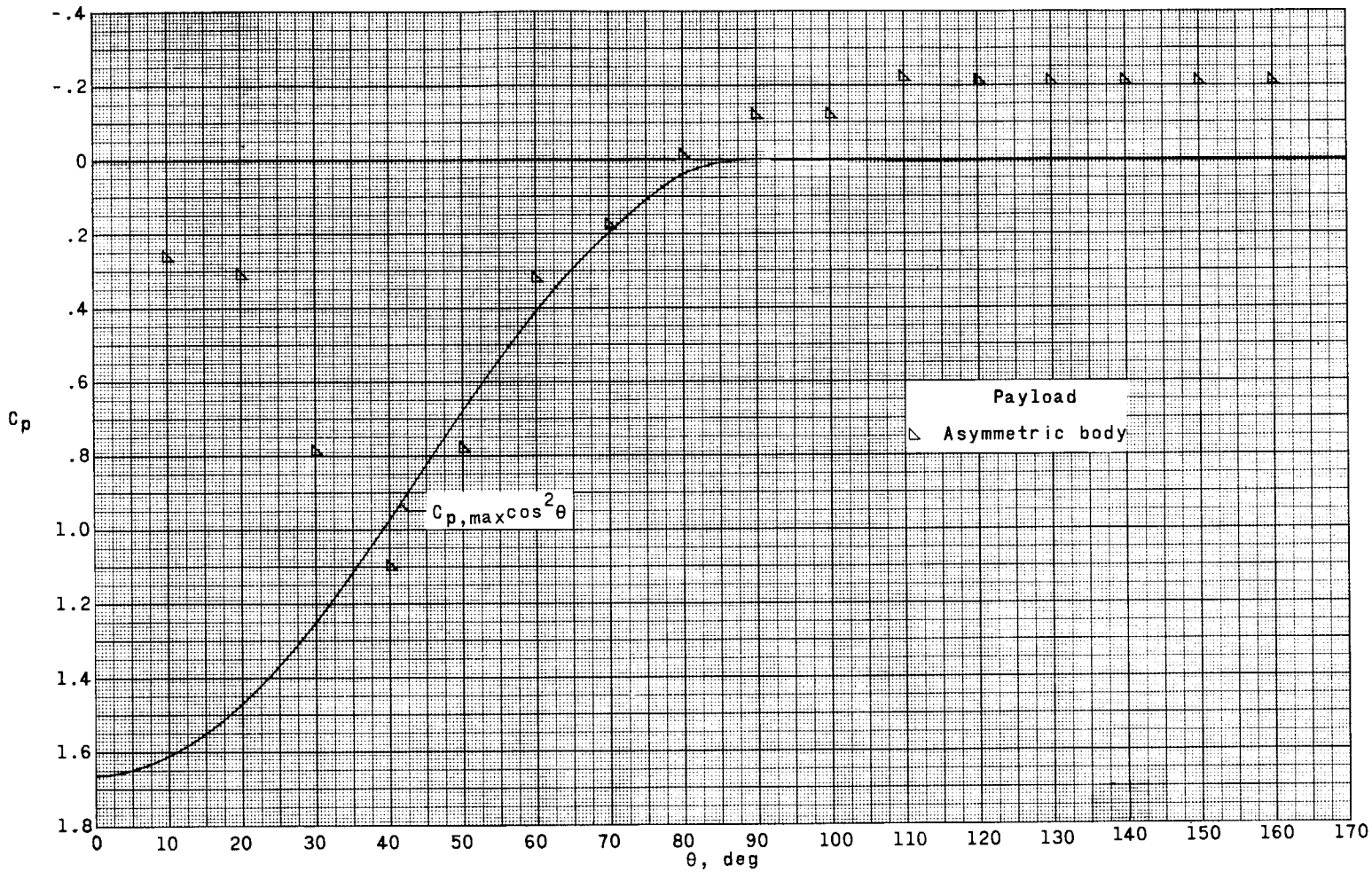

(k) Rigid balloon with fence and asymmetric body. M = 2.00.

Figure 14.- Continued.

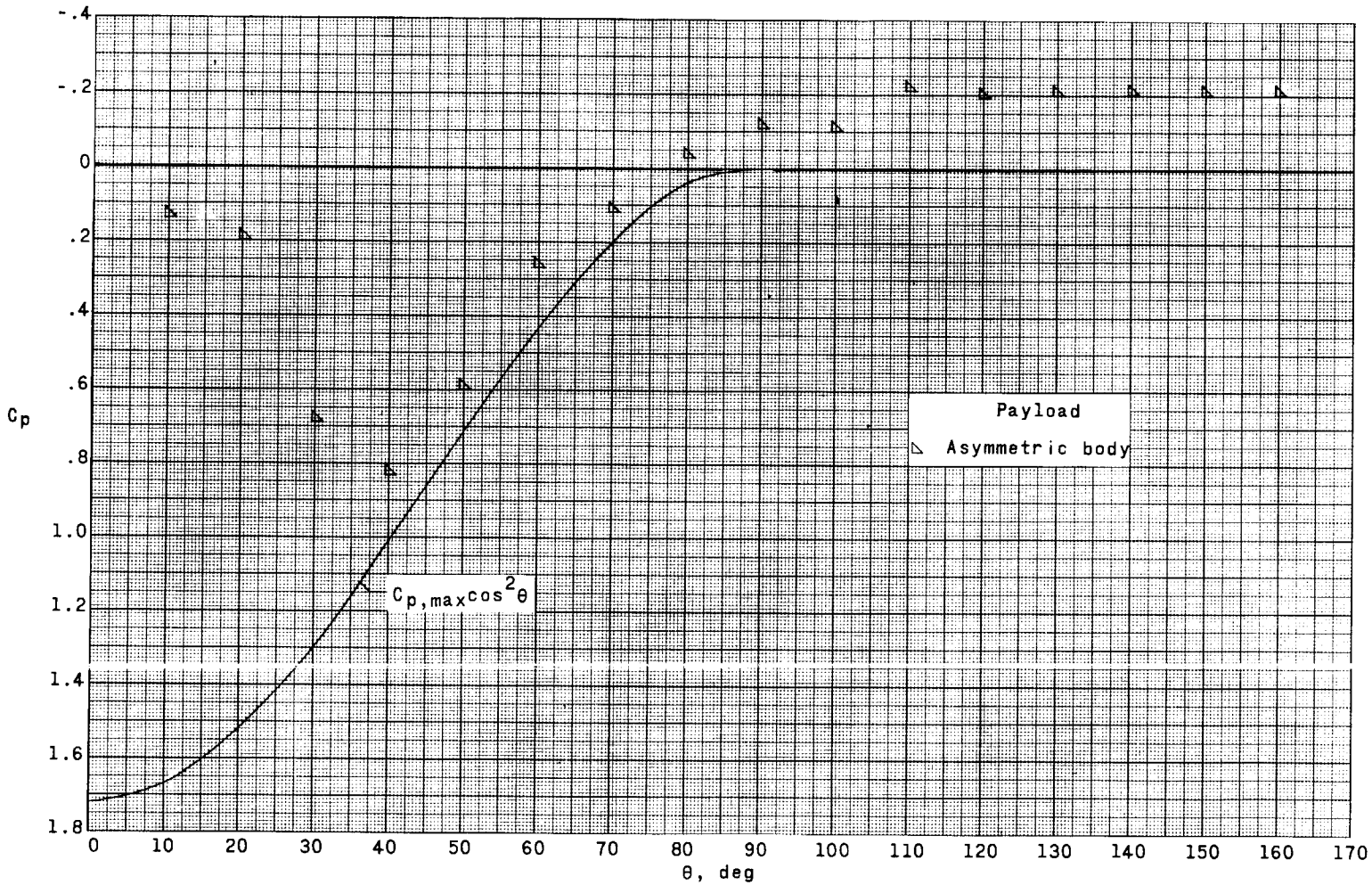

(l) Rigid balloon with fence and asymmetric body. M = 2.50.

Figure 14.- Concluded.

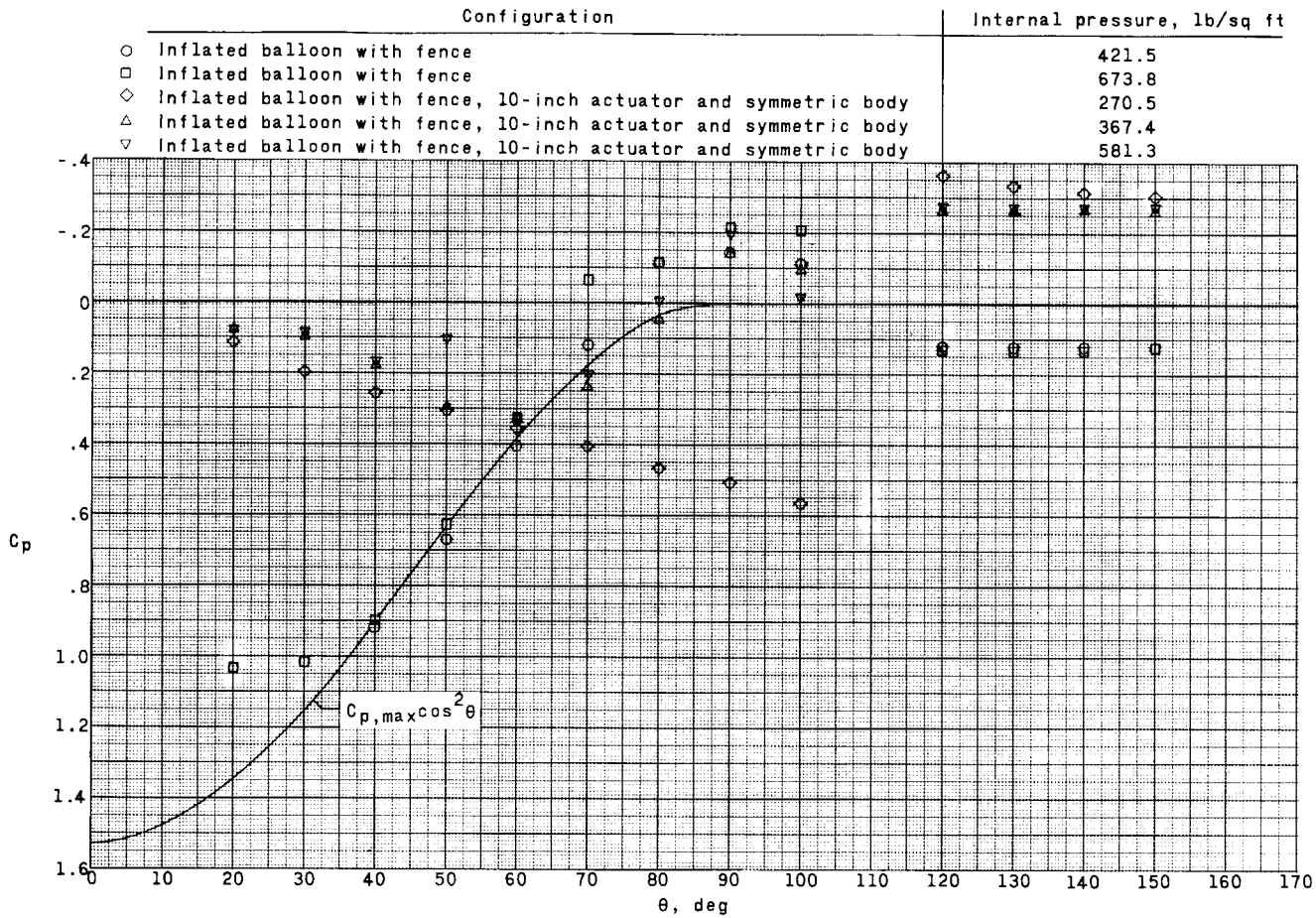

(a) M = 1.50.

Figure 15.- Comparison of experimental pressure coefficients with Newtonian distribution on the inflated balloon with fence, with and without actuator and payload, at different internal pressures. $\alpha_{nom} = 0^{\circ}$.

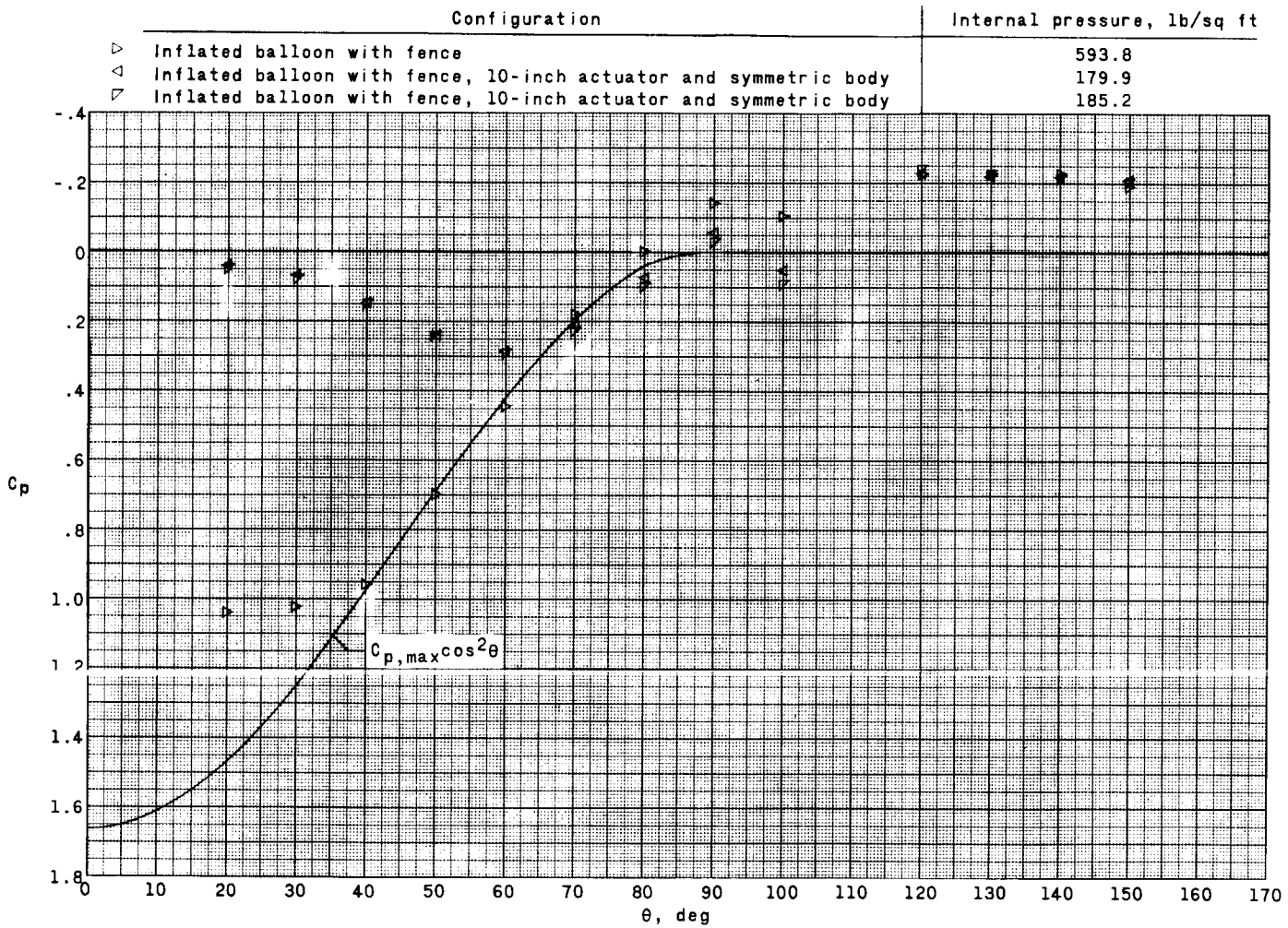

(b) M = 2.00.

Figure 15.- Continued.

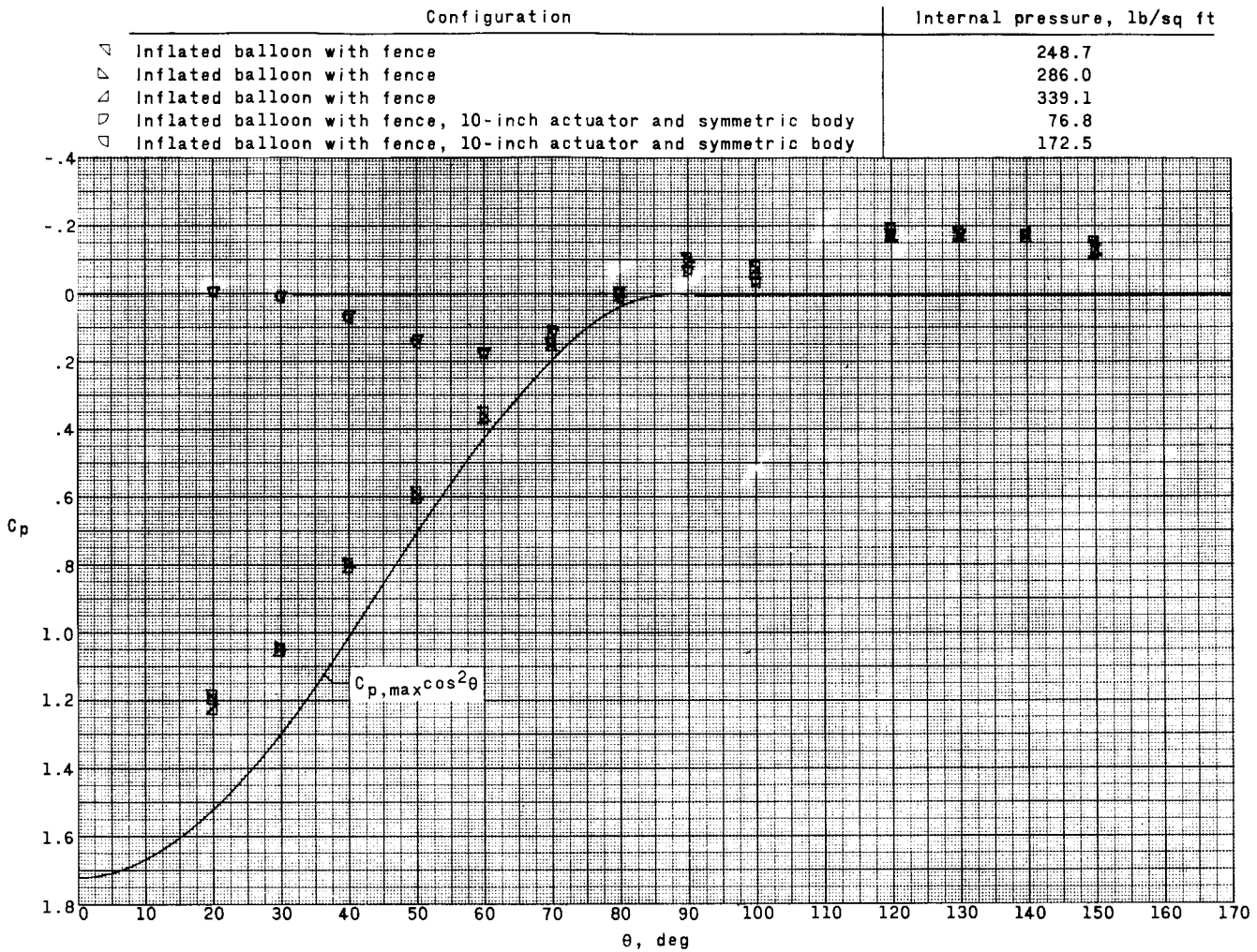

(c) M = 2.50.

Figure 15.- Concluded.

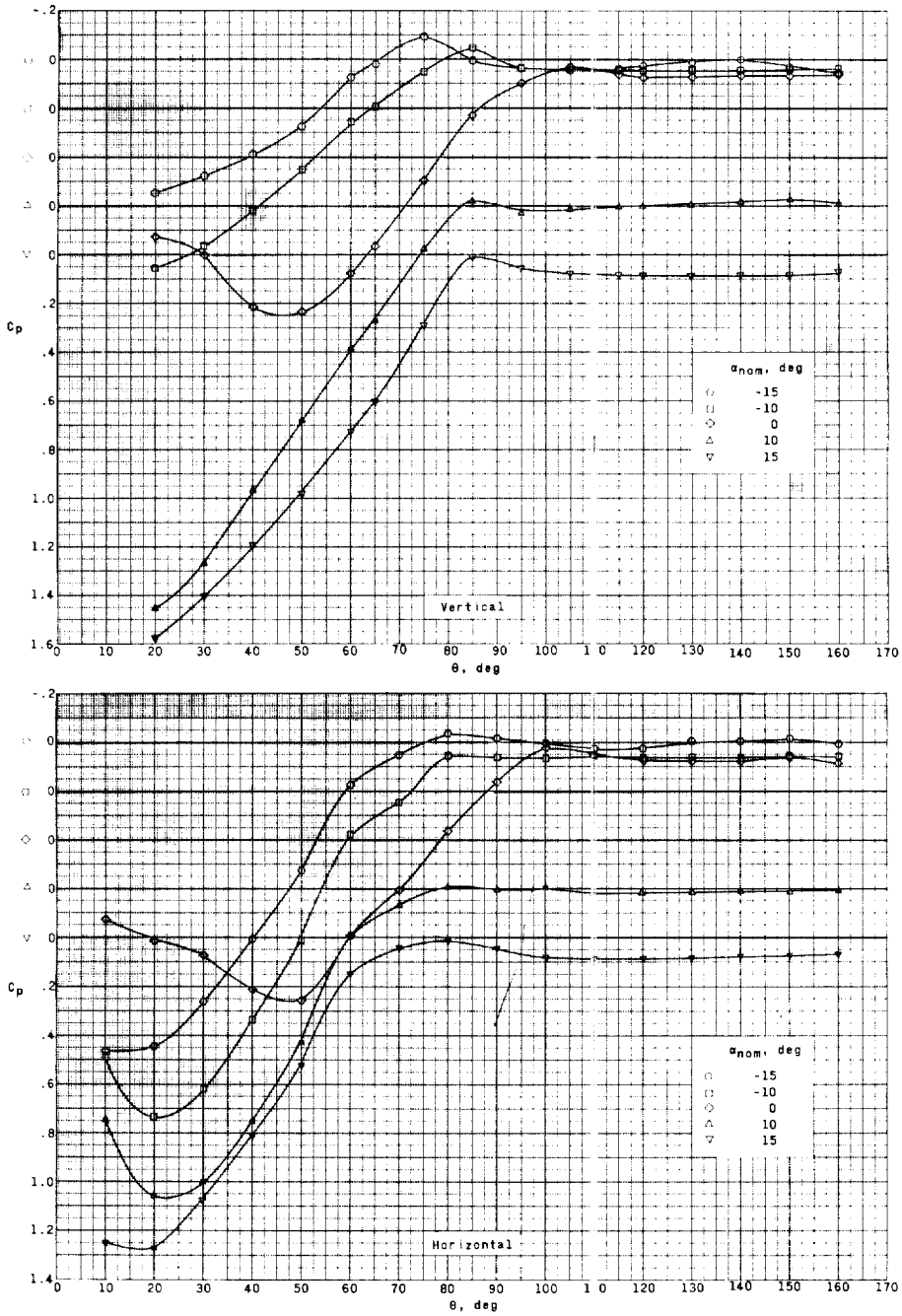

(a) Rigid balloon without fence and with 8-inch tow cable. M = 1.50.

Figure 16.- Results of pressure measurements around the rigid balloon at various angles of attack.

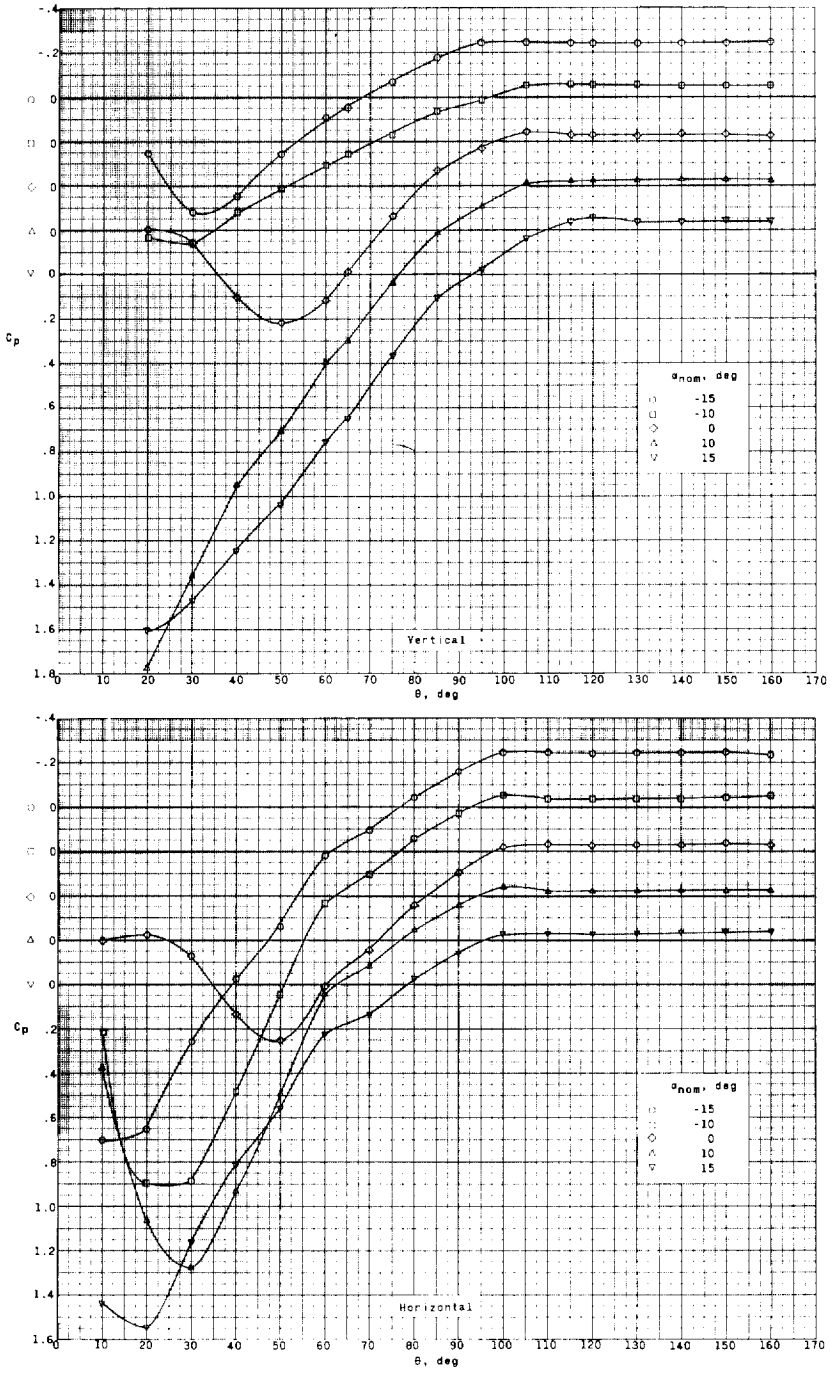

(b) Rigid balloon without fence and with 8-inch tow cable. M = 2.00.

Figure 16.- Continued.

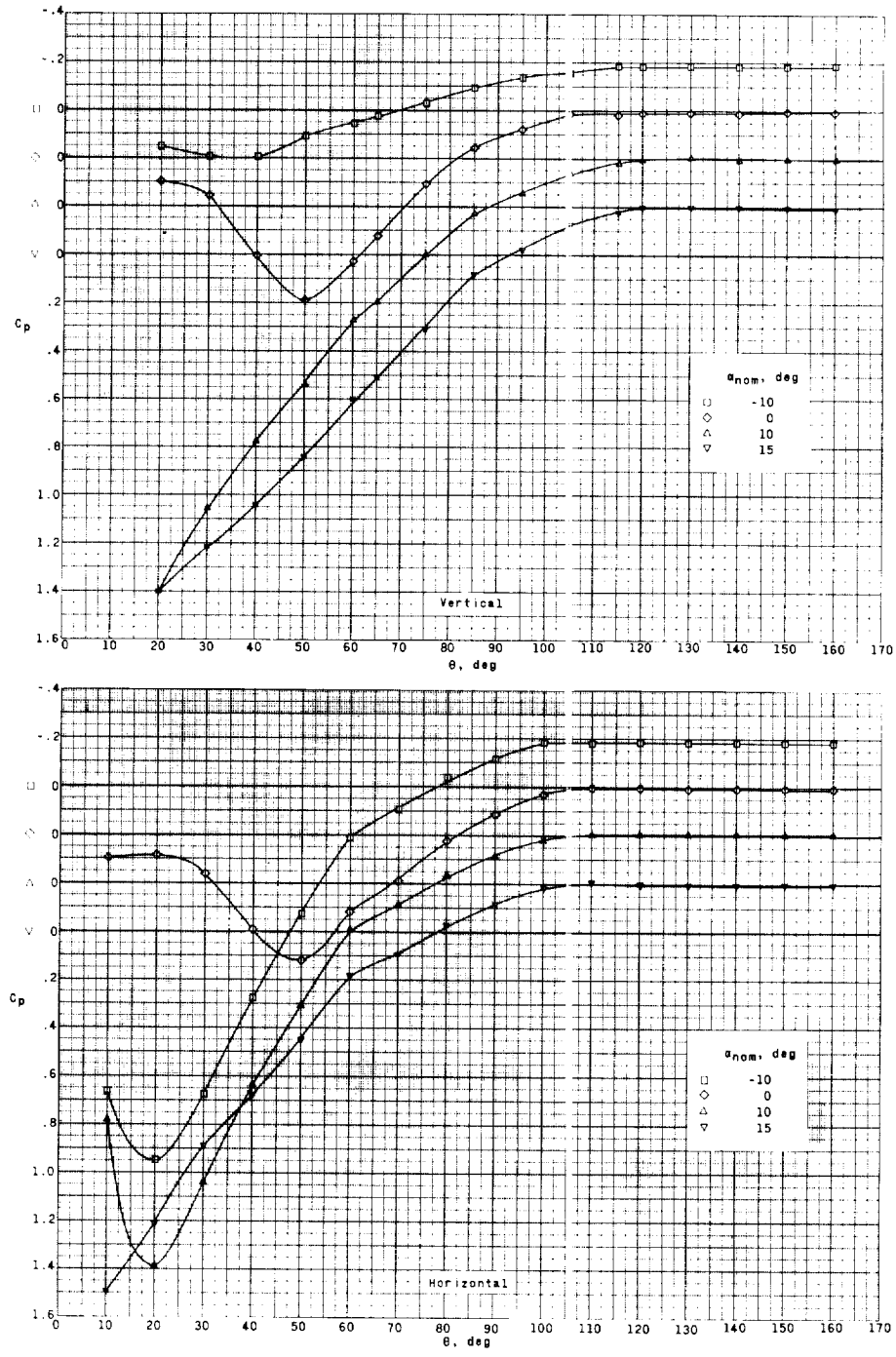

(c) Rigid balloon without fence and with 8-inch tow cable. M = 2.50.

Figure 16.- Continued.

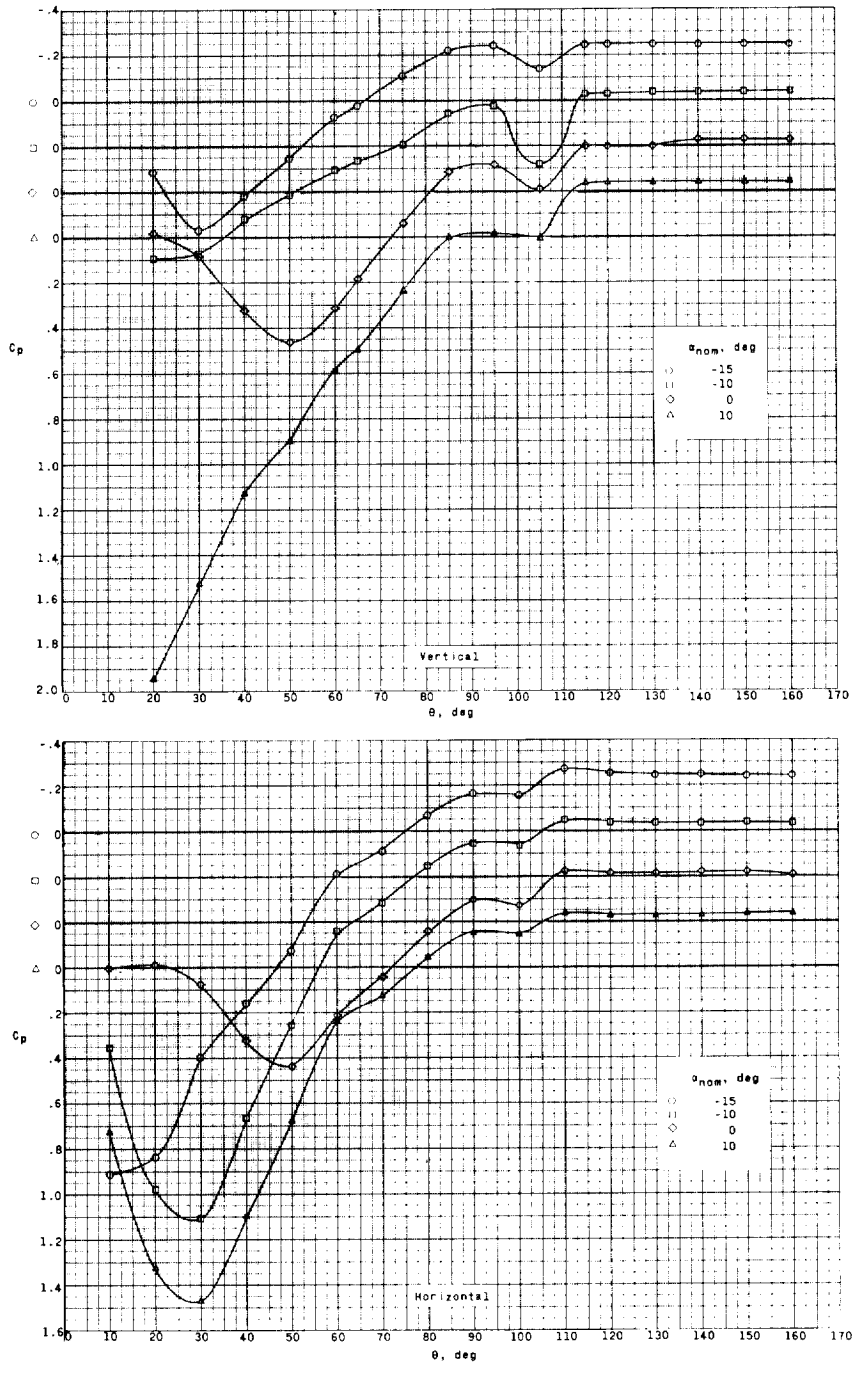

(d) Rigid balloon with fence and with 8-inch tow cable. M = 2.00.

Figure 16.- Continued.

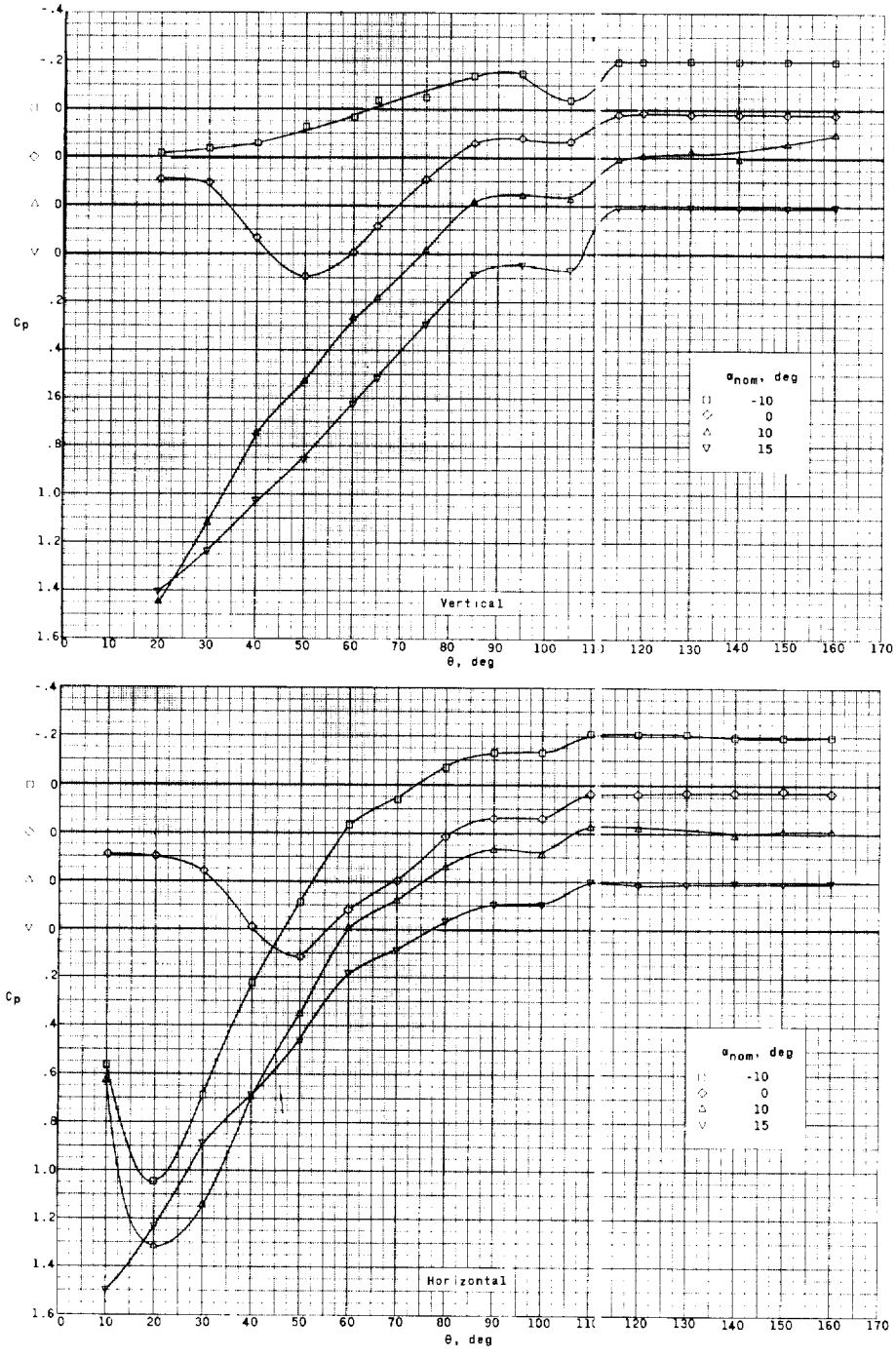

(e) Rigid balloon with fence and with 8-inch tow cable. M = 2.50.

Figure 16.- Continued.

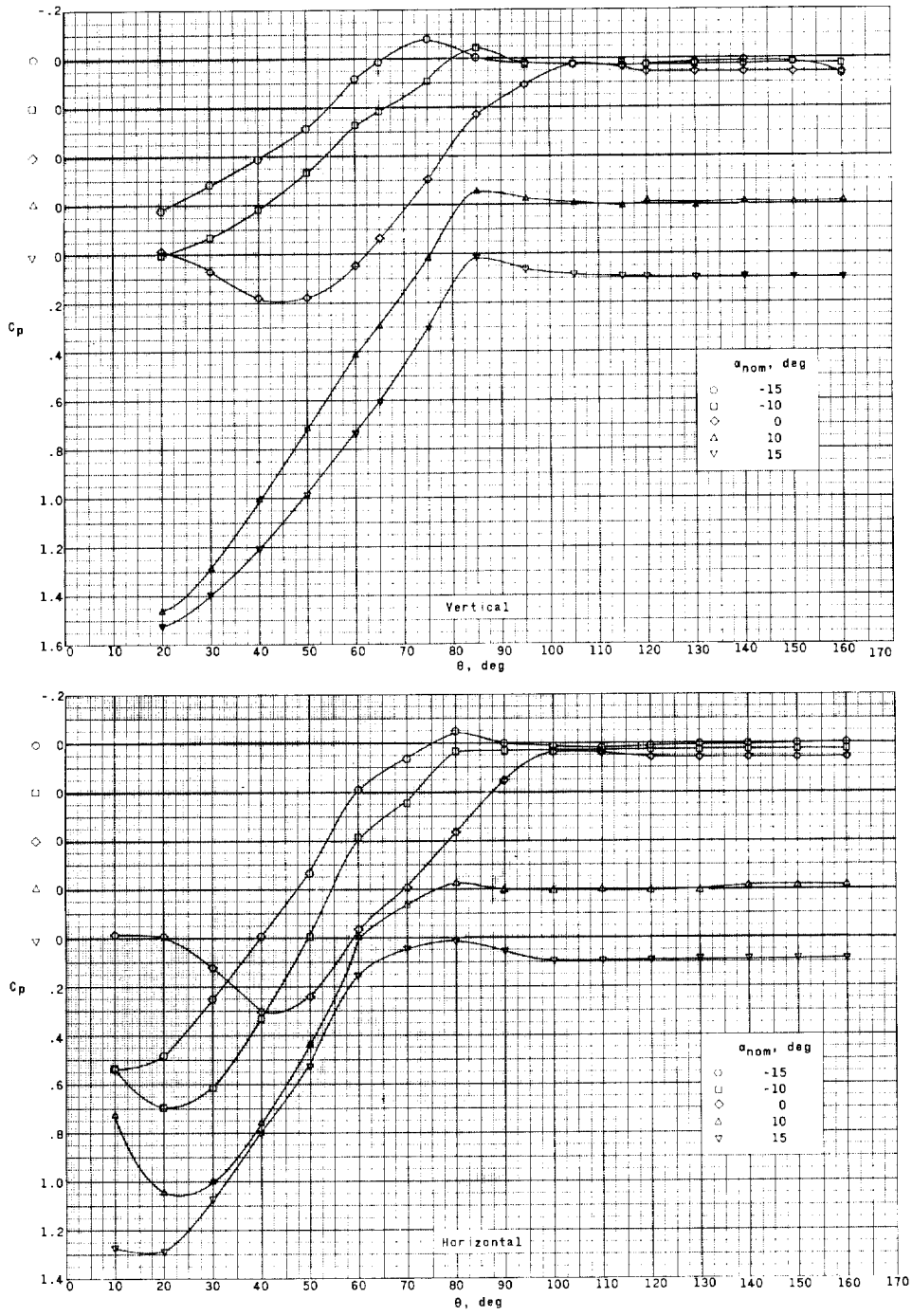

(f) Rigid balloon without fence and with 24-inch tow cable. M = 1.50.

Figure 16.- Continued.

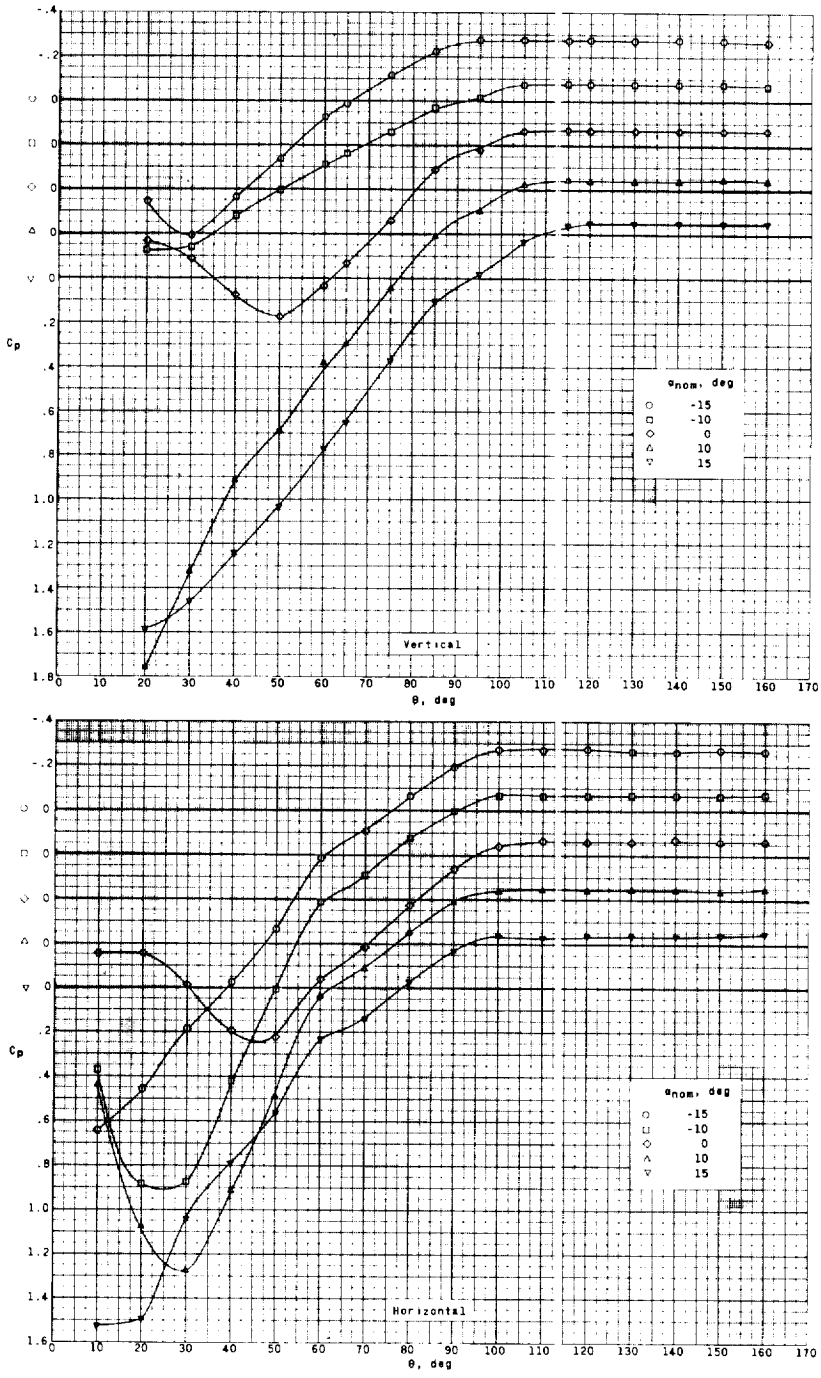

(g) Rigid balloon without fence and with 24-inch tow cable. M = 2.00.

Figure 16.- Continued.

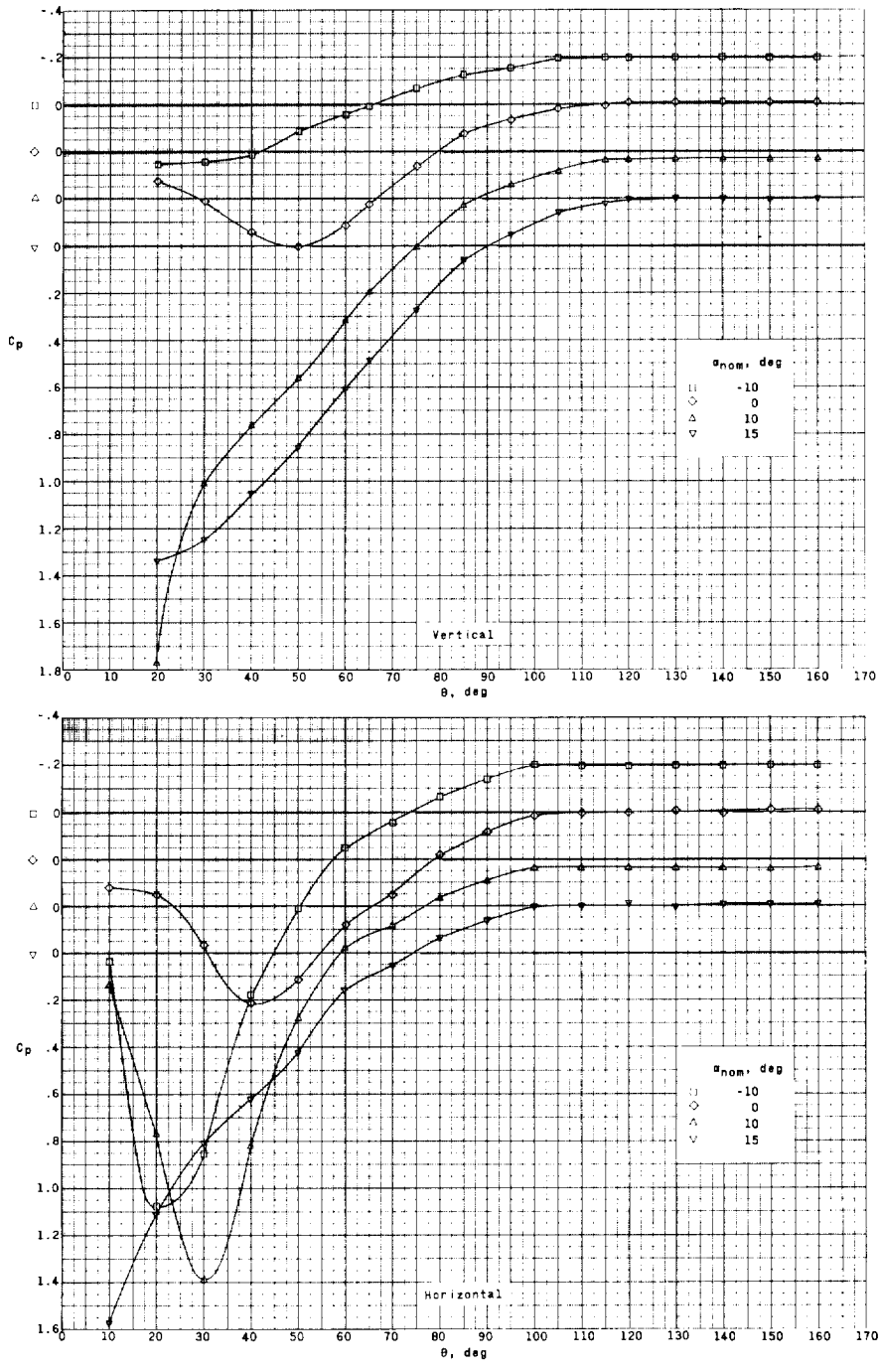

(h) Rigid balloon without fence and with 24-inch tow cable. M = 2.50.

Figure 16.- Continued.

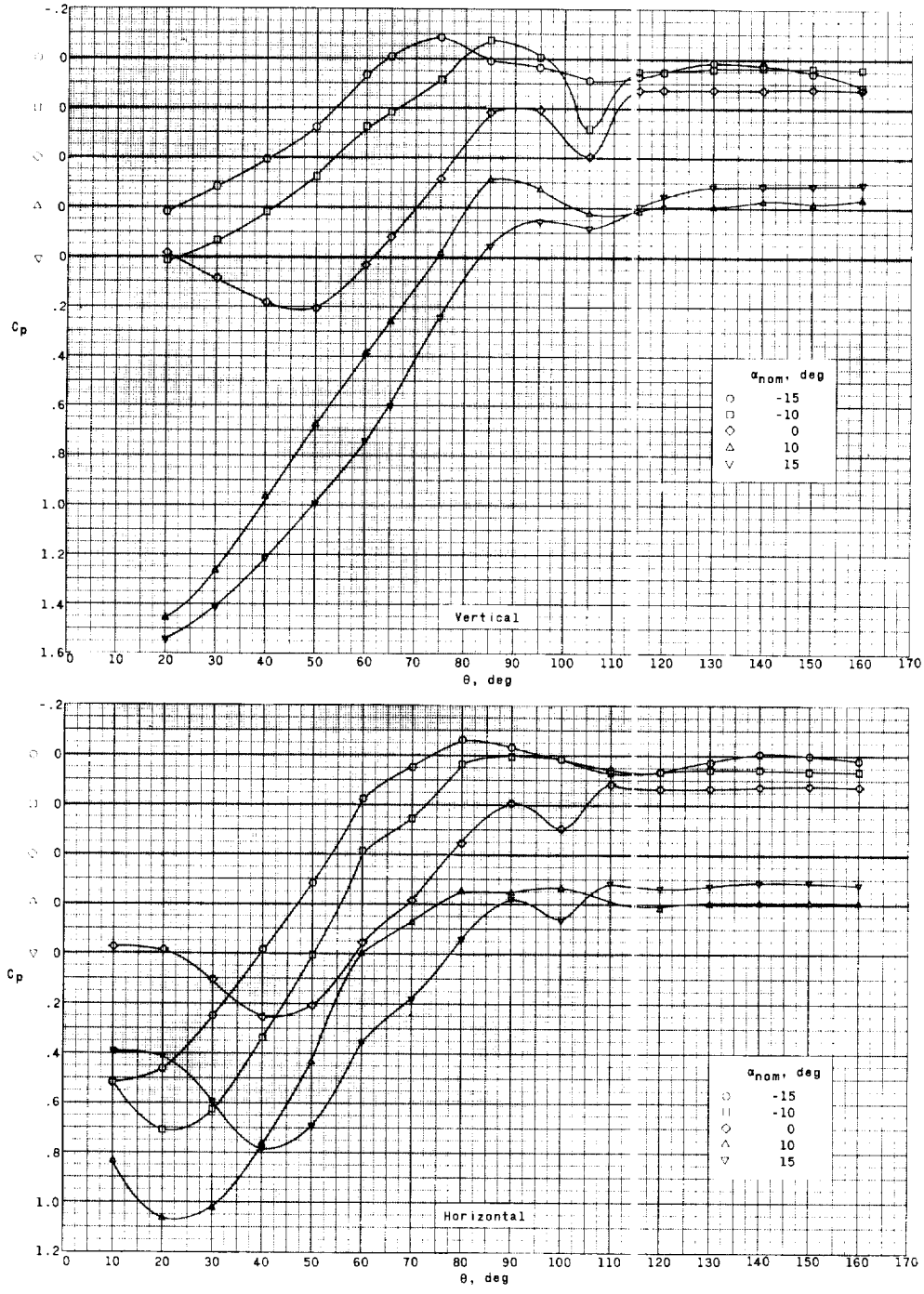

(i) Rigid balloon with fence and with 24-inch tow cable. M = 1.50.

Figure 16.- Continued.

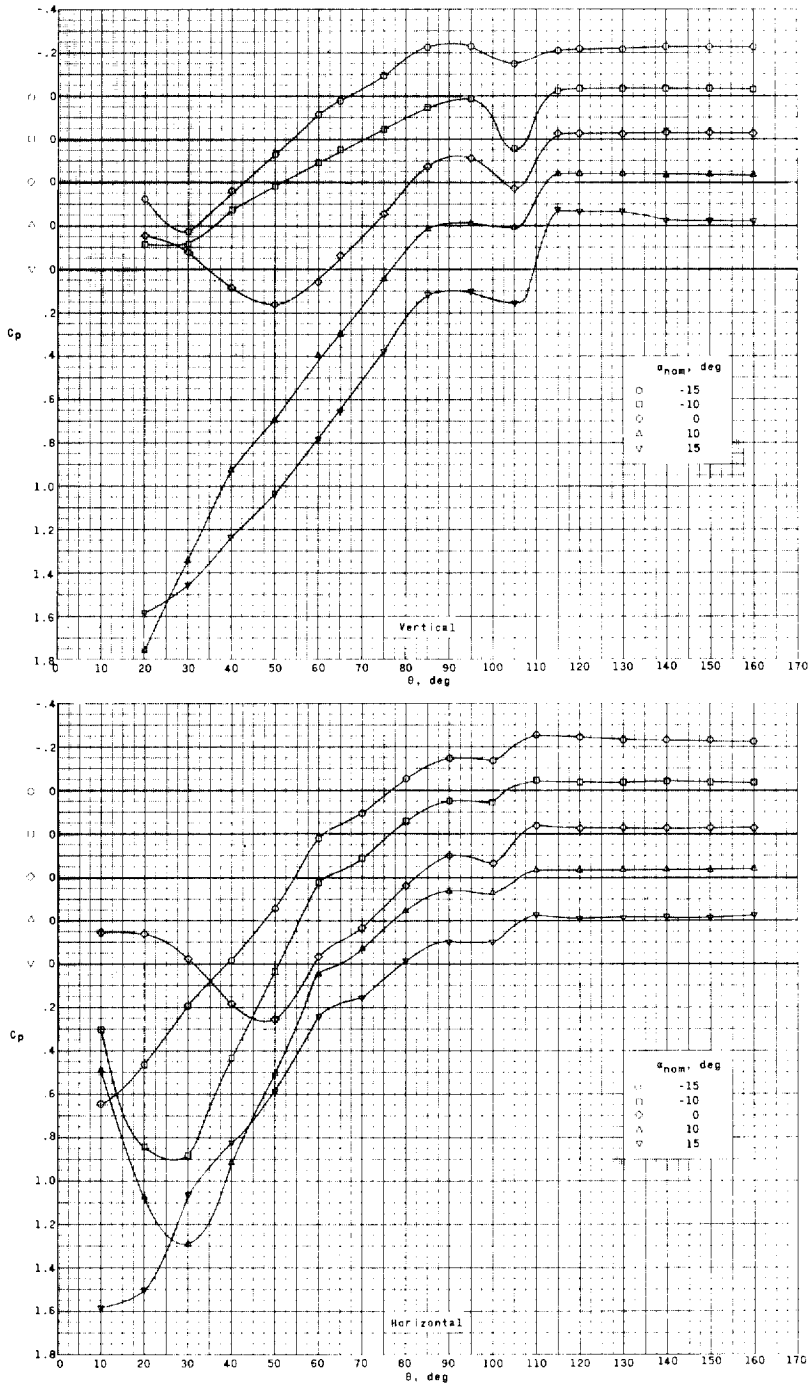

(j) Rigid balloon with fence and with 24-inch tow cable. M = 2.00.

Figure 16.- Continued.

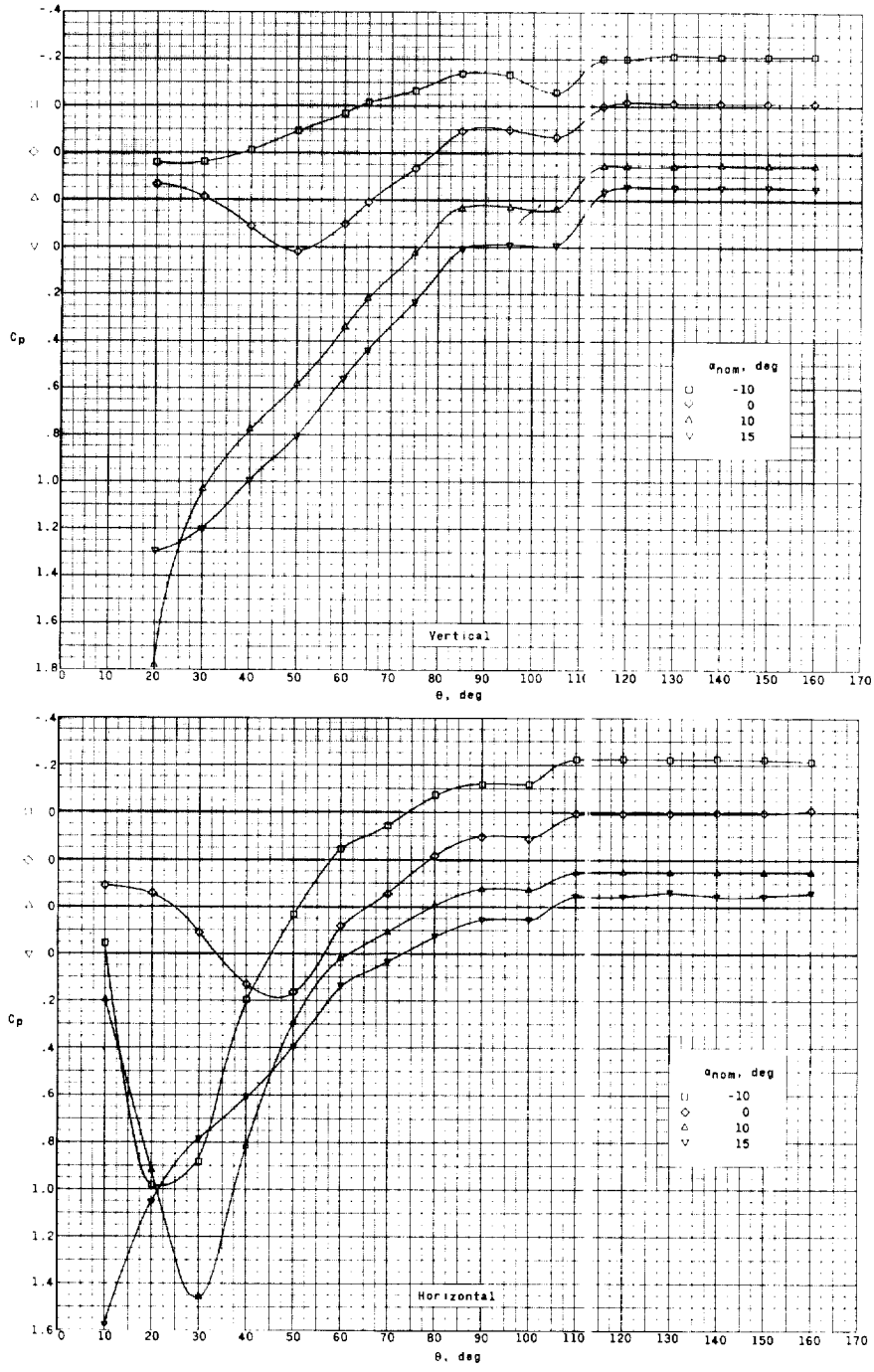

(k) Rigid balloon with fence and with 24-inch tow cable. M = 2.50.

Figure 16.- Continued.

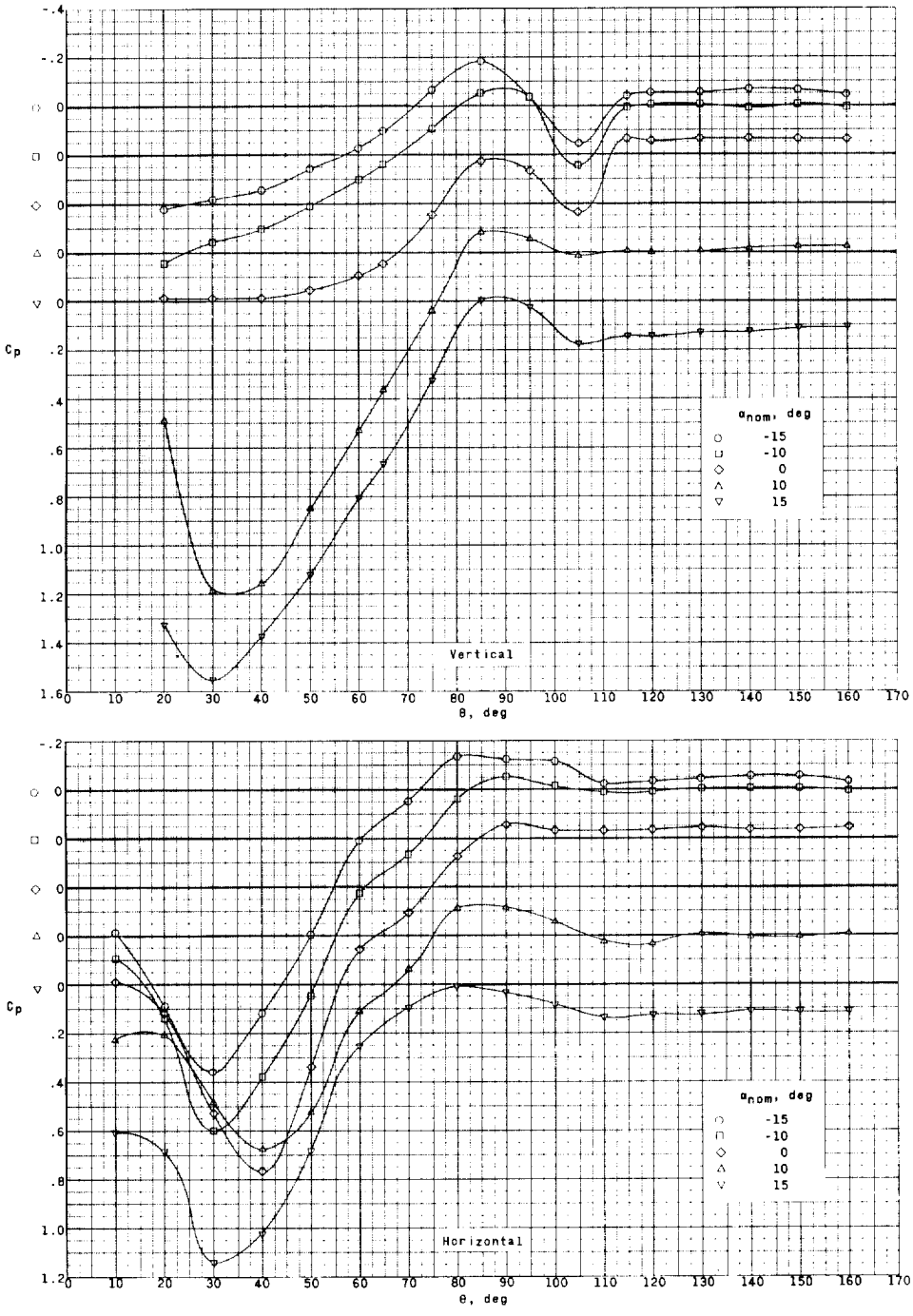

(l) Rigid balloon with fence and asymmetric body. M = 1.50.

Figure 16.- Continued.

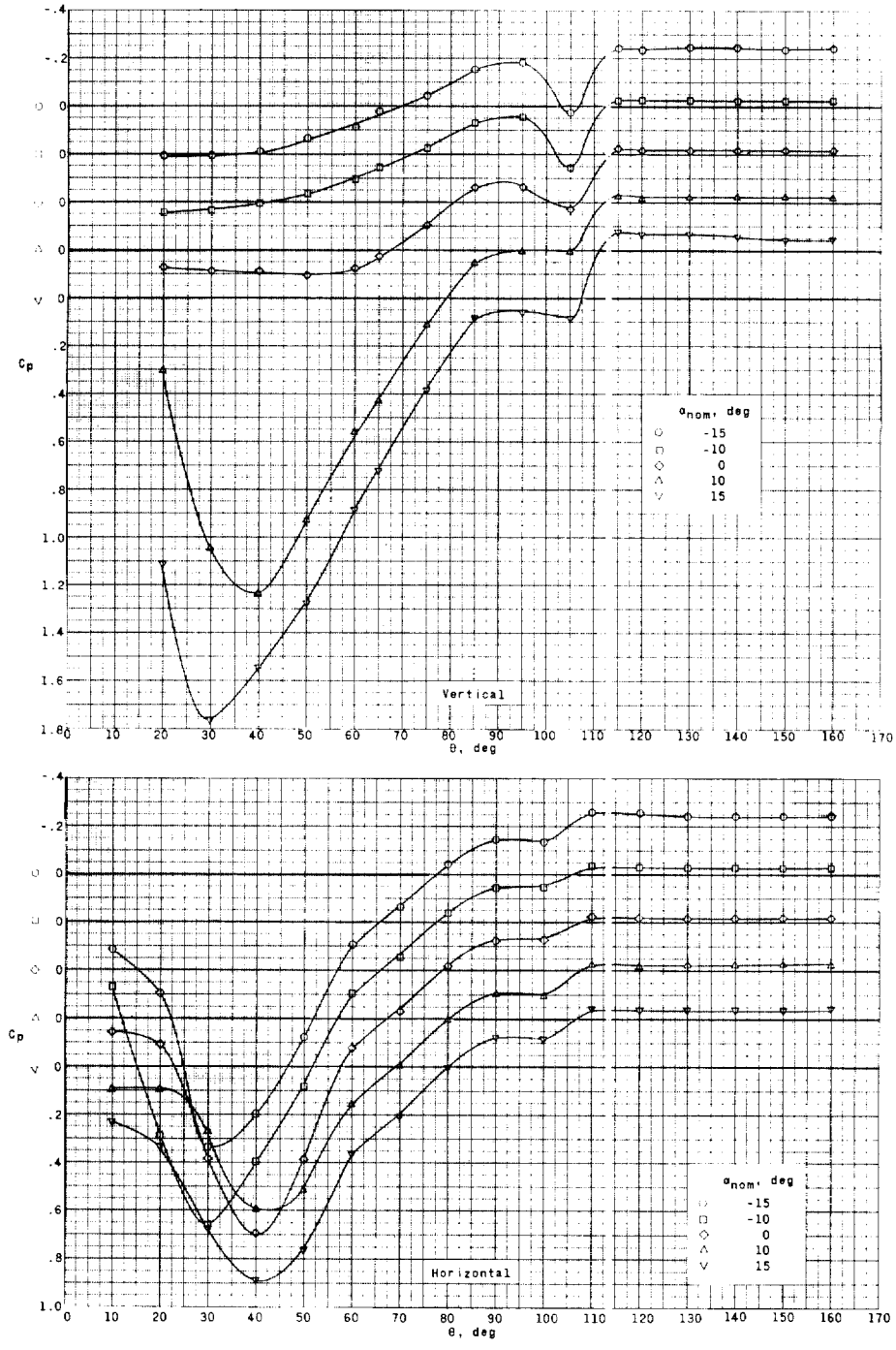

(m) Rigid balloon with fence and asymmetric body. M = 2.00.

Figure 16.- Continued.

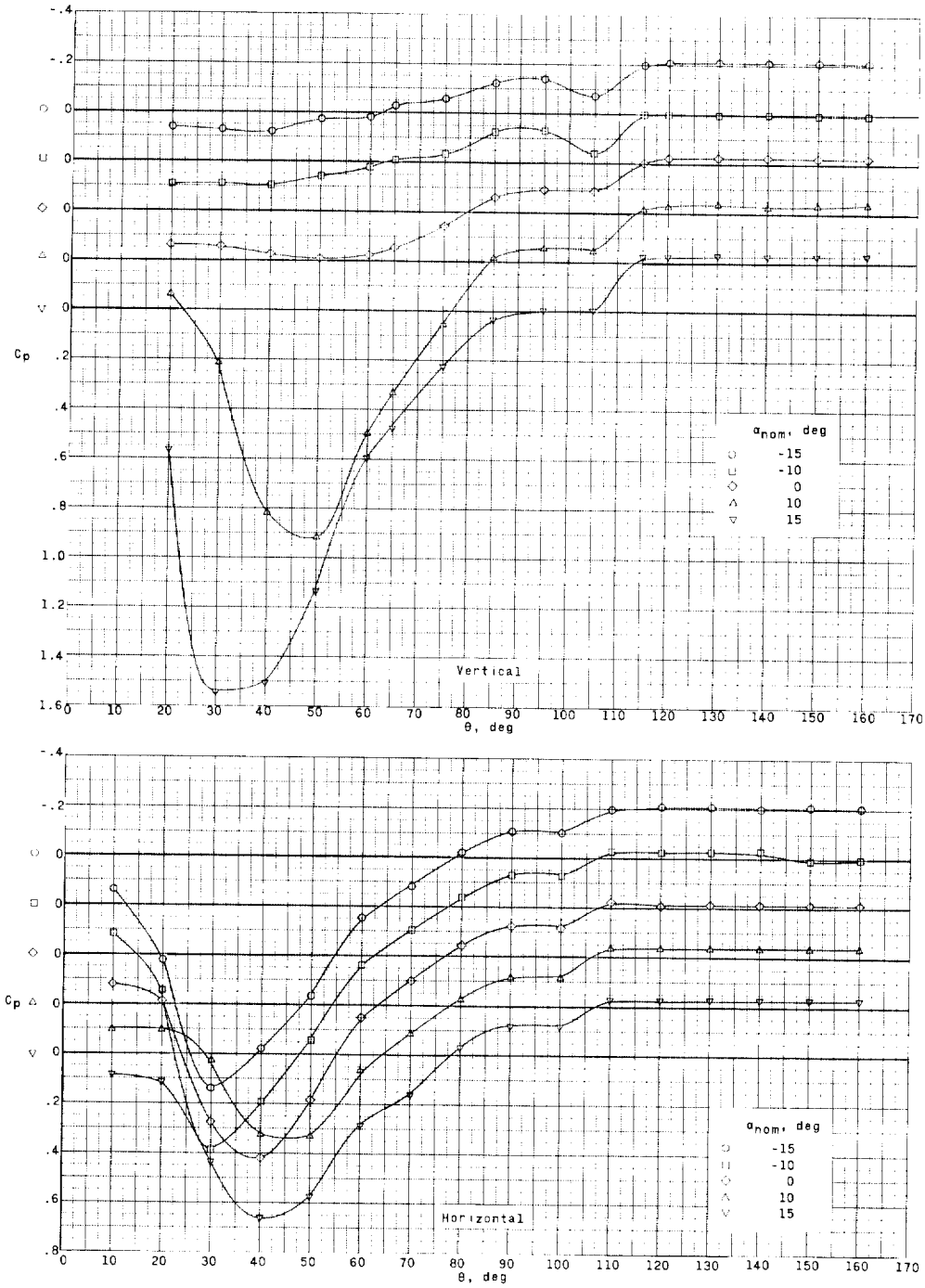

(n) Rigid balloon with fence and asymmetric body. M = 2.50.

Figure 16.- Concluded.

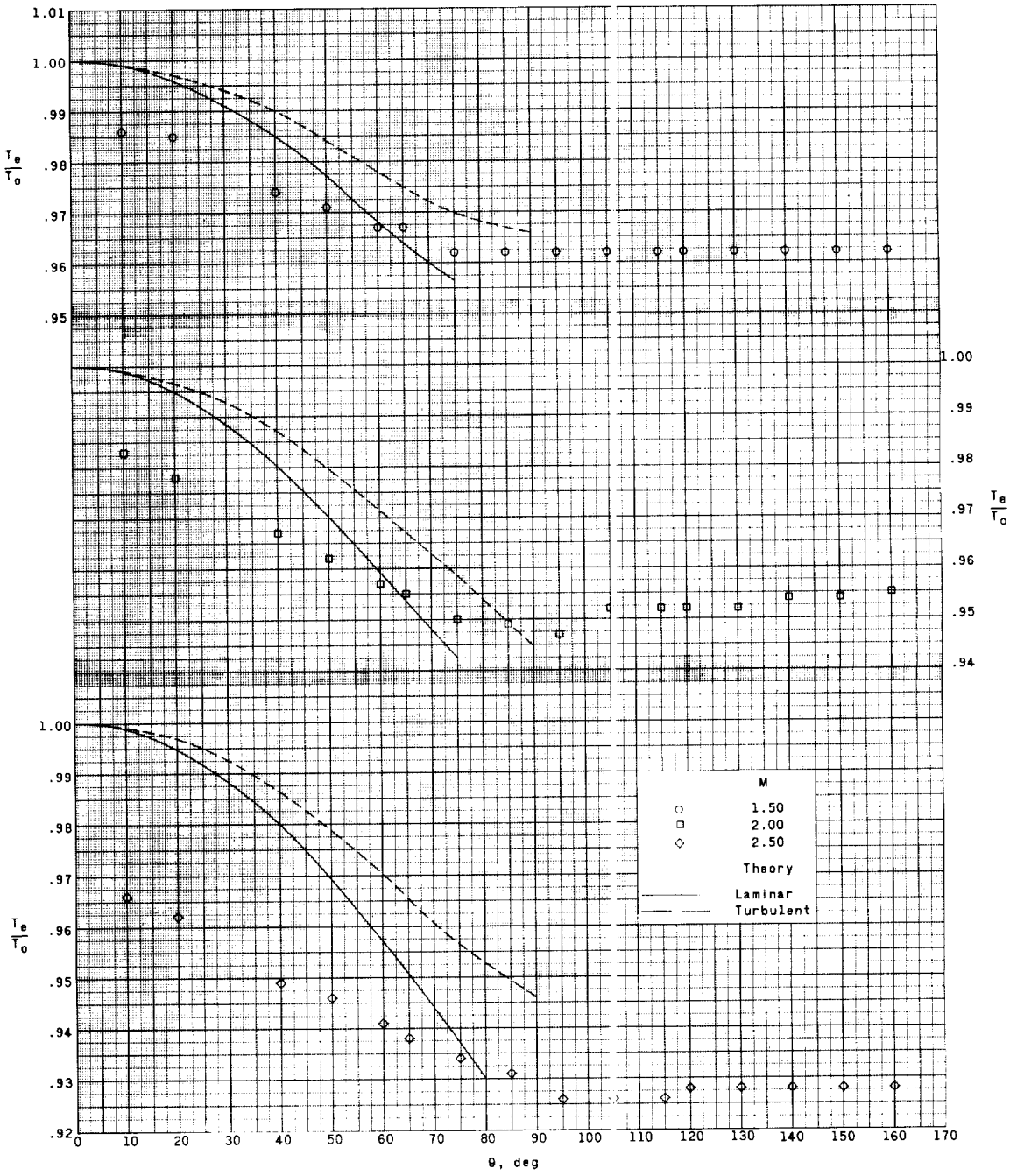

Figure 17.- Comparison of ratios of equilibrium temperature to stagnation temperature with laminar and turbulent flow theory around the clean rigid balloon. $\alpha_{nom} = 0^{o}$.

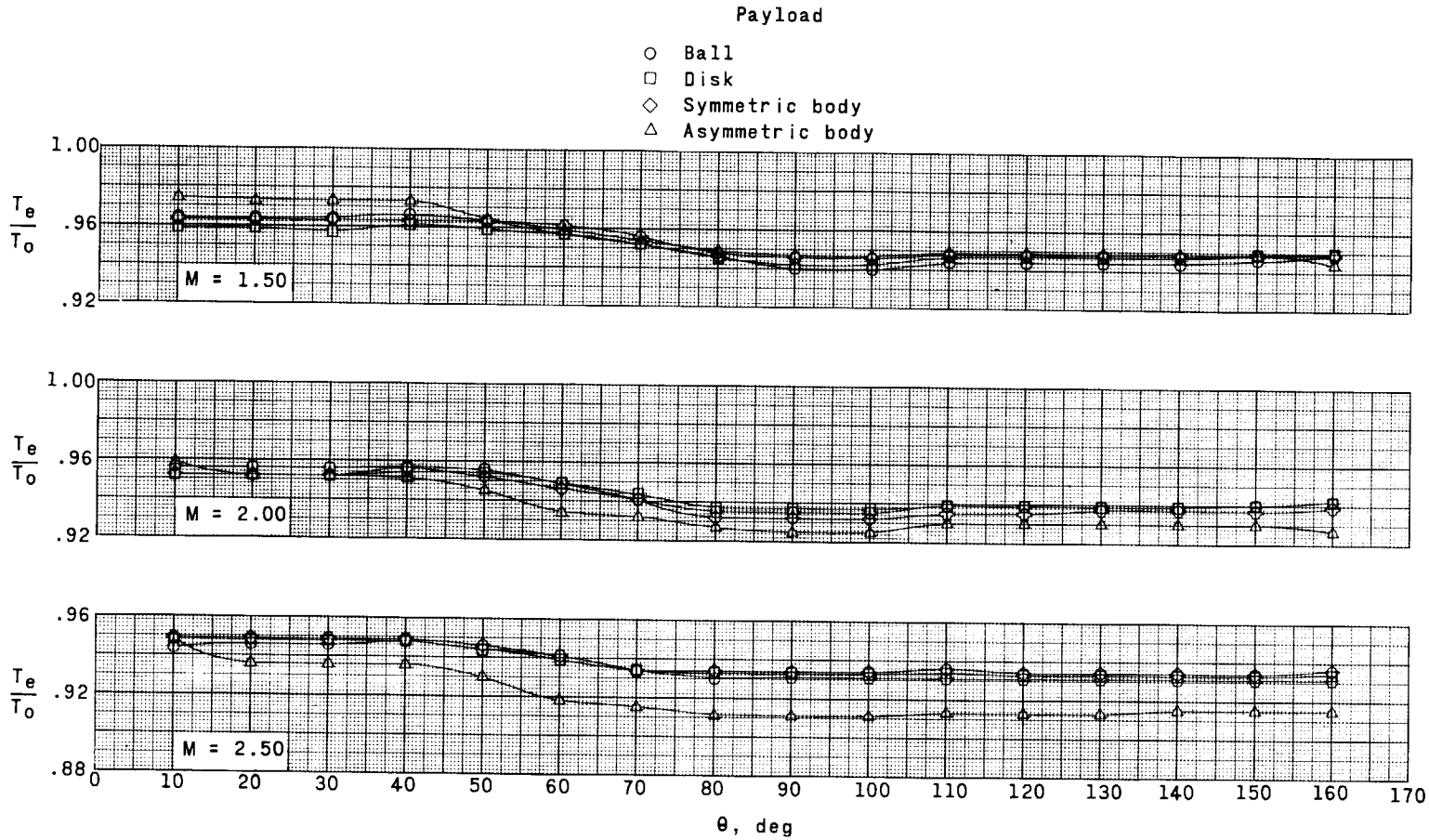

(a) 10-inch actuator.

Figure 18.- Results of temperature measurements around the rigid balloon with fence, actuator, and various payloads. $\alpha_{nom} = 0^{\circ}$.

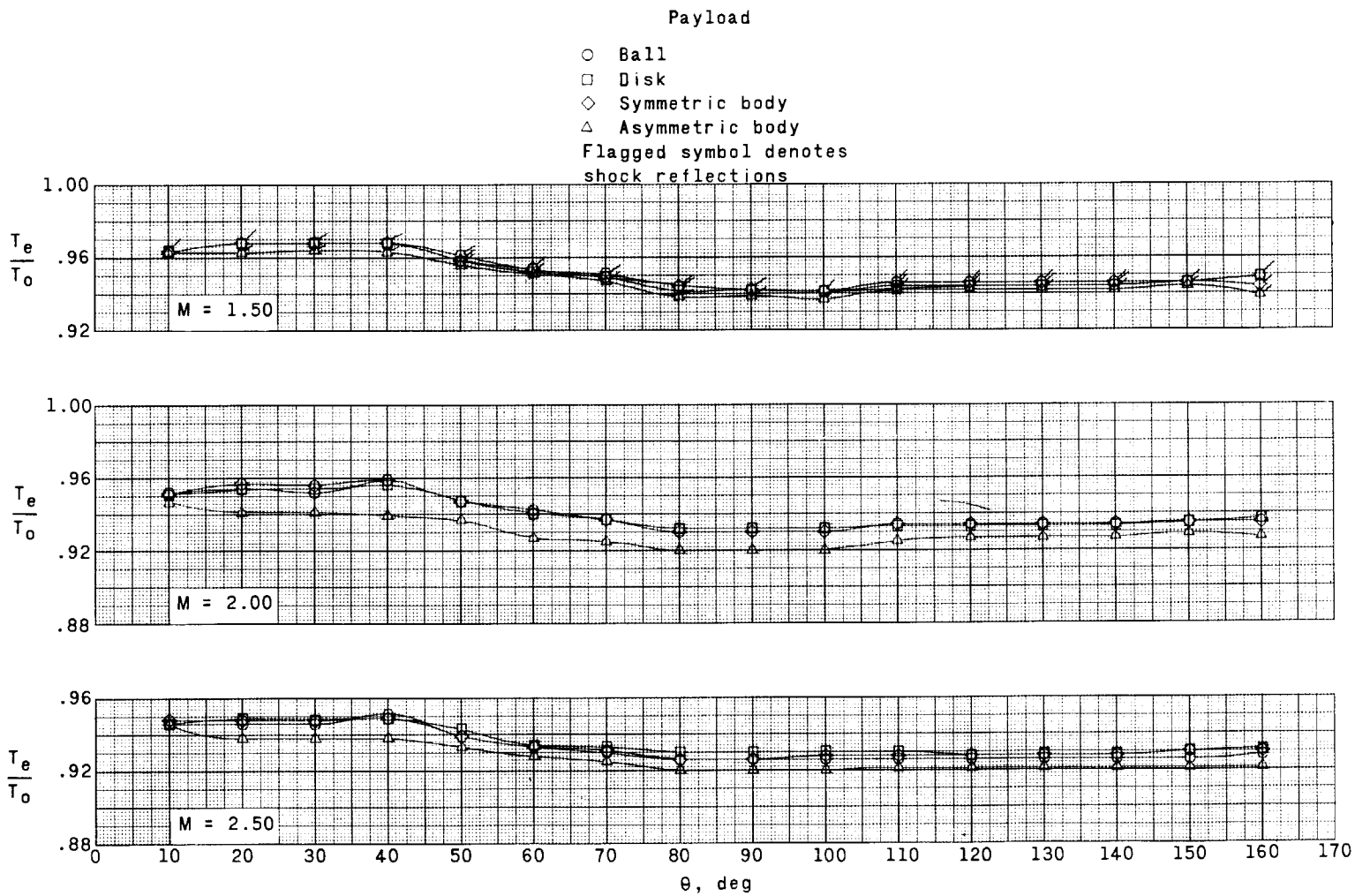

(b) 24-inch actuator.

Figure 18.- Concluded.

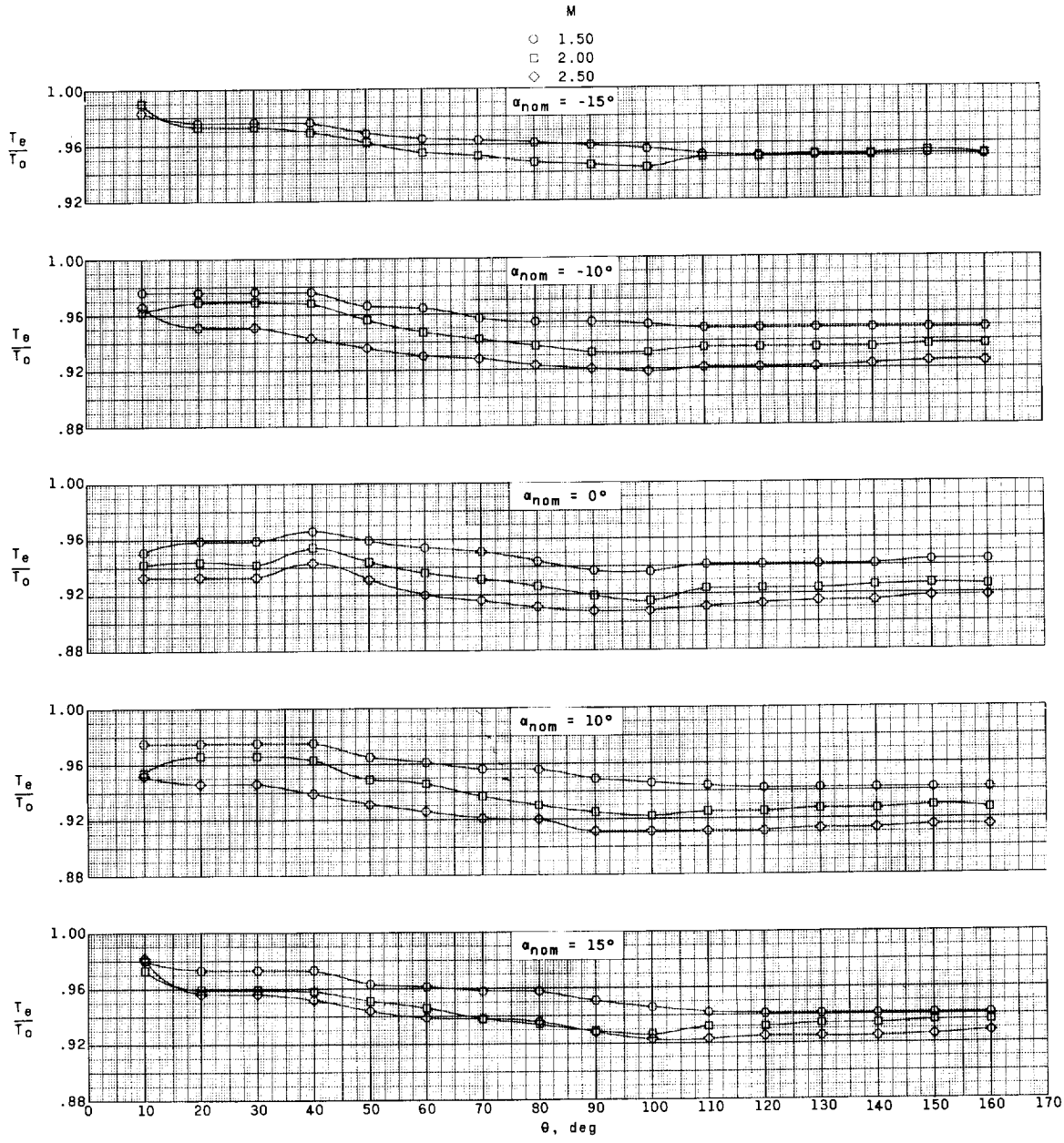

(a) Rigid balloon without fence and with 8-inch tow cable.

Figure 19.- Results of temperature measurements around the rigid balloon at various angles of attack.

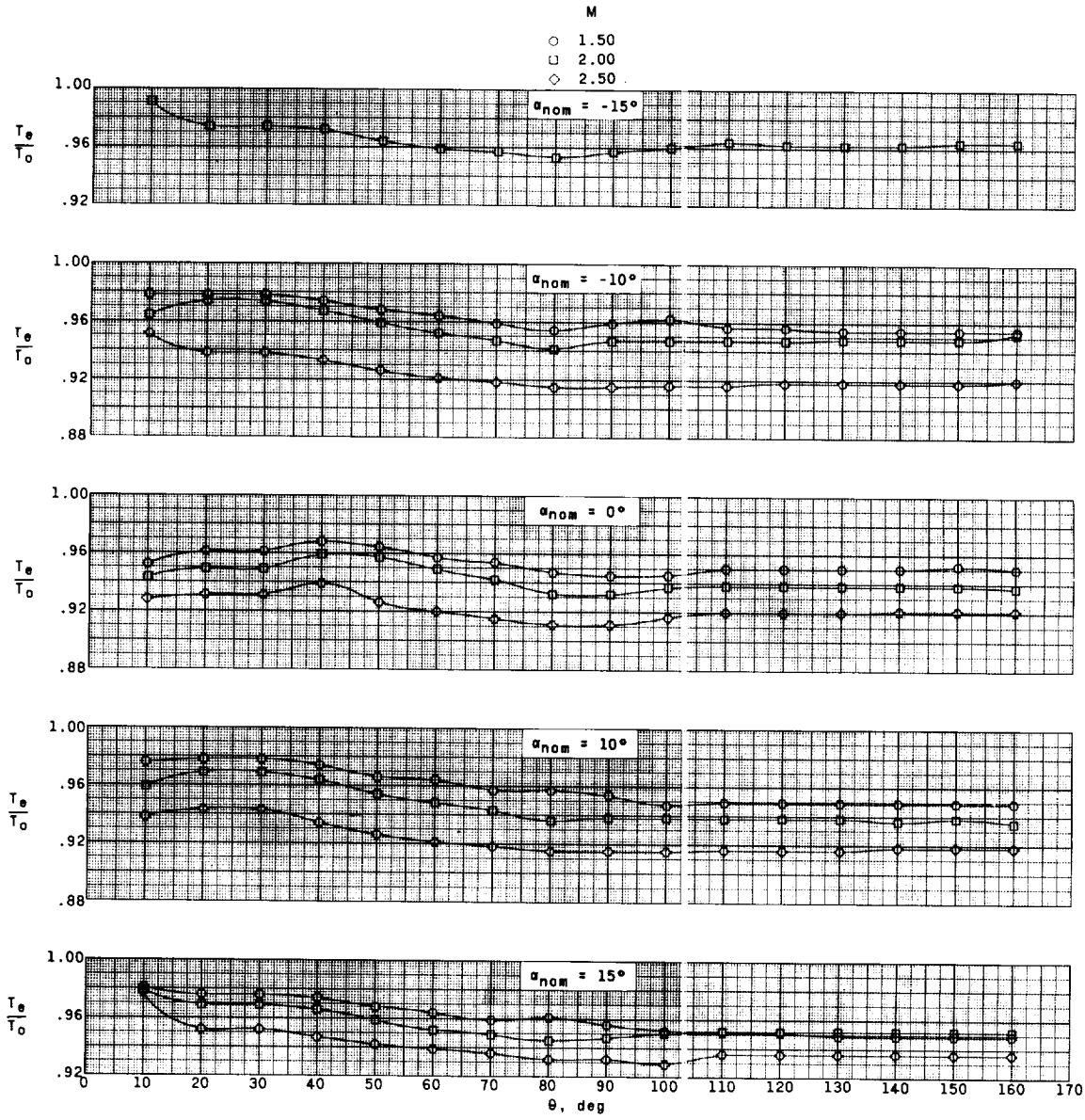

(b) Rigid balloon with fence and with 8-inch tow cable.

Figure 19.- Continued.

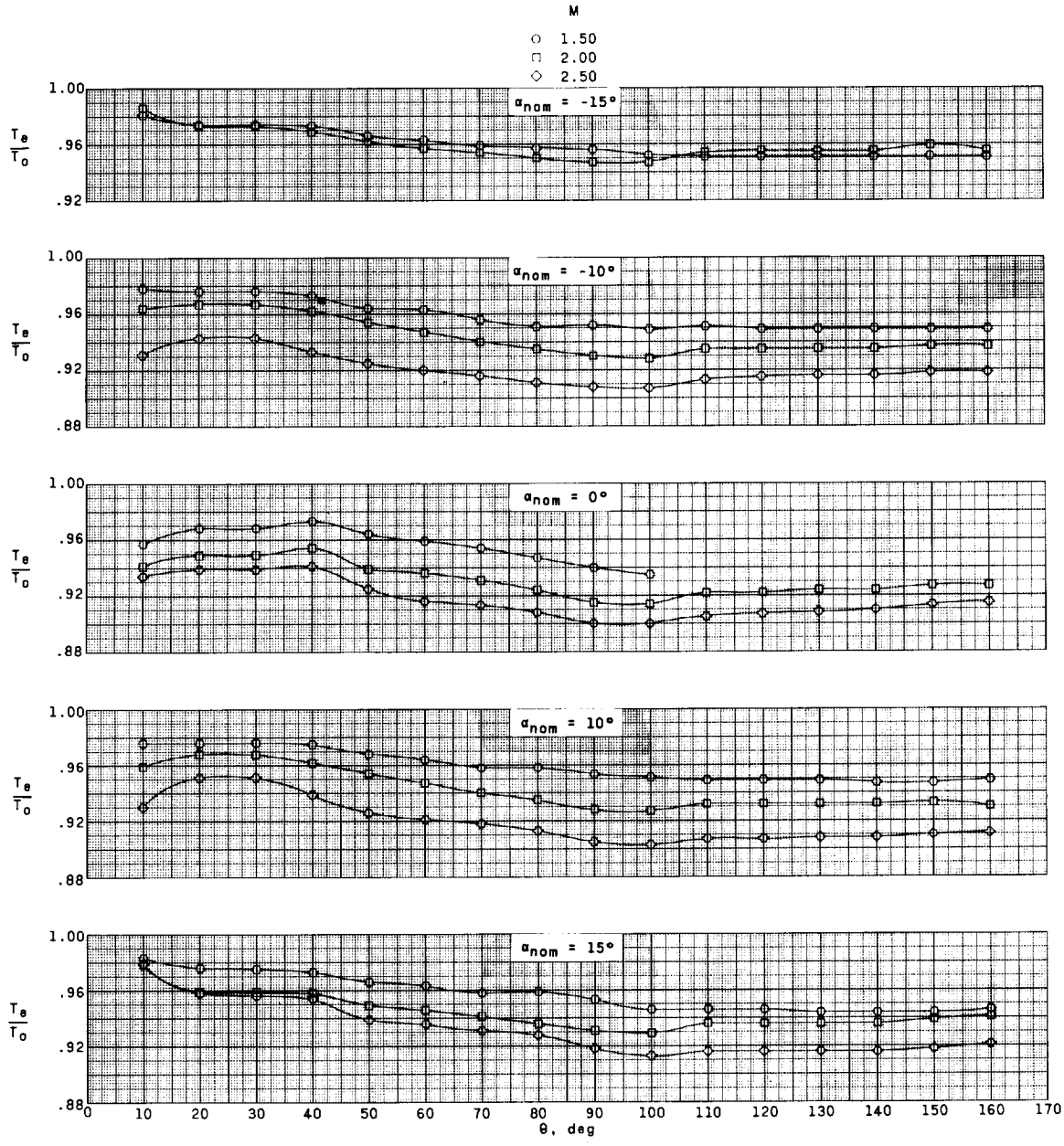

(c) Rigid balloon without fence and with 24-inch tow cable.

Figure 19.- Continued.

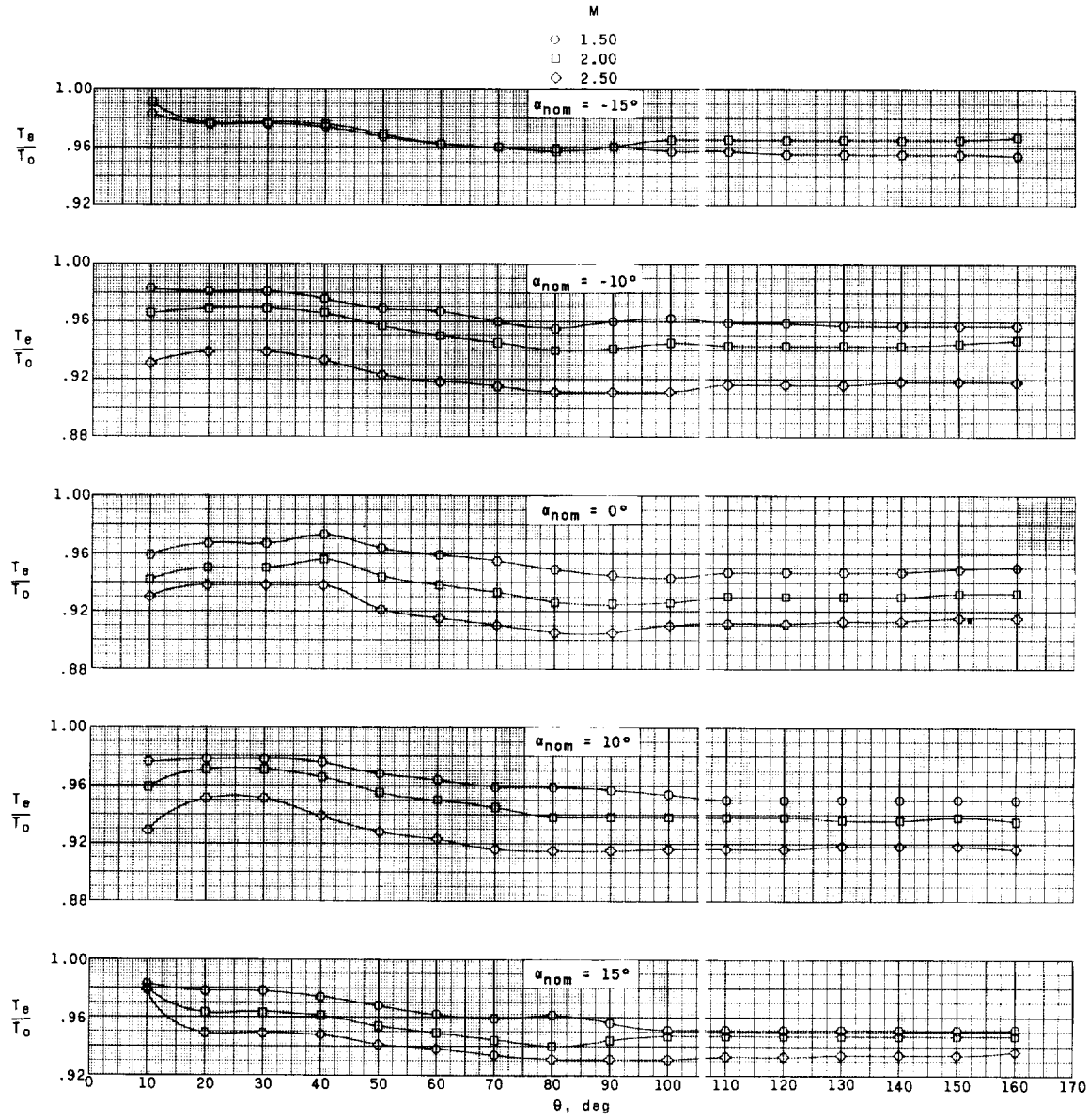

(d) Rigid balloon with fence and with 24-inch tow cable.

Figure 19.- Continued.

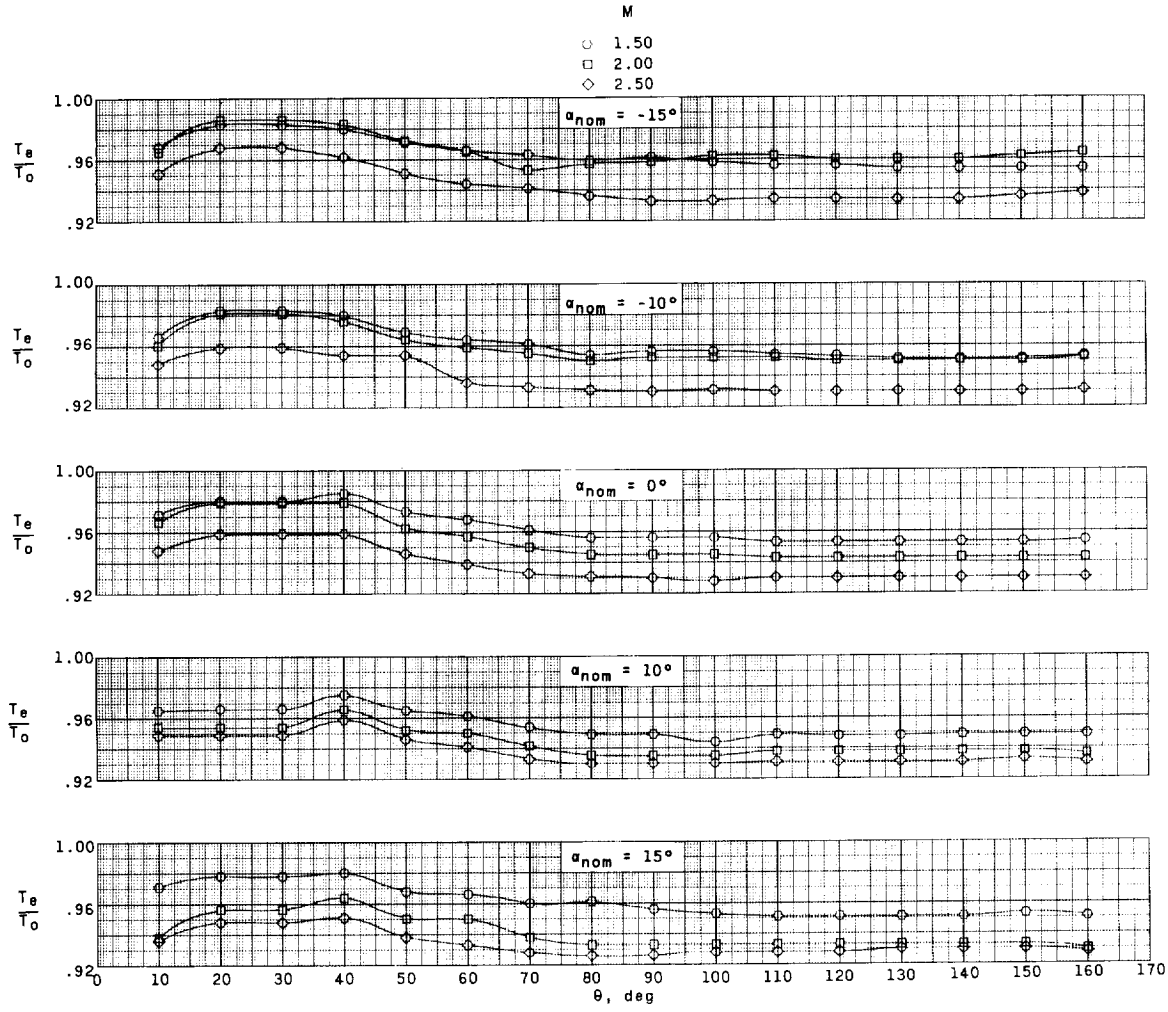

(e) Rigid balloon with fence and asymmetric body.

Figure 19.- Concluded.